1994

A comparative study of acoustic models in a range-independent shallow water environment

Duarte, Steven P.

Monterey, California. Naval Postgraduate School

NAVAL POSTGRADUATE SCHOOL
Monterey, California

THESIS

A COMPARATIVE STUDY OF ACOUSTIC MODELS IN A RANGE-INDEPENDENT SHALLOW WATER ENVIRONMENT

by
Steven P. Duarte

December, 1994

Thesis Advisors: Robert H. Bourke
James H. Wilson

Approved for public release; distribution is unlimited.

REPORT DOCUMENTATION PAGE

Form Approved OMB No. 0704-0188

1. AGENCY USE ONLY *(Leave blank)*	2. REPORT DATE December 1994	3. REPORT TYPE AND DATES COVERED Master's Thesis

4. TITLE AND SUBTITLE A Comparative Study of Acoustic Models in a Range-Independent Shallow Water Environment

5. FUNDING NUMBERS

6. AUTHOR(S) Steven P. Duarte

7. PERFORMING ORGANIZATION NAME(S) AND ADDRESS(ES)
Naval Postgraduate School
Monterey CA 93943-5000

8. PERFORMING ORGANIZATION REPORT NUMBER

9. SPONSORING/MONITORING AGENCY NAME(S) AND ADDRESS(ES)

10. SPONSORING/MONITORING AGENCY REPORT NUMBER

11. SUPPLEMENTARY NOTES The views expressed in this thesis are those of the author and do not reflect the official policy or position of the Department of Defense or the U.S. Government.

12a. DISTRIBUTION/AVAILABILITY STATEMENT
Approved for public release; distribution is unlimited.

12b. DISTRIBUTION CODE

13. ABSTRACT *(maximum 200 words)*

Project GEMINI was initiated to study the sound pressure fields in a range-independent, benign shallow water environment. The project consisted of five separate experiments conducted at a shallow site (~20 m), a relatively deep water site (~60 m) and a 30 m deep site previously studied by Rubano (1980). The experiments were carried out at both 50 and 140 Hz with measurements collected on two hydrophones at each site. The resulting data set was analyzed and compared to various acoustic propagation models approved or under consideration for inclusion in the Navy's Ocean Atmospheric Master Library (OAML). The following models were considered in the analysis: PE, utilizing the OAML approved LFBL database, FEPE and SNAP. FEPE and SNAP used a Hamilton "point" geoacoustic model as bottom model inputs. The models show varying ability to accurately model the average transmission loss (TL) and TL data intensity fluctuations at both frequencies. PE was not generally effective in modeling the TL data while FEPE was only slightly more accurate. SNAP proved to be the most successful at predicting the average TL and TL data fluctuations. SNAP was especially accurate in modeling TL at the Rubano site where an accurate Hamilton geoacoustic model was derived. SNAP's accuracy in modeling TL was significantly degraded at the deep and shallow water sites, where no site-specific Hamilton geoacoustic data existed and the Rubano geoacoustic parameters were used. Since the three sites were separated by only a few kilometers, the assumption of using a single site-specific geoacoustic model over a large area of shallow water does not seem feasible from the results of this data set.

14. SUBJECT TERMS PE, FEPE, SNAP, LFBL, normal mode model, Hamilton geoacoustic model, Project GEMINI.			15. NUMBER OF PAGES 123 16. PRICE CODE
17. SECURITY CLASSIFICATION OF REPORT Unclassified	18. SECURITY CLASSIFICATION OF THIS PAGE Unclassified	19. SECURITY CLASSIFICATION OF ABSTRACT Unclassified	20. LIMITATION OF ABSTRACT UL

NSN 7540-01-280-5500 Standard Form 298 (Rev. 2-89)

Prescribed by ANSI Std. 239-18

Approved for public release; distribution is unlimited.

A Comparative Study of Acoustic Models in a Range-Independent Shallow Water Environment

by

Steven P. Duarte
Lieutenant, United States Navy
B.S., Oral Roberts University, 1986

Submitted in partial fulfillment
of the requirements for the degree of

MASTER OF SCIENCE IN METEOROLOGY
and
PHYSICAL OCEANOGRAPHY

from the

NAVAL POSTGRADUATE SCHOOL
December, 1994

Author: [redacted]
Steven P. Duarte

Approved by: [redacted]
Robert H. Bourke, Thesis Advisor

[redacted]
James H. Wilson, Thesis Advisor

[redacted]
Robert H. Bourke, Chairman
Department of Oceanography

ABSTRACT

Project GEMINI was initiated to study the sound pressure fields in a range-independent, benign shallow water environment. The project consisted of five separate experiments conducted at a shallow site (~20 m), a relatively deep water site (~60 m) and a 30 m site previously studied by Rubano (1980). The experiments were carried out at both 50 and 140 Hz with measurements collected on two hydrophones at each site. The resulting data set was analyzed and compared to various acoustic propagation models approved or under consideration for inclusion in the Navy's Ocean Atmospheric Master Library (OAML). The following models were considered in the analysis: PE, utilizing the OAML approved LFBL database, FEPE and SNAP. FEPE and SNAP used a Hamilton "point" geoacoustic model as bottom model inputs.

The models show varying ability to accurately model the average transmission loss (TL) and TL data intensity fluctuations at both frequencies. PE was not generally effective in modeling the TL data while FEPE was only slightly more accurate. SNAP proved to be the most successful at predicting the average TL and TL data fluctuations. SNAP was especially accurate in modeling TL at the Rubano site where an accurate Hamilton geoacoustic model was derived. SNAP's accuracy in modeling TL was significantly degraded at the deep and shallow water sites, where no site-specific Hamilton geoacoustic data existed, and the Rubano geoacoustic parameters were used. Since the three sites were separated by only a few kilometers, the assumption of using a single site-specific geoacoustic model over a large area of shallow water does not seem feasible from the results of this data set.

TABLE OF CONTENTS

ACKNOWLEDGMENTS

The author would like to thank and extend my appreciation to Professors Robert H. Bourke and James H. Wilson for their overwhelming support, guidance and patience in the preparation of this thesis. Additionally, I would like to express my gratitude to Ms. Josie Paquin of Neptune Science, Inc. for all her help with the acoustic models. I am forever in your debt. Finally, I would like to thank my wife for all her support and patience, and my son for providing me numerous opportunities for taking breaks away from long hours of writing.

I. INTRODUCTION

A. BACKGROUND

With the downfall of the Soviet Union and the end of the cold war, a shift from deep water anti-submarine warfare (ASW) to shallow water undersea warfare (USW) has been undertaken by the Navy. The threat of a submarine attack in shallow water upon a friendly merchant vessel or warship has replaced the threat of Soviet submarine attacks on US ballistic missile submarines in the deep ocean. Concurrent with this shift in threats, the U.S. Navy needs to better understand the physical oceanographic and acoustic processes occurring in shallow, coastal waters and in particular, to develop an accurate acoustic model for sound propagation in shallow coastal waters.

Modern technology has allowed the development of quieter, more capable diesel-electric submarines (such as Germany's type 209 and the export Kilos from the former Soviet Union) which smaller countries are able to afford and operate. The U.S. Navy is very concerned about the submarine threat of such countries as North Korea with its numerous Romeo and Whiskey class submarines, Algeria with it's two Kilo class and two Romeo class submarines, Libya with it's six Foxtrot class submarines, and Syria with it's three Romeo class submarines (Morton, 1993). With the recent transfer of two export Kilo class submarines to Iran, the Navy is becoming increasingly interested in shallow water ASW (Morton, 1993). The technical difficulties in dealing with the rest-of-the-world (ROW) diesel submarines are

numerous. They have a low target strength and are much quieter (when not snorkeling) than nuclear submarines. With the advent of higher capacity batteries, the small diesel submarines are able to extend the submerged interval between snorkel operations, thus reducing the time and opportunity to detect a noisy snorkeling sub.

Some research efforts are now focusing attention on the development and evaluation of shallow water propagation models which incorporate a Hamilton (1980) sub-bottom geoacoustic "point" model to determine the bottom loss component of the overall propagation loss. A Hamilton geoacoustic model presents a realistic treatment of the ocean bottom in the vertical dimension at a single location or point. Both reflection from the sediment-water interface and refraction through the sub-bottom are included. The Navy currently uses the Ocean and Atmospheric Master Library (OAML) approved geoacoustic model, Low Frequency Bottom Loss (LFBL), formerly known as BLUG (Bottom Loss Upgrade), to model low frequency bottom interaction. This geoacoustic model was developed from mostly deep water data for frequencies between 50 Hz and 1000 Hz and treats the bottom as a single sediment with an acoustic basement (Etter, 1991) (see section II A 3 for a more detailed discussion). The bottom layering structure in shallow water is much more complex than this and LFBL may not be an adequate shallow water approximation at low frequencies to model sound propagation in the sub-bottom (Holland, 1992).

In shallow water, modeling propagation loss accurately means modeling both the TL versus range curve and the TL fluctuations. Signal coherence in shallow water is influenced by interference among propagating normal

modes which are the cause of the large range-independent TL fluctuations frequently observed in measured TL data. In shallow water these large fluctuations generally occur at short (1 km to 20 km) intervals. Predicting detection ranges from deepwater figure of merit (FOM) concepts is not meaningful when the FOM intersects the TL versus range curve several (3 to 10) times over wide (20 km) range intervals. New detection range concepts must be developed for shallow water to account for the large (10 dB to 15 dB) TL fluctuations along the acoustic path. The objective of this thesis is to assess the accuracy of several propagation models using average TL and TL fluctuations compared with measured data for several shallow water environments. Shallow water detection range prediction concepts are not discussed further, but provide the need to model TL range fluctuations accurately.

Recently Lynch et al. (1991) used an inversion technique to accurately estimate the TL fluctuations with range using data in the shallow waters off Corpus Christi, Texas. Although this inversion technique resulted in excellent agreement between fluctuations in modeled and observed data, the absolute or average TL level was not estimated well and the model estimates were "adjusted" in level and "shifted" in range to obtain a "best fit." Only a limited amount of the total Corpus Christi data were analyzed (Lynch et al., 1991) and the use of the Hamilton geoacoustic model at nearby measurement sites was not addressed. Additionally, two major disadvantages arise in using this inversion approach. First, the inversion algorithm requires an extensive observation program to obtain high resolution propagation measurements. Such a requirement is not likely to be possible to conduct in a hostile shallow

water area in wartime. Second, the geoacoustic parameters derived from the inversion technique (e.g., the vertical compressional sound speed profile of the sedimentary layers) were in disagreement with well established geoacoustic sub-bottom features derived from seismic surveys and other independent geoacoustic information (Matthews et al., 1985).

These disadvantages of inversion theory suggest that it is important to start with a geologically sound Hamilton geoacoustic model imbedded in an accurate shallow water propagation model, and integrate inversion theory techniques to estimate the horizontal variability of geoacoustic properties between Hamilton "point" model observations. In this thesis, the first part of this technical approach is addressed: can propagation be accurately estimated in a shallow water range-independent environment using only a Hamilton "point" model ?

B. OBJECTIVE

The objective of this study is to compare model estimates of TL with low frequency (50 Hz and 140 Hz) propagation data collected during the 1985 exercise, Project GEMINI, in the shallow waters near Corpus Christi, Texas. The OAML approved, Navy standard shallow water propagation model, Colossus II, is considered inadequate to estimate TL fluctuations accurately due to its empirical nature and hence was not considered in this study. The acoustic propagation models selected for use in this study are the SACLANTCEN normal mode acoustic propagation model (SNAP), finite element parabolic equation (FEPE) model, and the Navy OAML standard parabolic equation (PE) model. The comparison of the model TL estimates with the observed TL data will result in both a comparison of the PE and

normal mode models as well as the Navy standard geoacoustic model LFBL to a Hamilton "point" geoacoustic model. The TL and bottom loss models utilized do not require an extensive acoustic survey of the area as is required by the inversion technique of Lynch et al. (1991).

C. PROJECT GEMINI

Project GEMINI was a part of the Naval Electronics Systems Command (ELEX-612) Bottom Interaction Program (BIP) initiated to investigate the nature of the interaction of acoustic energy with the sea floor (Matthews et al., 1985). GEMINI was intended to be a baseline shallow water experiment containing as few geoacoustic complexities (i.e., range-independent sub-bottom layering) as possible. Project GEMINI was located in shallow water off the shores of Corpus Christi, Texas. This area is characterized by a mildly sloping, relatively smooth bottom and horizontal sub-bottom layering, a "benign" acoustic environment[1] with approximately range-independent geoacoustic conditions. If the propagation models are to be scientifically assessed and improved, they must be first evaluated in geoacoustically simple shallow water areas before applying them to more complex shallow water areas. If a propagation model does not perform well in the GEMINI area, it is not likely to perform well in a geoacoustically more complex shallow water area.

Project GEMINI data were obtained from researchers at the Woods Hole Oceanographic Institute and the Naval Research Laboratory-Stennis Space Center (NRL-Stennis) who performed the initial analysis of the data (Lynch

[1] "Benign" is defined as "an environment that is simple enough for essentially all of the assumptions and boundary conditions of acoustic field calculations to be met." (Matthews et al., p. 21, 1985).

et al., 1991). Project GEMINI consisted of a series of five experiments. A complete listing of date, location, bottom depth, and receiver depths of each experiment conducted is presented in Table 1.

Table 1: A DESCRIPTION OF THE PROJECT GEMINI TEST AREA CONDUCTED FROM 8 TO 12 SEPTEMBER 1985.

Run #	Date	Water Depth (m)	Location	Description	Receiver Depths (m)
1	9/08/85	30	27° 30' N, 97° 00' W	Rubano site	15 and 29
2	9/09/85	30	27° 30' N, 97° 00' W	Rubano site	15 and 29
3	9/10/85	62	27° 30' N, 96° 40' W	Deep site	32 and 61
4	9/11/85	21	27° 44' N, 97° 00' W	Shallow site	16 and 20
5	9/12/85	62	27° 30' N, 96° 40' W	Deep site	32 and 61

These experiments were conducted between 8 and 12 September 1985 with the Rubano site referring to the area previously studied by Rubano in 1980 (Rubano, 1980). Figure 1 shows the geographical location along with bottom depth information for the entire area of interest. Notice that the deep and shallow water sites are each less than 15 nm from the Rubano site. It was hoped that the Hamilton geoacoustic model previously developed at the Rubano site could be used at the other two sites due both to their close proximity and the benign geoacoustic properties of the area.

The experiment consisted of towing a narrow-band noise source (NRL J15-3) at frequencies of 50 and 140 Hz away from a pair of hydrophones moored at the locations given in Table 1. As seen in Table 1 and Figure 1,

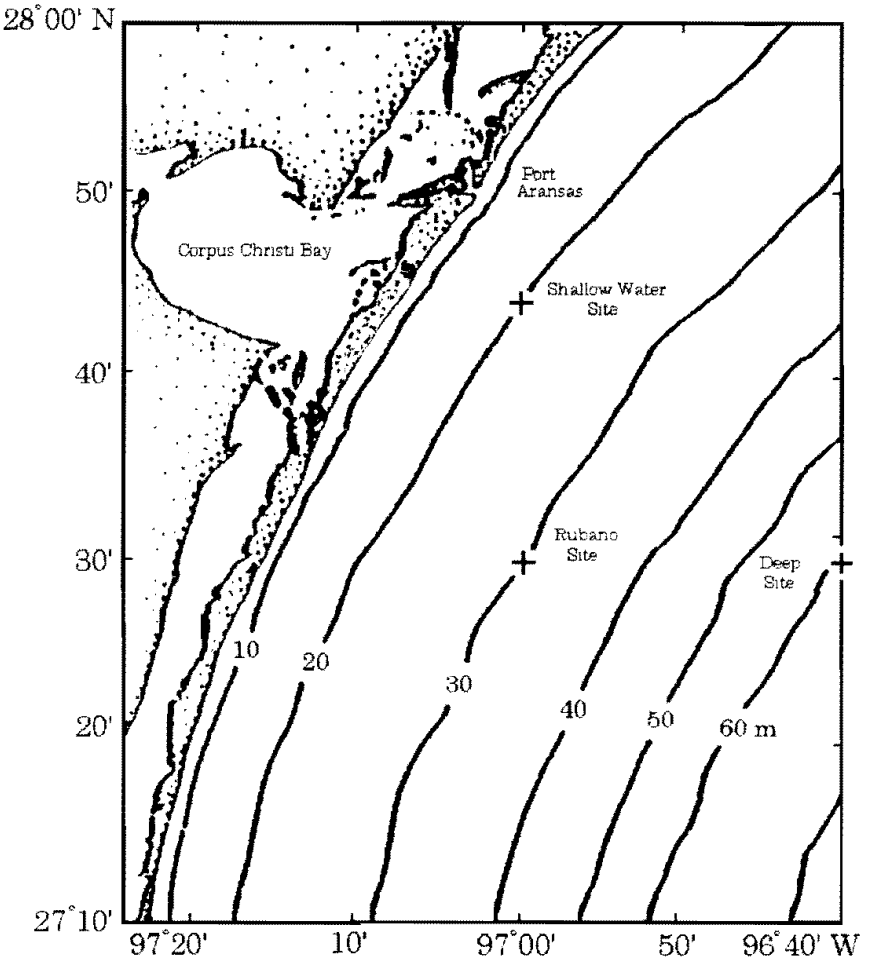

Figure 1: Geographical location of Project GEMINI experimental sites located off the shores of Corpus Christi, Texas (from Lynch et al., 1991).

the experiment was conducted at three different test sites: a relatively deep site, a shallow site, and the Rubano site. Figure 2 is a schematic of the experimental set up. The two receivers were placed midway in the water column and approximately 1.5 m above the bottom, respectively. Sound speed profiles were determined from CTD casts taken daily during the period 8-12 September. A Neil Brown, internally recording CTD was used to conduct the CTD casts and in most cases readings were taken on both the down and the up cast. Two weeks prior to the experiment, Hurricane Elena swept through the Gulf of Mexico and as a result the water columns for the three sites were fairly well mixed (Lynch et al., 1991).

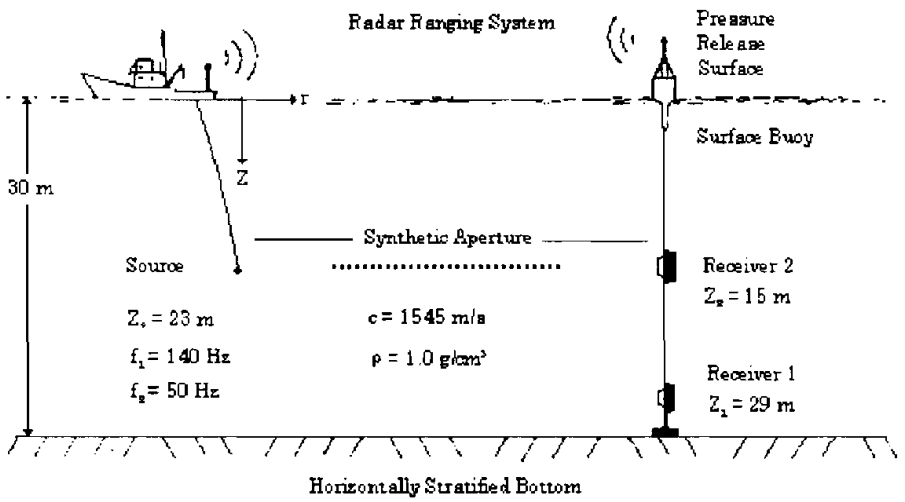

Figure 2: The experimental geometry for Project GEMINI. The depths indicated are for the September 9 experiment conducted at the Rubano site (from Lynch et al., 1991).

II. ACOUSTIC MODEL SUMMARY

Propagation models used to estimate TL in shallow water will be discussed briefly in this section. No attempt will be made to describe each model and its applications in detail. The parabolic equation (PE) and the finite element PE (FEPE) models are discussed in Section II A. A development of normal mode theory and the isospeed/hard bottom problem is presented in Section II 2a. This is followed by a brief comparison of LFBL and the Hamilton geoacoustic model. The sound speed profiles and the bathymetry of the GEMINI test site areas are shown in the last part of Section II.

A. TRANSMISSION LOSS (TL) MODELS

1. Parabolic Equation (PE)

The derivation of the parabolic equation begins with the reduced wave equation or Helmholtz equation:

$$\left\{\frac{\partial^2}{\partial r^2} + \left[\frac{\partial^2}{\partial z^2} + k_o^2 n^2\right]\right\}\psi(r,z) = 0 \tag{1}$$

$$n = \frac{c_o}{c(z)} \tag{2}$$

$$k_o = \frac{\omega}{c_o} \tag{3}$$

where n is the refractive index, k_o is the wave number, c_o is the reference

sound speed. The second order differential operator in Eq. (1) is factored into two first order complex operators using the following identity:

$$(a^2 + b^2) = (a + jb)(a - jb) \tag{4}$$

by setting

$$a = \frac{\partial}{\partial r} \tag{5}$$

and

$$b = \left[\frac{\partial^2}{\partial z^2} + k_o^2 n^2 \right]^{1/2}. \tag{6}$$

The Helmholtz equation is then rewritten into the following form:

$$\left[\frac{\partial}{\partial r} + j\left(\frac{\partial^2}{\partial z^2} + k_o^2 n^2 \right)^{1/2} \right] \left[\frac{\partial}{\partial r} - j\left(\frac{\partial^2}{\partial z^2} + k_o^2 n^2 \right)^{1/2} \right] \psi = 0 \tag{7}$$

Backward Propagating Energy

Forward Propagating Energy

Next, consider only forward propagating energy where the wave equation (Eq. 1) has been reduced to a first order partial differential equation in the range (r) variable, but a "non-sensical" (i. e., mathematically undefined) square root operator of a second order derivative in the depth variable (z) is introduced:

$$\left[\frac{\partial}{\partial r} - j\left(\frac{\partial^2}{\partial z^2} + k_o^2 n^2\right)^{1/2}\right]\psi = 0 \tag{8}$$

The undefined square root operator can be expanded in a Taylor Series by rewriting Eq. (8) in the following form:

$$\left[\frac{\partial^2}{\partial z^2} + k_o^2 n^2\right]^{1/2} = \left[\frac{\partial^2}{\partial z^2} + k_o^2(n^2 - 1) + k_o^2\right]^{1/2}$$

$$= k_o\left[1 + \frac{1}{k_o^2}\frac{\partial^2}{\partial z^2} + (n^2 - 1)\right]^{1/2}. \tag{9}$$

The square root operator in Eq. (9) can be approximated by

$$\sqrt{1 + x} \approx 1 + \frac{x}{2} \qquad x << 1 \tag{10}$$

where x is defined as:

$$x \equiv \frac{1}{k_o^2}\frac{\partial^2}{\partial z^2} + (n^2 - 1). \tag{11}$$

The differential operator

$$\frac{\partial^2}{\partial z^2} \tag{12}$$

is now well defined (where $\sqrt{1+\frac{\partial^2}{\partial z^2}}$ is not) and the parabolic equation can now be written as:

$$\frac{\partial \psi}{\partial r} = j\left[k_o + \frac{1}{2k_o}\frac{\partial^2}{\partial z^2} + \frac{k_o}{2}(n^2 - 1)\right]\psi \,. \tag{13}$$

The price to be paid for the PE approximation is that large source angles are not well modeled. More terms can be retained in the expansion for $\sqrt{1+x}$, but the time to compute the solution increases significantly with the number of terms calculated in the Taylor series. Thus, the Navy standard PE is valid in deep water only where high source angle energy is not important at long ranges. The parabolic equation can be solved efficiently for range-dependent environments (Etter, 1991). The split-step algorithm developed by Tappert (1977) has the advantage of being able to determine the acoustic pressure at each range step. This makes the PE easy to interface with range-dependent environments (sound speed, bathymetry, and geoacoustic variations) (Etter, 1991).

a. Finite Element Parabolic Equation (FEPE)

The finite element parabolic equation (FEPE) model is a numerical solution to the PE equation for sound propagation in an ocean overlying a sediment that supports only compressional energy propagation in the sub-bottom. FEPE is based on very efficient algorithms and solves the second order parabolic partial differential equation based on a Pade' series approximation (Collins, 1991) of the square root operator (see Eq. 8 through 12) in the parabolic equation. While the split-step PE model is confined by

computational limitations to propagation angles less than $\pm$ 40° from the horizontal, FEPE can calculate angles up to $\pm$ 89° when seven Pade' terms are used. FEPE can handle large variations in sound speed, density, and bathymetry, unlike the split-step PE. These features make FEPE an attractive candidate for shallow water modeling where high angle propagation paths are an important part of the total transmission path. Thus it is utilized in this study to model sound propagation for the GEMINI site with a Hamilton "point" geoacoustic model for the three sites developed as FEPE inputs.

2. Normal Mode Model

a. The Normal Mode Solution

The normal mode solution is a complete solution to the wave equation and avoids the limitations inherent to the parabolic approximation. For the simple case of an isospeed sound speed profile and a hard bottom the normal mode solution consists of a series of characteristic functions which vary with depth (z), known as normal modes, each of which is a solution to the wave equation. The normal mode functions are multiplied by the range solution to the wave equation and summed to satisfy the boundary and source conditions under consideration (Urick, 1991). The present discussion provides a simple derivation of the normal mode solution for the environment above using the technique of separation of variables and are developed in this chapter for the range-independent environment only. The purpose of deriving the solution for a simple environment is to illustrate general characteristics of the normal mode solution explicitly that are present

implicitly in more complex environments requiring numerical methods to solve the partial differential equations with boundary conditions.
The following discussion is based upon material derived from Porter (1991).

Starting with an idealized, symmetric, range-independent acoustic waveguide, given a sound source within this layer the solution is governed by the acoustic wave equation:

$$\nabla \cdot \left(\frac{1}{\rho} \nabla P \right) - \frac{1}{\rho c^2(z)} P_{tt} = - s(t) \frac{\delta(z - z_s)\delta(r)}{2\pi r} \tag{14}$$

where $P(r,z,t)$ represents the acoustic pressure as a function of depth (z), time (t), and range (r). Also, $s(t)$ is an isotropic point source located at depth $z = z_s$ and range $r = 0$, $c(z)$ is the sound speed, and $\rho(z)$is the density. Assuming that the ocean surface is a pressure release surface and that the bottom (at a depth D) is a perfectly reflecting rigid boundary, the following boundary conditions apply:

$$\begin{aligned} P(r,0,t) &= 0, \\ \frac{\partial P}{\partial z}(r,D,t) &= 0, \end{aligned} \tag{15}$$

The hard or rigid boundary is an approximation to the ocean bottom used only to derive analytic solutions to the wave equation that illustrate characteristics of the normal mode solution. A better approximation is that of a layered geoacoustic, elastic boundary used in all later TL calculations for GEMINI data. In addition, it is required that

$$P(r,z,t) \rightarrow \text{zero for outgoing waves as } r \rightarrow \infty. \tag{16}$$

A sinusoidal time dependence is assumed which leads to a pressure field with the time-dependence:

$$P(r,z,t) = p(r,z)\, e^{-j\omega t}. \tag{17}$$

Substituting this equation into the wave equation (Eq. 14) results in the Helmholtz equation, or the reduced wave equation:

$$\frac{1}{r}\frac{\partial}{\partial r}\left(r\frac{\partial p}{\partial r}\right) + \rho(z)\frac{\partial}{\partial z}\left(\frac{1}{\rho(z)}\frac{\partial p}{\partial z}\right) + \frac{\omega^2}{c^2(z)}p = \frac{-\delta(z-z_s)\delta(r)}{2\pi r} \tag{18}$$

Using the technique of separation of variables a solution of the unforced, or free field, equation (without the source) is obtained in the form:

$$p(r,z) = Z(z)R(r). \tag{19}$$

Substituting Eq. (19) into Eq. (18) for source free space leads to the following equation:

$$\frac{1}{R}\left[\frac{1}{r}\frac{\partial}{\partial r}\left(r\frac{\partial R}{\partial r}\right)\right] + \frac{1}{Z}\left[\rho(z)\frac{\partial}{\partial z}\left(\frac{1}{\rho(z)}\frac{\partial Z}{\partial z}\right) + \frac{\omega^2}{c^2(z)}\right] = \frac{-\delta(z-z_s)\delta(r)}{2\pi r} \tag{20}$$

The first term within the first square bracket is a function of r only and the term in the second square bracket is a function of z only. To satisfy Eq. (20)

both components are set equal to a constant. Representing this separation constant as k^2, the modal (z dependent) equation is obtained:

$$\rho(z)\frac{d}{dz}\left(\frac{1}{\rho(z)}\frac{dZ(z)}{dz}\right)+\left(\frac{\omega^2}{c^2(z)}-k^2\right)Z(z)=0$$

$$Z(0)=0$$

$$\frac{dZ}{dz}(D)=0. \tag{21}$$

This is an example of a classical Sturm-Liouville eigenvalue problem and the properties of this equation are well known. Assuming that $\rho(z)$ and $c(z)$ are real functions, there exists an infinite number of solutions (normal modes) to the modal equation (Eq. 21) which are represented by a normal mode function, $Z_m(z)$, and a horizontal propagation constant, k_m. The propagation constants (k_m) are all distinct eigenvalues and the function $Z_m(z)$ is the corresponding eigenfunction. The mth mode consists of a function that has m zeroes in the depth interval between 0 and D. All the corresponding eigenvalues are real and are ordered such that $k_1^2 > k_2^2 > \cdots$. It can also be shown that all the eigenvalues are less than $\omega/c_{\min}$ where $c_{\min}$ is the minimum sound speed in the water column. The normal modes or eigenfunctions of the Sturm-Liouville problem are *orthogonal* if scaled by the density in the water column:

$$\int_0^D \frac{Z_m(z)Z_l(z)}{\rho(z)}\,dz=0, \qquad \text{for } m\neq n \tag{22}$$

To simplify the derivation further, assume that the modes are orthonormal or normalized so that

$$\int_0^D \frac{Z_m^2(z)}{\rho(z)}\,dz = 1 \tag{23}$$

With this scaling, the modes form a complete *orthonormal* set and hence the name "normal modes" follows. A complete set means that any arbitrary function can be expanded in a series of all the normal modes. The pressure field can then be written as

$$p(r,z) = \sum_{m=1}^{\infty} R_m(r)\, Z_m(z). \tag{24}$$

where the range functions $R_m(r)$ are, as yet, not determined. Substituting this expression for pressure into Eq. (18) yields:

$$\sum_{m=1}^{\infty} \left\{ \frac{\rho(z)}{r} \frac{\partial}{\partial r}\left(\frac{r}{\rho(z)} \frac{\partial R_m}{\partial r} \right) Z_m(z) \right.$$

$$\left. + R_m(r)\left[\rho(z) \frac{d}{dz}\left(\frac{1}{\rho(z)} \frac{dZ(z)}{dz} \right) + \frac{\omega^2}{c^2(z)} Z_m(z) \right] \right\} = \frac{-\delta(r)\delta(z-z_s)}{2\pi r}. \tag{25}$$

which simplifies to the following equation:

$$\sum_{m=1}^{\infty} \left[\frac{1}{r} \frac{\partial}{\partial r}\left(r \frac{\partial R_m(r)}{\partial r} \right) Z_m(z) + k_m^2 R_m(r)\, Z_m(z) \right] = \frac{-\delta(r)\delta(z-z_s)}{2\pi r}. \tag{26}$$

The next step is to multiply the operator

$$\int_0^D (\bullet)\frac{Z_l(z)}{\rho(z)}dz \tag{27}$$

to both sides of Eq. (26). Applying the orthogonality property (Eq. 23), the following equation is obtained:

$$\frac{1}{r}\frac{\partial}{\partial r}\left(r\frac{\partial R_l(r)}{\partial r}\right) + k_l^2 R_l(r) = \frac{-\delta(r)Z_l(z_s)}{2\pi r\rho(z_s)}. \tag{28}$$

The solution to Eq. (28) is a Hankel function of the first kind:

$$R_l(r) = \frac{j}{4\rho(z_s)} Z_l(z_s) H_0^{(1)}(k_l r). \tag{29}$$

The full normal mode solution for the pressure field is given by;

$$p(r,z) = \frac{j}{4\rho(z_s)} \sum_{m=1}^{\infty} Z_m(z_s)\, Z_m(z)\, H_0^{(1)}(k_m r), \tag{30}$$

and using the asymptotic approximation to the Hankel function,

$$H_0^{(1)}(k_m r) \approx \sqrt{\frac{2}{\pi k_m r}}\; e^{j\left(k_m r - \frac{\pi}{4}\right)} \tag{31}$$

the approximate solution for the pressure field is given by:

$$p(r,z) \approx \frac{j}{\rho(z_s)\sqrt{8\pi r}}\, e^{-j\frac{\pi}{4}} \sum_{m=1}^{\infty} Z_m(z_s)\, Z_m(z) \frac{e^{jk_m r}}{\sqrt{k_m}}. \tag{32}$$

This equation represents the complex pressure field and the magnitude of $p(r,z)$ transmission loss (TL) and is given by the following equation:

$$TL(r,z) = -20\log\left|\frac{p(r,z)}{p^0(r=1)}\right|, \tag{33}$$

where

$$p^0(r) = \frac{e^{jk_0 r}}{4\pi r} \tag{34}$$

is the pressure for the source in free space. Finally transmission loss can be expressed as:

$$TL(r,z) \approx -20\log\left|\frac{1}{\rho(z_s)}\sqrt{\frac{2\pi}{r}} \sum_{m=1}^{\infty} Z_m(z_s)\, Z_m(z) \frac{e^{jk_m r}}{\sqrt{k_m}}\right|. \tag{35}$$

b. The Isospeed Problem

A specific normal mode solution for the boundary conditions given in the previous section is obtained by assuming that the sound speed c and the density ρ in the water column are constant. The general solution to this problem is

$$Z_m(z) = A\sin\gamma z + B\cos\gamma z, \tag{36}$$

where

$$\gamma = \sqrt{\frac{\omega^2}{c^2} - k^2}. \tag{37}$$

The boundary conditions given in (Eq. 21) lead to:

$$A\gamma \cos \gamma D = 0, \tag{38}$$

where D is the bottom depth. Since $A = 0$ represents the trivial solution, the solution must be:

$$\gamma D = (m + \tfrac{1}{2})\pi, \quad m = 1,2,..., \tag{39}$$

k must assume the particular values given by

$$k_m = \sqrt{\frac{\omega^2}{c^2} - \left[(m + \tfrac{1}{2})\frac{\pi}{D}\right]^2}, \quad m = 1,2,.... \tag{40}$$

with the corresponding eigenfunctions, or normal modes, given by

$$Z_m(z) = \sqrt{\frac{2}{D}} \sin \gamma_m z. \tag{41}$$

Equation 40 gives the modal wavenumber k_m as a function of frequency ω and is known as the *dispersion relation*. Substituting Eq. (41) into Eq. (31) one obtains a representation for the complex pressure field:

$$p(r,z) = \frac{j}{2D}\sum_{m=1}^{\infty}\sin(\gamma_m z_s)\sin(\gamma_m z)H_0^{(1)}(k_m r). \tag{42}$$

The magnitude of pressure is given by

$$|p(r,z)| = \left|\frac{1}{D}\sqrt{\frac{8\pi}{r}}\sum_{m=1}^{\infty}\sin(\gamma_m z_s)\sin(\gamma_m z)\frac{e^{jk_m r}}{\sqrt{k_m}}\right|. \tag{43}$$

This leads to the following equation for TL:

$$TL(r,z) = -20\log\left|\frac{p(r,z)}{p^0(r=1)}\right|. \tag{44}$$

Although the "hard bottom" boundary condition is not a good assumption for the GEMINI area, this solution is used to represent an "optimistic upper bound" for transmission loss in the GEMINI test area. The individual model data comparisons are shown in Section III.

3. Low Frequency Bottom Loss (LFBL) vs. Hamilton Geoacoustic Model

For low frequency (< 300 Hz) propagation in shallow water the energy propagation through the sub-bottom layers becomes significant. LFBL, formerly called Bottom Loss Upgrade (BLUG), is the Navy's OAML-approved database used to describe the acoustic reflection and sub-bottom refraction characteristics of the ocean bottom for frequencies of 50 to 1000 Hz. Ten geoacoustic inputs are used in LFBL to describe the sub-bottom propagation environment as shown in Figure 3. LFBL contains a thin

surficial or "stainless steel" layer, a fluid sediment layer of variable thickness, and a reflective sub-bottom half space (Holland and Muncil, 1992). Figure 3 illustrates an example of a typical LFBL bottom/sub-bottom.

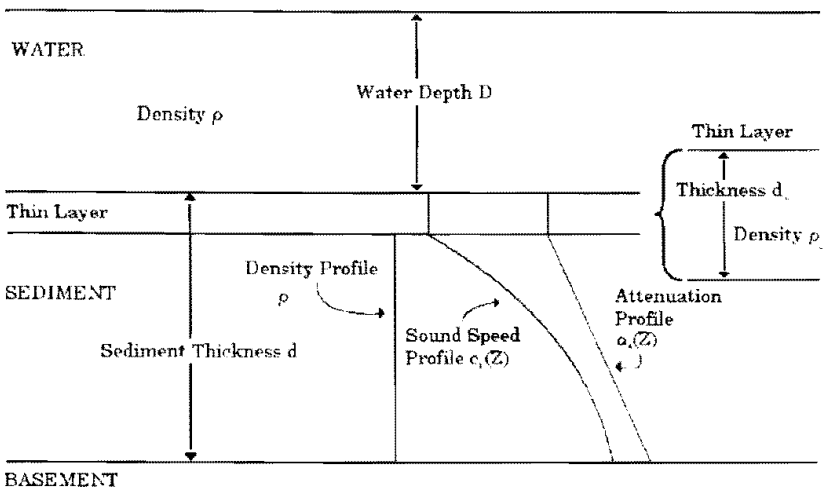

Figure 3: A typical LFBL bottom with a "stainless steel" thin layer (from Holland and Muncil, 1992).

LFBL is based upon a simplified model of the bottom sediment and, as stated previously, the ocean bottom layering is much more geoacoustically complex than assumed by this model. A full or exact geoacoustic model is needed to adequately model the ocean sediment in shallow water environments where there is significant energy propagating through the bottom. Hamilton (p. 1313, 1980) defines a geoacoustic model as:

> a model of the real sea floor with emphasis on measured, extrapolated, and predicted values of those properties important in underwater acoustics and those aspects of geophysics involving sound transmission. In general, a geoacoustic model details the true thicknesses and

properties of sediment and rock layers in the sea floor. A complete model includes water-mass data, a detailed bathymetric chart, and profiles of the sea floor (to obtain relief and slopes).

Table 2 lists the ten LFBL parameters required as model inputs.

TABLE 2: DESCRIPTION OF LFBL PARAMETERS

PARAMETER	UNITS
Ratio of sediment sound to water sound speed	none
Thin layer thickness	*m*
Thin layer density	g / cm^3
Sediment surface density	g / cm^3
Sediment sound speed gradient at the water/sediment interface	1/s
Surface attenuation	*dB / m / kHz*
Attenuation gradient (constant)	*dB / m / kHz / m*
Attenuation exponent	none
Basement reflection coefficient	none
Two-way travel time	*s*

A realistic treatment of the sediment bottom should include all of the sediment layers present in the area of interest. Figure 4 shows a more accurate depiction of the sediment bottom. This more accurate representation of the ocean bottom is called a Hamilton geoacoustic "point" model where the geoacoustic properties are range-independent. A description of the development of the geoacoustic model used for the GEMINI area is discussed in Section III.

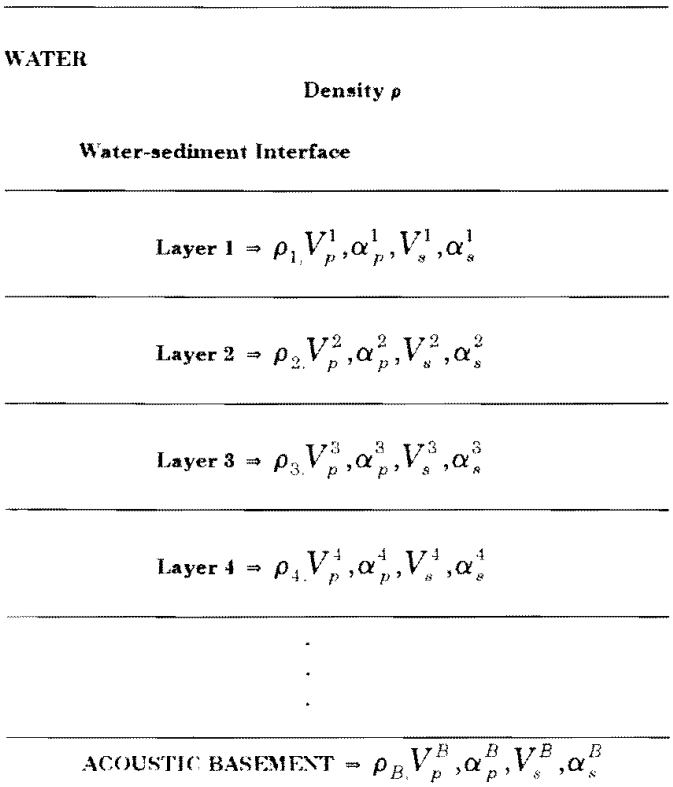

Figure 4: A more realistic depiction of the ocean bottom, geoacoustic environment.

B. THE GEOACOUSTIC MODEL FOR THE GEMINI AREA

1. Background

A full Hamilton geoacoustic model is developed in this section in order to compare SNAP and FEPE model estimates of TL to measured data in the GEMINI area. The Navy standard PE model with LFBL will also be used to estimate TL for comparison purposes. The Hamilton and LFBL geoacoustic models are incorporated into the propagation models as specified above and TL model estimates are compared to measured TL data to show the relative accuracy of the two geoacoustic models.

A preliminary assessment of the Rubano test site area was conducted by Matthews et al. (1985). In this assessment a Hamilton geoacoustic model of the Rubano site was developed using historical environmental data as well as the most recent seismic surveys of the test area (Berryhill and Tippet, 1981). Based on this pre-assessment and study of the regional seismic stratigraphy of the Rubano test site area, Matthews et al. showed that the local lithology consists of a Holocene silty clay sediment over a very fine sand, late to early Wisconsin sediment layer. Table 3 presents a simplified geological time scale to be used as a reference.

Since one of the basic prerequisites for the GEMINI experiment was for a smooth, nearly flat environment, the assumption is made that the geoacoustic model developed by Matthews et al. (1985) (and discussed here) can be extended to the other two test site areas, i.e., the deep and shallow sites, with reasonable confidence. Figure 5 shows clearly the range-independent, nearly horizontal sediment layers characteristic of the Corpus Christi coast line. This requirement for a benign area was critical in the

selection of this experimental area. The development of the geoacoustic model for the Rubano site follows.

Table 3: GEOLOGIC TIME SCALE FROM THE QUATERNARY PERIOD (FROM MATTHEWS ET AL., 1985).

PERIOD	EPOCH	GLACIAL STAGE	SEA LEVEL
Quaternary	Holocene		Transgression
	Pleistocene	Late Wisconsin	Regression
		Mid Wisconsin	Transgression
		Early Wisconsin	Regression
		Sangamon	Transgression
		Late Illinoian	Regression
		Mid Illinoian	Transgression
		Early Illinoian	Regression
		Yarmouth	Transgression
		Kansan	Regression
		Aftonian	Transgression
		Nebraskan	Regression
Tertiary	Pliocene		

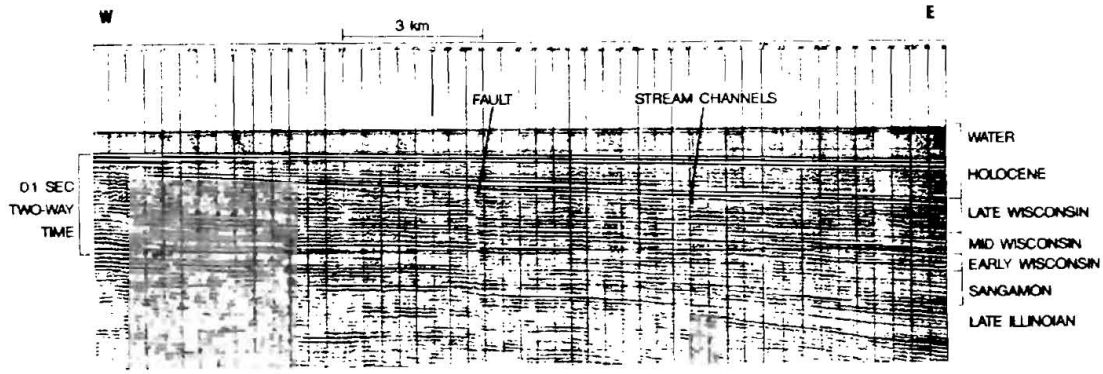

Figure 5: High resolution seismic reflection record across the continental shelf of Corpus Christi (from Matthews et al., 1985).

2. Development of The Geoacoustic Model

a. The Holocene Sediment Layer

The Holocene sedimentary sequence was shown by Matthews et al. (1985) to have a two way travel time of 23 ms. According to Hamilton (1980) in shallow water this should relate to a silty clay sediment having a density of $1.421 \pm 0.015\ g/cm^3$ and a relative sound speed 0.994 ± 0.002. The relative sound speed is the ratio of the surface sediment sound speed to the sound speed at the bottom of the overlying water column.

The Naval Oceanographic Office (NAVOCEANO) and other researchers (Rubano, 1980; Ross et al., 1978) conducted an experiment during which 16 gravity core samples were collected in the Rubano test site area. Their analysis indicated a mean density of $1.557\ g/cm^3$ and a mean relative sound speed of 0.987. Based on the NAVOCEANO data, Matthews et al. (1985) chose to use this site specific data to develop their geoacoustic model.

The compressional sound speed as a function of depth in the sediment layer for silty clay was calculated from Hamilton (1980) using the following linear regression equation:

$$V_p = Ss(.987) + 1.3\, s^{-1}(D) \tag{45}$$

where V_p is the compressional sound speed in m/s, Ss is the sound speed at the bottom of the water column (the water-sediment interface) in m/s and D is the depth of the sediment layer below the sea floor in meters. The thickness of the Holocene layer does not exceed more than a few tens of meters. As a result, the higher order terms (not shown) of the linear regression equation (Eq. 45) used to calculate compressional sound speed make very small contributions to the sound speed in this sediment layer and are therefore neglected (Matthews et al., 1985). The sound speed regression equation (Eq. 45) is therefore a linear function of depth below the sea floor.

The sound speed at the bottom of the water column greatly effects the sound speed in the first few meters of the bottom sediment. If a periodic thermal fluctuation is applied to the water-sediment interface, a thermal wave will propagate into the sediment. The amplitude of this wave will decay exponentially below the water-sediment interface and the temperature fluctuations will oscillate around a relatively stable geothermal gradient. This geothermal gradient is a function of sediment thermal conductivity and heat flow (Matthews et al., 1985). Lee and Cox, (1966) have shown that these thermal oscillations can be expected to essentially cease by a depth of approximately 3 m where the level of thermal stability is reached.

In this study, Matthews et al.(1985) assume a depth for thermal stability of 2.5 m. This is reflected by incorporating a negative sound speed gradient in the sediment until a depth of 2.5 m. The sound speed profile follows that of Eq. (45) after the initial 2.5 m to a depth of 47.8 m.

The sediment density as a function of depth below the sea floor for a silty clay bottom was calculated from Hamilton (1978). The sediment density is considered a linear function of depth below the sea floor. The following equation was used to calculate the sediment density:

$$\rho = \frac{1.135\,(Ss\,)}{1000} - 0.155, \tag{46}$$

The regression constant (0.155) was adjusted to match the mean surface density of the 16 NAVOCEANO sediment coring samples.

The sound attenuation coefficients were calculated from Hamilton (1976) and proved to be the most unreliable of all the acoustic estimates. Assuming that the sound attenuation (dB/m) is linearly proportional to the acoustic frequency (kHz), the proportionality constant k[(2)] is estimated using the sediment porosity and the mean grain size (Matthews et al., 1985). According to Hamilton (1980), the sediment porosity and the mean grain size for silty clay are 75.9% and 8.52 ϕ[(3)], respectively. Similar experiments in deep-water with the same sediment type indicate much lower values for sediment porosity and mean grain size (Mitchell and Focke, 1980).

---

(2) Proportionality constant k: $\alpha = kf^{n}$.

(3) Wentworth scale: $\phi = \log_2 mm = (-\log_{10} mm / \log_{10} 2)$, where mm = grain size in mm.

Matthews et al. chose to use values for sediment porosity and mean grain size between those determined by Hamilton and those values indicated by Mitchell and Focke. Specifically, these values correspond to the lower error bar values of sediment porosity and mean grain size determined by Hamilton (1980). The proportionality constant used for the lower error bar value (8.0 ϕ) is 0.03 dB/m/kHz. This value is used for the Holocene sediment layer.

Both Hamilton (1980) and Mitchell and Focke (1980) have shown that attenuation (for silty clay) increases with depth below the sea floor for several hundred meters. The attenuation profile was determined using Hamilton techniques (1980) and is shown in Table 4. The linear regression equation is as follows:

$$\alpha = 0.030 + 0.0016\,(D) \tag{47}$$

where α is sound attenuation given in dB/m/kHz and D is defined as before.

Table 4 indicates large steep gradients in compressional wave speed (V_p), density (ρ), attenuation (α), and shear speed (V_s) at the Holocene-Pleistocene interface (47.80 m). This sharp interface along with the water-air interface combine to form a well defined waveguide.

The shear wave speed was calculated from Hamilton (1980) using the following regression equation:

$$V_s = \frac{3.884\,(V_p)}{1000} - 5.757 \tag{48}$$

Table 4: GEOACOUSTIC MODEL FOR THE RUBANO EXPERIMENTAL SITE CONDUCTED 8 SEPTEMBER 1985 OFF CORPUS CHRISTI, TEXAS (FROM MATTHEWS ET AL., 1985).

Material	Depth (m)	V_p (m/s)	ρ(g/cm^3)	α^a	V_s (m/s)
Sea Surface	0.00	1544.58	1.0	0.0	0.0
	1.70	1544.58	1.0	0.0	0.0
	2.70	1544.65	1.0	0.0	0.0
	3.40	1544.69	1.0	0.0	0.0
	4.60	1544.72	1.0	0.0	0.0
	5.60	1544.75	1.0	0.0	0.0
	6.70	1544.75	1.0	0.0	0.0
	7.50	1544.74	1.0	0.0	0.0
	8.50	1544.79	1.0	0.0	0.0
	9.70	1544.82	1.0	0.0	0.0
	10.50	1544.85	1.0	0.0	0.0
	11.50	1544.87	1.0	0.0	0.0
	12.80	1544.91	1.0	0.0	0.0
	13.20	1544.92	1.0	0.0	0.0
	14.90	1544.97	1.0	0.0	0.0
	15.60	1544.98	1.0	0.0	0.0
Sea Water	16.60	1545.00	1.0	0.0	0.0
	17.50	1545.04	1.0	0.0	0.0
	18.60	1545.05	1.0	0.0	0.0
	19.50	1545.07	1.0	0.0	0.0
	20.50	1545.09	1.0	0.0	0.0
	21.60	1545.11	1.0	0.0	0.0
	22.80	1545.13	1.0	0.0	0.0
	23.60	1545.16	1.0	0.0	0.0
	24.50	1545.17	1.0	0.0	0.0
	25.60	1545.19	1.0	0.0	0.0
	26.60	1545.20	1.0	0.0	0.0
	27.70	1545.24	1.0	0.0	0.0
	28.40	1545.25	1.0	0.0	0.0
	29.80	1545.29	1.0	0.0	0.0
Water-sediment interface	30.30	1545.30	1.0	0.0	0.0
	30.40	1525.2	1.58	0.030	166.88
	32.80	1519.6	1.57	0.034	145.13
	35.30	1522.9	1.57	0.038	157.94
Holocene silty clay	37.80	1526.1	1.58	0.042	170.37
	40.30	1529.4	1.58	0.046	183.19
	42.80	1532.6	1.58	0.050	195.62
	45.30	1535.9	1.59	0.054	208.44
	47.80	1539.1	1.59	0.058	220.86

[a] α = attenuation coefficient given in dB/m/kHz.

Material	Depth (m)	V_p (m/s)	ρ (g/cm^3)	α^a	V_s (m/s)
Holocene-Pleistocene	47.90	1737.1	1.84	0.288	435.89
boundary	50.30	1741.2	1.84	0.286	437.93
	52.80	1744.7	1.84	0.284	439.69
	55.30	1747.8	1.85	0.282	441.26
	57.80	1750.4	1.85	0.280	442.58
Late Wisconsin very fine	60.30	1752.8	1.85	0.277	443.80
sand	62.80	1755.0	1.86	0.275	444.93
	65.30	1757.0	1.86	0.274	445.96
	70.30	1760.0	1.86	0.270	447.51
	75.30	1763.0	1.87	0.266	449.07
Late Wisconsin	80.30	1766.3	1.87	0.263	450.80
parameters extended to	85.30	1768.7	1.87	0.259	452.06
approximate mid and	90.30	1770.9	1.87	0.256	453.22
early Wisconsin sediments	95.30	1772.9	1.88	0.253	454.28
	100.30	1775.4	1.88	0.250	455.61
	110.30	1780.4	1.88	0.244	458.28
	120.30	1785.4	1.89	0.239	460.98
	130.30	1790.4	1.89	0.234	463.71

where V_s is the shear wave speed in m/s, and V_p is the compressional wave speed in m/s. This equation was used for both the Holocene and the late Wisconsin sedimentary sequences.

b. The Wisconsin Sediment Layer

Matthews et al. (1985) have shown that the late Wisconsin sediment layer is composed of very fine sand. According to Hamilton (1980) this sediment type in shallow water should have a density of 1.77 g/cm^3 and a relative sound speed of 1.080. Hamilton (1976) has shown that the compressional sound speed increases at a rate depending on the nature of the sediment (1976). Matthews et al. (1980) estimated the compressional wave speed at the top of the late Wisconsin sediment layer to be 1737.1 m/s. This

[a] α = attenuation coefficient given in dB/m/kHz.

value was estimated by comparing the lithostatic load corresponding to the Holocene-Pleistocene boundary (17.5 m depth) to a similar lithostatic load at the appropriate depth for the late Wisconsin sediment layer. Table 4 gives values for compressional sound speed calculated from Hamilton (1976) by Matthews et al. using an initial value of 1737.1 m/s as discussed above. The density and sound attenuation were calculated as a function of depth below the sea floor according to Hamilton (1980) using an initial intercept value of 0.177 for density. Equation (48) was used to calculate shear speed (V_s) for the late Wisconsin sedimentary sequence as indicated in the previous section.

C. SOUND SPEED PROFILES AND BATHYMETRY OF THE PROJECT GEMINI TEST SITE AREA

CTD casts were conducted daily during the GEMINI experiment and in some instances twice a day. The acoustic models analyzed in this study utilized the sound speed profiles derived from these casts. Figures 6-8 show the sound speed profiles for the Rubano, deep, and shallow water sites, respectively. Figure 9 presents the bathymetric profiles along the propagation radials at each of the three sites.

A preliminary environmental assessment of the GEMINI area was conducted by Matthews et al. (1985) and preliminary acoustic studies were based on this assessment. This study utilizes the results reported by them but are modified using the in-situ environmental data.

Two weeks prior to the commencement of the experiment, hurricane Elena passed through the Gulf of Mexico which caused the water column to become fairly well-mixed. This is evident in Figure 6 which suggests an

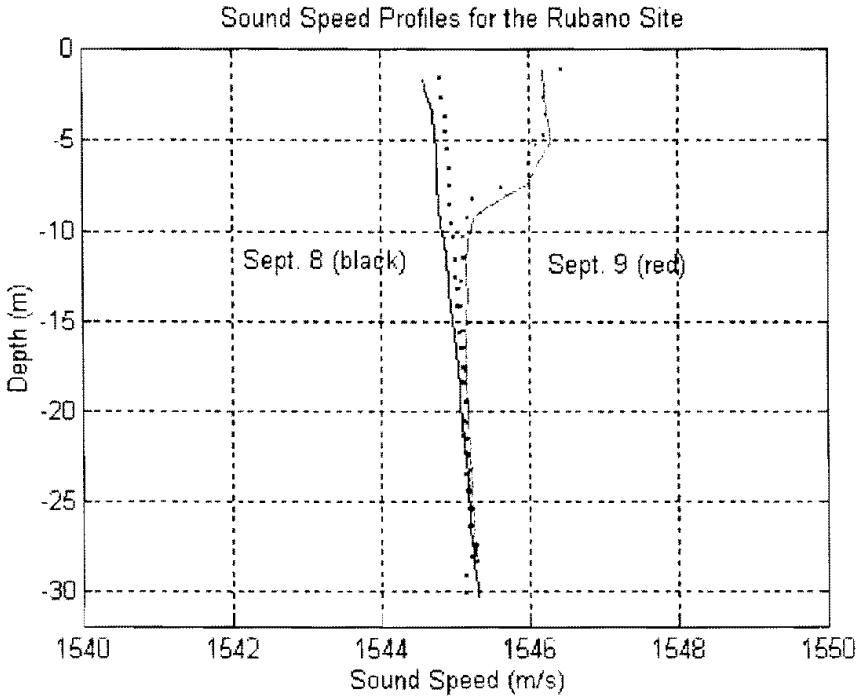

Figure 6: Sound speed profiles for the Rubano site conducted 8 and 9 September 1985. The solid line represents the downcast and the dotted line represents the upcast. The casts were taken 32 hr apart.

essentially isothermal water column to 30 m depth for the 8 September profile. Thirty-two hours later the upper 10 m shows signs of warming (9 September profile). The deep site (Figure 7) shows the presence of isospeed water to approximately 42 m overlying a low speed (low temperature) bottom layer approximately 10 m thick resulting in a thermocline gradient of $-0.789\ s^{-1}$ for the 10 September profile. Two days later the 12 September profile shows a slightly weaker thermocline at 41 m depth. The shallow site (Figure 8) was visited once and only one CTD cast was obtained. The sound

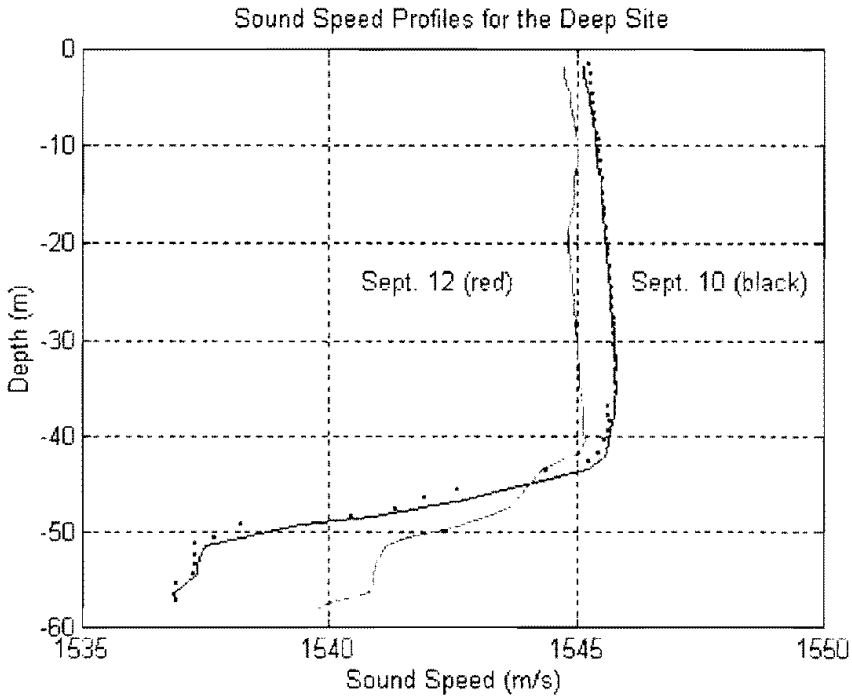

Figure 7: Sound speed profiles for the deep site experiment conducted 10 and 12 September 1985. The solid line represents the downcast and the dotted line represents the upcast. No upcast data were obtained on 12 September. The casts were taken 47 hr apart.

speed profile for the 11 September experiment indicated isothermal conditions over the entire water column (21 m). Bathymetric information was also determined with a high degree of accuracy along each propagation path (Figure 9). It is clear from Figure 5 (Section II B) and Figure 9 that the requirement for a flat, horizontally layered bottom was met. Figure 9 indicates that the bottom is mildly sloping at all three test site areas. The Rubano site had an average bottom slope of 0.0351° for the 8 September experiment and the average bottom slope for the 9 September experiment was 0.0439°.

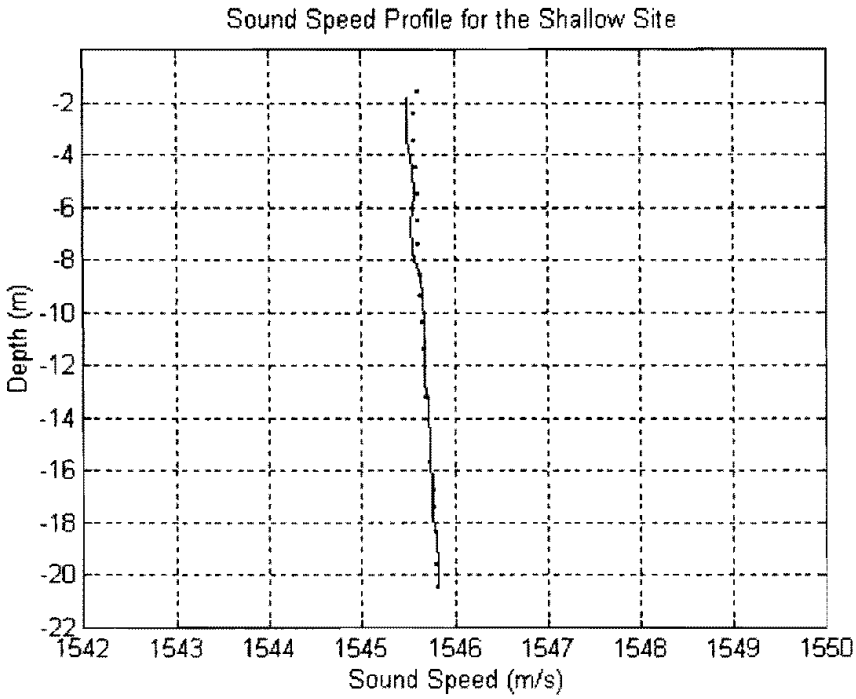

Figure 8: Sound speed profile for the shallow site experiment conducted 11 September 1985 at 1045 CST. The solid line represents the downcast and the dotted line represents the upcast.

The deep water site showed an average bottom slope of 0.0601° for the 10 September experiment and the average bottom slope for 12 September was 0.0542°. The shallow water site showed an average bottom slope of 0.0176°. The bathymetry varies only slightly (i. e., all bottom slopes << 1°) with range.

The SSP's varied each day from site to site but one can assume along a propagation path little change is experienced in SSP (based upon an average of the upper 20 m of all profiles). It is clear that the GEMINI test site area is approximately range-independent.

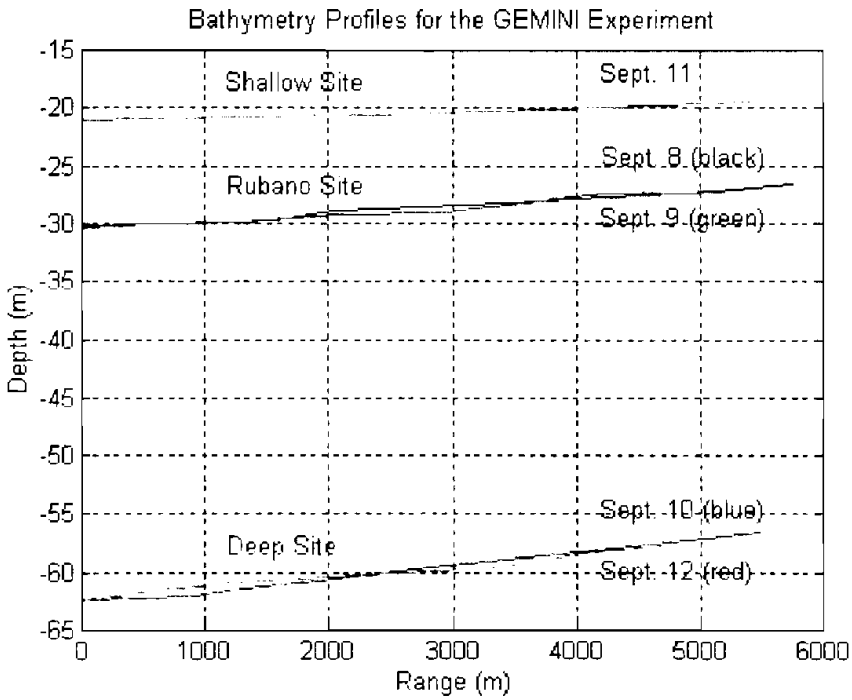

Figure 9: Bathymetry profiles for the three sites visited on 8-12 September 1985.

D. MEASURES OF EFFECTIVENESS (MOE) FOR EVALUATING SHALLOW WATER TL PREDICTIONS

The figure of merit (FOM) approach to estimating detection range in deep water has a clear and useful interpretation and has been widely accepted and long used by the Navy ASW community. As Figure 10 shows, an FOM results in a direct path detection range and the range to one or more convergence zones. There is little or no ambiguity in identifying these detection ranges because fluctuations in the TL curve generally occur in the "shadow zone" between the direct path and CZ due to bottom interactions at TL levels well below realistic FOMs. For an FOM of 70 dB the direct path detection range is approximately 15 km and only 1st CZ detections are permitted (Figure 10a).

In shallow water large fluctuations in TL curves are routinely observed due to frequent, often periodic, interactions with the sea floor. Fluctuations of 10-15 dB, such as experienced in the GEMINI data analyzed in this thesis, occur throughout the typical direct path detection interval causing significant problems in the application of deep water FOM concepts to estimate detection range. This is illustrated in Figure 10b which shows, for an FOM of 65 dB and TL fluctuations on the order of 10 dB to 15 dB, that no clear cut direct path detection range is obvious. Many intersections of the FOM line occur due to the influence of the many multipaths or normal modes interacting with the bottom, sub-bottom, and ocean surface. The modal or interference pattern can be shifted in range or amplitude due to small

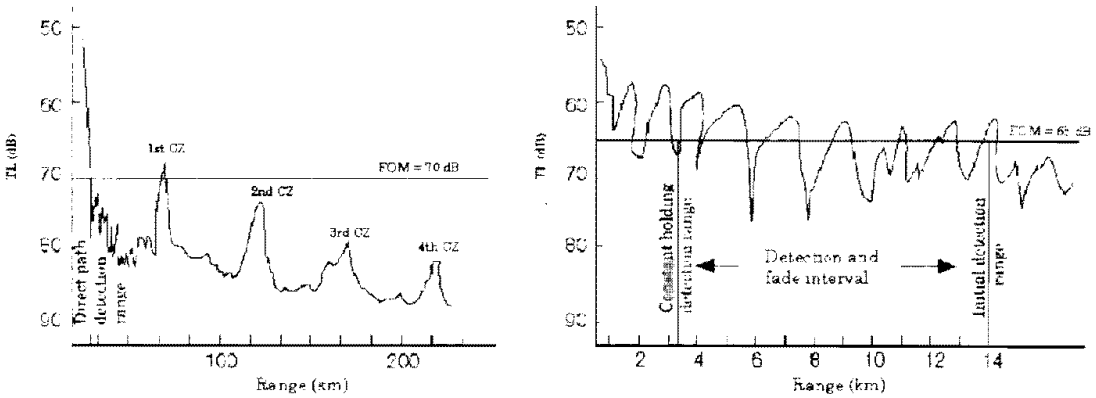

(a) Deep Water (b) Shallow Water

Figure 10: Use of the figure of merit (FOM) for detection range estimation in (a) deep and (b) shallow water.

changes in the sound speed profile, bottom geoacoustic properties and source and receiver position.

Therefore, some MOE is needed in the shallow water case to determine how "well" or "poorly" a model estimate of TL compares with measured data. An ASW approach, rather than a basic TL modeling research approach, is adopted in this thesis due to the thesis objectives. For shallow water situations we propose that the detection range be determined by the reverse of the deep water procedure. That is, imagine the FOM line is drawn from right (long range) to left (short range) on Figure 10 and label the first or longest range at which the TL and FOM line intersect as the "initial detection range." Proceeding farther to the left (towards shorter ranges) on the FOM line, one may encounter a range interval, which can be large compared to the initial detection range, during which the signal fades in and out. For a slow speed ROW diesel in shallow water and a slow speed ASW platform closing upon each other, transitioning through the fade periods can

last a long time (upwards to 30 min or longer). For a submarine in an approach and attack phase or a P-3 in the localization and kill phase of an ASW threat a 30 min period of repeated loss and regain of contact is unacceptable unless the TL fluctuations can be estimated accurately to give the simple message "just keep closing the target/receiver range." Thus, it is desired that for shallow water operations the TL model predict both the "initial detection range and fade interval" (see Figure 10) and estimate the "constant holding detection range" inside which of there are no more signal fades.

Since the objective of this thesis is only to assess the performance of several widely used TL models to simulate the TL measured in the GEMINI experiment and its range independent geoacoustic environment, the FOM approach to detection range estimation in shallow water described above will be used only to guide the selection of MOEs for model TL estimates. For this purpose the following two MOEs are adopted in this thesis:

MOE	Purpose
1. Range averaged TL or "average TL"	Accurate estimates of range averaged TL are necessary to estimate detection range intervals as illustrated in Figure 10.
2. TL fluctuations	Once the range averaged TL has been estimated accurately by a TL model, an accurate estimation of the TL fluctuations about this average will allow assessment of signal fade and holding periods illustrated in Figure 10.

A TL model is not expected to exactly retrace the observed or measured propagation loss without error to be considered as excellent performance.

However, the TL model is expected to agree with the observed TL when both are range averaged (eyeball averages are used in this thesis). As a secondary characteristic, the number and magnitude of TL fluctuations are expected to be modeled accurately. For example, if the measured data demonstrate 12 TL peaks (and nulls) over a given range interval that average 11dB (peak to null) in magnitude and the model estimates 25 TL peaks (and nulls) of 4 dB average peak to null magnitude, then the TL fluctuations are considered to be poorly modeled even though the range averaged TL may be modeled accurately. If there are approximately the same number of peaks with the same average peak to null magnitude in both model and observed data sets, but the fluctuations occur at slightly different ranges, then the TL model is still assessed to perform well for the purposes of this thesis.

III. SHALLOW WATER TL CHARACTERISTICS IN A RANGE INDEPENDENT ENVIRONMENT USING PROJECT GEMINI TL DATA AND ACOUSTIC MODEL ESTIMATES

In deep water the average value of TL at low frequencies and ranges less than 5 km can be approximated by spherical spreading to ranges of a few kilometers followed by cylindrical spreading thereafter. Assuming a range of 2 km for the transition from spherical to cylindrical spreading for purposes of illustration, deep water, short range TL is plotted on Figure 11a. Some characteristics of TL at 140 Hz in the shallow water GEMINI area are also illustrated by Figure 11a. First, the initial spreading loss in shallow water is much less than it is in deep water and overall propagation is far better at short ranges and low frequencies than it is in deep water. Second, although bottom attenuation is greater in shallow water than in deep water, the average TL increase with range is only slightly greater than cylindrical spreading resulting in better overall propagation at low frequencies in the GEMINI area out to 5 km than could be expected in a typical deep water environment. Third, the TL fluctuations with range can be 10 dB to 20 dB and occur at very short range intervals (e.g., 300 m) while deep water fluctuations at short ranges are typically very small.

The impact of the above three contrasting characteristics of shallow and deep water TL can be illustrated in Figure 11a by discussing the impact on detection of a quiet diesel submarine at short ranges. Assuming an FOM of 55 dB, in deep water one could expect a direct path detection range of about 700 m (0.7 km) with no further detection opportunities thereafter unless an unusually strong convergence zone was present near 60 km in range. In

shallow water the situation is significantly different. Multiple detection opportunities are present to 5 km (the limit of measured GEMINI data) and probably beyond, but the very large TL fluctuations due to normal mode interference will cause very short holding periods interspersed among total fade periods at "normal mode nulls." From Figure 11a an FOM of 55 dB would imply constant holding only for ranges less than approximately 750 m (0.75 km), but over 15 short holding periods between 0.75 km and 4.2 km. For a tactical approach with a closing range rate of 6 knots, these 15 holding/ fade periods occur within 20 minutes. To say that this will cause havoc in obtaining a firing control solution is a dramatic understatement, because sonar operators on board most surface and submarine platforms require much longer holding times to obtain target range, course, and speed estimates that are accurate enough to permit weapon launch. It seems obvious that new tactics will need to be developed to exploit shallow water TL characteristics. For example, remaining within the range bin of a "normal mode TL peak" for an extended period (several minutes) of time may be desirable to provide sonar operators enough time to provide accurate target range, course, and speed estimates. Although the objectives of this thesis are not directly related to shallow water tactics, it is emphasized that it is extremely important to model the TL fluctuations in shallow water, as shown in Figure 11a, in order to provide useful input to Navy shallow water tactical development. The deep water concept of 50% probability of detection range is not useful in shallow water areas like the GEMINI exercise area.

To measure the impact of bottom reflection loss and sub-bottom refraction loss in the GEMINI data, a TL curve for an isospeed, perfectly

reflecting bottom at 140 Hz for the Rubano site (30 m depth) is shown on Figure 11a as an optimistic upper bound for TL. The difference between this curve and the observed GEMINI TL curve shows that indeed a significant bottom loss component is present and must be adequately represented in any predictive model.

The preceding discussion has shown that propagation in shallow water is highly variable at low frequencies and, compared to deep water TL, is a balance between reduced spreading loss and increased bottom/sub-bottom losses. The remainder of this section investigates data and model estimates at three shallow water sites that are separated by approximately 12 nm. It was hoped that the Hamilton geoacoustic model, developed for the Rubano site, could be successfully used at the other two sites since the GEMINI area was selected based on its apparent geoacoustically benign (range independent) character. In fact, it was hoped that LFBL could be used to accurately model the GEMINI TL data. However, based on this analysis the TL data was found to be very sensitive to the Hamilton geoacoustic parameters at each site and a major conclusion of this thesis is that site specific Hamilton geoacoustic models are needed for sites as close as 12 km from one another, even in a benign, nearly range independent geoacoustic environment. A follow on study (Null, 1994) is addressing the resultant improvements in TL modeling when site specific geoacoustic models are developed for the three GEMINI sites and the use of inversion theory when detailed geoacoustic information is not available about the shallow water area of interest.

Figure 11b shows that the TL at 50 Hz exhibits less fluctuation than at 140 Hz (Figure 11a) because fewer normal modes are present to contribute to the interference pattern at 50 Hz. The overall rate of loss is slightly greater at 50 Hz than 140 Hz. The isospeed, hard bottom wave guide exhibits no modal interference patterns as at 140 Hz because the 50 Hz is well below the cut off frequency that can efficiently propagate in the 30 m channel.

Acoustic pressure data were collected at the three GEMINI sites from 8-12 September 1985 as previously discussed. The measured TL data were compared to the acoustic model estimates for each individual site visited. The Rubano site was visited on 8 and 9 September. The deep water site (deep relative to the Rubano and shallow water sites) was visited on 10 and 12 September and the shallow water site was visited on 11 September.

The pressure field at the Rubano site was measured at very short ranges from the source (3-12 m) and found to approximate spherical spreading, on the average, at these short ranges. Using this spherical spreading assumption, a pressure magnitude of (3.2654 μPa) was determined at 1 m and this value was used at all three sites. Several measured values at different (but nearby) ranges were used to insure that a normal mode null or peak did not bias the source level estimate. If the level was changed inadvertently during the experiment, there would be a bias between the measured TL data and model estimates. Since no obvious bias was seen in the model/data comparisons, this permitted the source level calculated at the Rubano site to be used at the other sites as well.

In the analysis that follows the TL range fluctuations due to modal interference for each site are also discussed. The WHOI inverse technique TL

results (Frisk et al., 1991) are also presented but the exceptionally good results they obtained were partially a result of moving the measured TL data vertically and "aligning" the TL data with horizontal range shifts to obtain a "best fit." Since this analysis is focused on assessing various TL models for accuracy, absolutely no shifting of the data up or down, left or right was permitted. In the Navy's use of TL models for sonar performance prediction, the model must estimate TL without prior knowledge of how to "shift" the TL estimate. The focus of the discussion will be on assessing the capability of each TL model to estimate the average TL and the TL fluctuations in shallow water at 50 and 140 Hz. The frequency dependence and the receiver depth dependence will be examined for each site individually. For those sites which were visited on two days (i.e., the Rubano and deep sites) the individual measured data TL curves for both days are compared.

A. THE RUBANO SITE

The TL measured on 8 and 9 September 1985 was for both a shallow source (8 September) and a deep source (9 September). The TL data were measured at 50 Hz and 140 Hz using a mid depth receiver (15 m) and a deep, near-bottom receiver (29 m). Table 5 shows the experimental parameters for the experiment conducted at the Rubano site. Due to the difference in source depth, it is not possible to intercompare the results obtained on these two days.

TABLE 5: MEASURED DATA BASE AT RUBANO SITE

Date	SSP	Frequency (Hz)	Source depth (m)	Receiver depth (m)	Water depth (m)
8 Sept. 85	Mixed layer entire depth (see Figure 6)	50	9	15 and 29	30
		140	9	15 and 29	
9 Sept. 85	Surface mixed layer (0-5 m); negative profile (5-10 m); mixed layer (10-30 m); (see Figure 6)	50	23	15 and 29	30
		140	23	15 and 29	

Figures 11-25 show a comparison of measured TL data with the TL model estimates for the GEMINI data collected on 8 and 9 September, 1985. The individual acoustic models are indicated for each figure as well as the individual parameters of each model run. Table 6 gives a brief summary of results.

TABLE 6: SUMMARY OF TL RESULTS AT THE RUBANO SITE

Frequency Dependence of TL Data: 50 Hz vs. 140 Hz	• in general, TL shows little frequency dependence. • large (up to 30 dB) TL fluctuations at 140 Hz due to normal mode interference. More normal modes contributed at 140 Hz. • much smaller TL fluctuations at 50 Hz due to fewer interfering normal modes.
Receiver Depth Dependence of TL Data: 15 m vs. 29 m	• in general, TL showed little receiver depth dependence. • large TL fluctuations (up to 30 dB) at 140 Hz for both shallow and deep receivers (both deep and shallow source). • large TL fluctuations at 50 Hz for shallow receiver (both deep and shallow source). • relatively small TL fluctuations at 50 Hz for deep receiver (both deep and shallow source).
Model Data Comparison	• SNAP by far the most accurate in estimating TL and TL fluctuations. • FEPE estimates of TL fluctuations at 50 Hz poor, good at 140 Hz. • PE estimates of TL fluctuations poor at all frequencies.

1. Frequency Dependence: Shallow Source, Deep Receiver

Figures 11a and 11b show the measured TL data along with the model TL estimates for 140 Hz and 50 Hz on 8 September. For a source depth of 9 m, a large surface decoupling loss was expected at 50 Hz (30 m acoustic wavelength). However, examining both data sets for TL frequency dependence, it is clear that there is only slightly less loss at 140 Hz inside of 3000 m. The reason that no surface decoupling loss is observed is not known, but may be due to the very shallow depth. Surface decoupling loss is observed at 50 Hz at the deep site as will be discussed in the next section.

There are more TL fluctuations at 140 Hz due to more propagating normal modes. The TL fluctuations are not modeled well by PE/LFBL as shown in Figures 12a and 12b. At 50 Hz, FEPE shows virtually no TL fluctuations (Figure 13b) and a possible explanation for this poor performance is the shallow water depth (measured in acoustic wavelengths) at 50 Hz. FEPE may break down as the water depth becomes shallower than one acoustic wavelength. A range step of $\lambda/6$ and a depth step of $\lambda/30$ were used as FEPE inputs. At 140 Hz the FEPE model estimate of TL fluctuations (Figure 13a) correctly shows the approximate number of peaks, but the peaks are out of phase with the TL data. More importantly, FEPE shows 4 dB to 7 dB more loss, on the average, than the measured TL data and the reason for this is unknown. Figures 14a and 14b show the GEMINI TL data and SNAP TL model estimates at 140 Hz and 50 Hz on 8 September. SNAP model TL estimates show excellent agreement at 140 Hz and good agreement at 50 Hz. The SNAP estimates of TL fluctuations at 140 Hz show excellent agreement

but at 50 Hz show approximately 5 dB less loss at TL peaks and the reason for this difference is unknown.

2. Frequency Dependence: Shallow Source, Shallow Receiver

Figures 15, 16, and 17 show TL for the mid-depth receiver and can be compared to Figures 12, 13, and 14 which show TL for the deep receiver. At these frequencies the measured data are remarkably similar in average TL considering the very large fluctuations. Generally, the TL data shown in Figures 11 through 17 have TL values between 55 dB and 65 dB at a range of 2.5 km and 60 dB to 70 dB at 5 km. The TL range slope beyond 2.5 km seems to be approximately 4 dB to 5 dB per doubling of the range, or slightly greater than cylindrical spreading. However, it is emphasized again that the initial spreading loss in typical deep water environments is greater than that in the GEMINI data, and thus, GEMINI TL at 5 km shows better propagation than the typical deep water case in spite of the increased bottom loss. The TL fluctuations are modeled well by SNAP but are not modeled well by FEPE or PE (Figures 15 through 17). As before, the FEPE TL estimates at 50 Hz show little TL fluctuations and are clearly inconsistent with measured TL fluctuations in the data.

3. Frequency Dependence: Deep Source, Deep Receiver

Measured and model TL comparisons when both source and receiver were located near the bottom are shown in Figures 18, 19, and 20. The average TL is approximately 5 dB better for the deep source than for the shallow source TL data discussed in the previous two sections and is probably due to decreased surface decoupling loss at the deep source depth. Little frequency dependence is noted when examining the average TL for the

deep source, but the TL fluctuations are significantly different. The TL fluctuations at 140 Hz are greater in magnitude and frequency of occurrence than the TL fluctuations at 50 Hz. The greater number of interfering normal modes at 140 Hz is the cause of this TL fluctuation difference.

The SNAP model shows excellent agreement in modeling TL fluctuations in the GEMINI data (Figure 20a) at 140 Hz. PE and FEPE show fair agreement in modeling the average TL at 140 Hz but poor agreement in modeling the TL fluctuations at 140 Hz (Figure 18a and 19a). FEPE and SNAP show less loss at 50 Hz than the TL data (Figures 19b and 20b) and PE shows greater loss than the TL data (Figure 18b). FEPE again shows a flat TL curve with range that is not characteristic of the data. The reason for the relatively poor model performance at 50 Hz at this site for the deep source and receiver is not known but could be very sensitive to near bottom sediment geoacoustic model errors.

4. Frequency Dependence: Deep Source, Shallow Receiver

Figures 21, 22, and 23 show a comparison of measured and model TL data on 9 September when the receiver was at mid-depth. Average TL levels were similar at both frequencies with the 50 Hz TL levels being 1 dB to 2 dB better than the 140 Hz TL levels on the average. The overall TL levels were similar to the shallow source levels shown in Figures 12 through 17, but were not as good as the average TL levels shown in Figures 18 through 20. The SNAP estimates provide good agreement in both TL and TL fluctuations at both 50 Hz and 140 Hz (Figures 23a and 23b). FEPE shows good agreement with the TL data at 140 Hz and shows poor agreement with TL fluctuations in the data (Figure 22a and 22b) at 50 Hz. PE shows more loss

than the data at 50 Hz (Figure 21b) and less loss than the data at 140 Hz (Figure 21a).

5. WHOI Narrow-band Modal Inversion Technique

The Woods Hole Oceanographic Institute utilized a narrow-band perturbation theory inversion technique to generate changes to the initial geoacoustic model and to estimate the TL fluctuations along the acoustic path based on the revised geoacoustic model for the GEMINI area (Frisk et al., 1990). Figures 24 and 25 show measured TL data compared with SNAP model TL estimates using the geoacoustic model generated by the WHOI inversion technique (Rajan, 1987). The figures are only given for the experiment conducted on 9 September 1985 at the Rubano site. The SNAP model at 140 Hz (Figure 24a) using the WHOI geoacoustic model generated by the inversion technique estimates lower TL than the data by 3-5 dB. SNAP, using the initial Hamilton geoacoustic model, accurately predicts the TL. Over the 5000 m transmission path the SNAP model (WHOI technique) predicts 23 TL peaks while the SNAP model (initial Hamilton model) predicted 20 peaks (the same number of TL peaks shown by the data). At 50 Hz (Figure 24b) the SNAP model (WHOI geoacoustic model) estimates are 2-3 dB less than the measured TL data, on the average. The SNAP (initial Hamilton geoacoustic model) shows 3-5 dB less loss than the measured TL data. The TL fluctuations for the measured TL data are modeled reasonably well by SNAP with the Hamilton geoacoustic model at 140 Hz and poorly at 50 Hz. The TL fluctuations are also modeled poorly by SNAP with the WHOI geoacoustic model derived from the WHOI inversion technique.

In Figure 25a, both SNAP estimates for average TL show very good agreement with the measured TL data. Over the 5000 m transmission path, of the 18 peaks present in the measured data, SNAP (WHOI geoacoustic model) predicts 23 peaks while SNAP (Hamilton geoacoustic model) predicts 21 peaks. Both SNAP models show fair agreement in their predictions of TL peaks in the measured TL data.

At 50 Hz (Figure 25b), SNAP (WHOI geoacoustic model) predicted average TL 3-5 dB greater (more loss) than the measured TL data. SNAP (Hamilton geoacoustic model) predicted 3-5 dB less loss, on the average, than the measured TL data. SNAP (WHOI geoacoustic model) predicted 13 of the 11 TL peaks present in the data while SNAP (Hamilton model) predicted 15 peaks. Both SNAP models show only fair agreement in their predictions of the measured TL modal fluctuations. SNAP (with the Hamilton geoacoustic model) performed equally as well as SNAP with the WHOI geoacoustic model when considering TL and TL fluctuations. Thus, if one is not allowed to shift the data or model estimates up or down, left or right, the WHOI inversion technique does not seem to improve performance with the SNAP model as it interferes with the Hamilton geoacoustic model currently.

The WHOI inversion technique (Frisk et al., 1990) showed much better results in their paper than presented above in Figures 24 and 25 not only because of shifting model TL estimates up/down or left/right but because the SNAP linear interpolation between discrete sub-bottom geoacoustic layers in the Hamilton model was changed to a "stairstep" model with no interpolation. In other words, the SNAP model was changed by WHOI so that geoacoustic parameters within each layer of the sub-bottom are constant.

Also, WHOI obtained excellent results by using SAFARI instead of SNAP (Rajan, private correspondence, 1994).

Since the objective of this analysis is to evaluate SNAP and other models as they exist, no attempt was made to change any model. The major weakness in changing model parameters (i.e., the model estimate level, the shift in range, and the SNAP geoacoustic model interpolation) at one time, is that it is very difficult to quantify the impact of each parameter separately. It is highly recommended in future research on shallow water TL that the source levels remain constant to eliminate the necessity of shifting SNAP TL model estimates in level, before adjusting the SNAP geoacoustic sub-bottom interpolation technique.

B. THE DEEP WATER SITE

Data were measured at the deep water site on 10 and 12 September. The experimental framework remained the same as that used for the Rubano site. The source depth was 46 m on 10 September and 9 m on 12 September.

The Rubano site geoacoustic characteristics discussed previously in Section II B were used as model inputs at the deep site. Use of the same Hamilton geoacoustic model was hoped to be possible because the two sites were only 12 nm apart in a shallow water region previously identified by Matthews et al. (1985) to be range independent or "geoacoustically benign." However, it now has been determined (Null, 1994) that the geoacoustic conditions were only superficially range independent and the TL results from the deep and shallow sites clearly show the need to calculate Hamilton geoacoustic bottom parameters at least every 10 nm. This is not a welcomed consideration for the Navy's need to establish a useful global geoacoustic

shallow water data base from which accurate TL model estimates can be made but it appears to be a requirement. This conclusion is analogous to the requirement for high resolution horizontal sampling of sound speed profiles across an oceanographic front. The TL results from Null's study demonstrates that Hamilton geoacoustic models can not be used at other close by locations without a thorough analysis at the new site, even for distances as small as 12 nm in seemingly benign geoacoustic environments. Despite this new finding, the Hamilton geoacoustic model, as derived for the Rubano site, was used as model input for the deep water site as no additional geoacoustic data are available. Table 7 lists experimental parameters for the deep site.

1. Frequency Dependence: Deep and Shallow Source

Figures 26 through 31 compare the measured and modeled TL plots for the deep source (10 September) for both 140 Hz and 50 Hz runs. Figures 32 through 37 show similar plots except for the shallow source (12 September). These comparisons show that there is a much greater (3 dB to 7 dB) TL loss, on the average, at 50 Hz than at 140 Hz for the shallow (9 m) source (Figures 32 through 37). This increased loss is most likely due to surface decoupling (image interference) related to the shallow source. At 50 Hz the acoustic wavelength is approximately 30 m and the 9 m source is well within one acoustic wavelength of the surface. The deep source/deep receiver TL plots in Figures 26 through 28 also show significantly more loss at 50 Hz than at 140 Hz. However, the 50 Hz measured data for the deep source and receiver are only available out to a range of 2 km and this lack of data is

TABLE 7: MEASURED DATA BASE AT THE DEEP SITE.

Date	SSP	Frequency (Hz)	Source depth (m)	Receiver depth (m)	Water depth (m)
10 Sept. 85	Mixed layer from surface to 42 m with negative SSP to bottom. (see Figure 7)	50	46	32 and 61	62
		140	46	32 and 61	
12 Sept. 85	Very similar to 10 Sept. 1985 SSP but less negative profile below 42 m. (See Figure 7)	50	9	32 and 61	62
		140	9	32 and 61	

most likely due to the data being lost during the actual experiment or possibly lost during the initial treatment of the data. As a result, the data may be of poor quality.

The TL model/data comparison at 50 Hz for the deep source (Figures 26b, 27b, 28b, 29b, 30b, and 31b) shows poor agreement for all models at both receiver depths. The models all perform better at 140 Hz for the deep source and both mid-column and deep receivers (Figures 26a, 27a, 28a, 29a, 30a, and 31a). The fact that all the 50 Hz model estimates show less loss than the measured data indicates that the geoacoustic model developed at the Rubano site is overly optimistic in portraying the bottom loss experienced at the deep site. When the improved geoacoustic model developed by Null (1994) is used, some slight improvement is noted at 50 Hz at the deep site for FEPE (compare Figures 38b and 30b) and SNAP (compare Figures 38b and 31b). Much more improvement in TL model accuracy was observed at the shallow site discussed in the next section when the improved Null geoacoustic model was used. The reason why the models

do not estimate the deep nulls at 50 Hz (Figures 30b, 31b, and 38b) is unknown at this time.

Figures 32-37 show the measured TL data for the shallow source compared with the model estimates for both receiver depths and both frequencies (see Table 7). Again the poor agreement between the TL models and data at 50 Hz suggests the need for a site specific geoacoustic model. At 140 Hz the TL models show only a slight improvement in estimating average TL and TL fluctuations. One is lead to believe this discrepancy is related to imperfect knowledge of the bottom loss parameters as the geoacoustic model derived for conditions at the Rubano site produced accurate TL results (especially SNAP) at both frequencies at the Rubano site. That this is the case may be proved by examining Figure 39b taken from Null (1994) which shows much improved TL at 50 Hz for the shallow source when the deep site-specific Hamilton geoacoustic model is used.

The TL data for the shallow receiver (deep and shallow source) at 50 Hz (Figures 29b, 30b, 31b, 35b, 36b, and 37b) show very large TL fluctuations. For example, Figure 31b shows the fluctuations at 50 Hz to be > 20 dB. These fluctuations are due possibly to interfering normal modes in the deeper water (62 m) at this site. The TL fluctuations at 50 Hz also were very wide (> 1000 m) in range. The 140 Hz run (Figure 31a) also showed large (> 20 dB) TL fluctuations with, as expected, more interfering normal modes than in the 50 Hz case. Differences in the 50 Hz and 140 Hz average TL was difficult to estimate due to the very large TL fluctuations. In general, the models did poorly in estimating the large 50 Hz TL fluctuations for the mid-column receiver even with the improved geoacoustic model (Null, 1994).

2. Receiver Depth Dependence: Deep and Shallow Source

Figures 26 through 37 show measured TL curves for both the deep and shallow receiver depths for both frequencies and source depths (see Table 7). Little or no difference is noted in the measured data for a shallow (Figures 29a and 35a) or deep (Figures 26a and 32a) receiver at 140 Hz. Little or no difference in TL is also observed at 50 Hz (Figures 26b, 29b, 32b, and 35b) at either receiver depth. This lack of receiver depth dependence is also reflected in the TL model estimates. Comparing TL model estimates for both receiver depths (compare Figures 26 and 29, 27 and 30, 28 and 31, 32 and 35, 33 and 36, 34 and 37) shows no evidence of receiver depth dependence in the models.

3. Summary of Results for the Deep Water Site

The poor agreement between the TL models and data at 50 Hz suggests the need for a site specific geoacoustic model. This is also true at 140 Hz where the TL models show only a slight improvement in estimating average TL and TL fluctuations. Source decoupling loss was evident at 50 Hz for the shallow source (9 m) and this decoupling was most likely due to the fact that at 50 Hz the acoustic wavelength was approximately 30 m and the 9 m source was well within one acoustic wavelength of the surface.

The lack of a site-specific geoacoustic model at the deep water site is likely the principle cause of the inaccuracy in estimating TL. When the improved geoacoustic model developed by Null (1994) was used, slight improvement was noted at 50 Hz at the deep site for FEPE and SNAP and a significant improvement was noted at 50 Hz for the shallow receiver for both deep and shallow source depths.

The geoacoustic model derived for conditions at the Rubano site produced accurate TL results (especially SNAP) at both frequencies at the Rubano site. However, its use at the deep site resulted in inaccurate TL estimates at 50 Hz in both average TL and TL fluctuations and also at 140 Hz to a lesser extent.

The Hamilton geoacoustic model may not be the only factor causing the inaccuracy in the models. The models performed much better in predicting TL at the Rubano site when the site-specific geoacoustic model was used along with isothermal water conditions. The SSP at the Rubano site showed isothermal water conditions (Figure 6) on 8 September and nearly isothermal conditions on 9 September (Figure 6). The SSP for 10 and 12 September (Figure 7) were completely different because both days showed a mixed layer from the surface to approximately 42 m in depth with negative SSP to the bottom. The SSP was incorporated into the geoacoustic model and the affect of the variability of the SSP is evident in the model results. The extent to which either the SSP and the geoacoustic model affects the propagation path is uncertain. The SSP was most likely range-dependent but the analysis was conducted using one profile, determined at one location, and applied to the entire water column.

C. THE SHALLOW WATER SITE

The shallow water site, so called because of it's 21 m water depth, was visited on 11 September. The source depth for this experiment was 9 m and the receiver depths were 20 m and 16 m. Figures 40 through 45 show measured TL plots along with the individual model estimates. There is less loss (~ 3 dB to 7 dB), on the average, at 140 Hz than at 50 Hz because the

water depth is much less than one acoustic wavelength at 50 Hz (~ 30 m). Thus, propagation at 50 Hz is effectively "cut off" (i.e., no propagating normal modes) by the shallow water wave guide.

The SNAP and PE models show good agreement in estimating the average TL, at both frequencies, but show only fair agreement in modeling the TL fluctuations. The FEPE model estimates were especially poor at 140 Hz showing 10 dB to 20 dB more loss, beyond 2.5 km. The SNAP plots show the best overall agreement with the measured average TL and TL fluctuations (Figures 42 and 45). However, at 50 Hz the SNAP curves underestimate the measured loss for ranges greater than 2.5 km. An improved geoacoustic model is not yet available at the shallow site to determine if an inaccurate representation of the bottom interaction is the cause of the SNAP model/data differences beyond 2.5 km.

In general, SNAP performs better at this shallow site than at the deep site previously discussed, but again the estimates of the TL fluctuations are poor. Both the 8 Sept. Rubano site and the shallow site had isothermal water conditions (see Figures 6 and 8). Since the shallow site depth is only 9 m shallower than the Rubano site and, assuming the bottom sedimentary sequences are similar, it is reasonable to assume that the measured TL data for both sites should be similar. Thus, SNAP TL estimates are expected to be accurate at the shallow site.

Figures 46 and 47 show a comparison of the TL curves measured at the Rubano site on 8 September and at the shallow site on 11 September. It is clear from these figures that the average TL levels are similar but the TL fluctuations vary considerably between these two sites. The fact that SNAP

TL estimates of TL fluctuations are excellent at the Rubano site but poorer at the shallow site implies that a site-specific Hamilton geoacoustic model is needed at the shallow site to improve SNAP's performance. The poor performance of FEPE at 50 Hz at the Rubano and shallow sites, and improved performance at the deep site, implies that there may be something fundamentally wrong with FEPE in water depths less than one acoustic wavelength.

Another possibility for FEPE's poor performance at both the Rubano and shallow sites at 50 Hz was recently discovered by Null (1994) where his preliminary geoacoustic model showed a 5 m sedimentary layer as opposed to a 17 m sedimentary layer as derived at the Rubano site. This appears to make an enormous difference in both the SNAP and FEPE TL model estimates as shown in Figure 48. If this is the case, it completely reverses the poor FEPE performance and good SNAP performance for this shallow water site. If this preliminary geoacoustic model proves to be accurate, the major issues change to (a) Why does SNAP show so much less TL loss than the data at 50 Hz ? and (b) Why don't SNAP and FEPE agree more closely at 50 Hz ?

D. DISCUSSION OF RESULTS

When examining frequency dependence at the Rubano site, it was found that little difference was noted in the overall transmission loss plots at 50 Hz and 140 Hz. More TL fluctuations were present in the measured TL plots at 140 Hz than at 50 Hz as more normal modes were present at 140 Hz to contribute to the interference pattern. Also, little receiver depth dependence was noted with the TL being similar for both mid-water column and near bottom receivers.

The PE model TL estimates were poor at all frequencies and all source/receiver depth combinations. It is believed that this is a result of the LFBL geoacoustic model which was used to calculate the bottom interaction in the PE model. The problem evidently resides in the construction of bottom loss in the LFBL pre-processor (Holland, 1992). Holland has proposed a "fix" to the problem, consisting of modifying LFBL by using a plane wave model for bottom loss. The current concept of a point source-point receiver model of bottom loss, employed by LFBL, is believed to be flawed. The implementation of the more robust plane wave model will significantly improves PE's poor performance at low frequency and in shallow water.

FEPE showed virtually no TL fluctuations at 50 Hz at the Rubano site. At the two shallow water sites the FEPE results were also poor demonstrating 10 dB to 20 dB more loss than the measured TL data. This is in contrast to the deep water site where much closer agreement between FEPE and measured TL occurred. No such problem existed at 140 Hz. This implies that there may be something fundamentally wrong with FEPE when used in water depths less than one acoustic wavelength. SNAP was by far the most accurate in estimating TL and TL fluctuations when the site-specific geoacoustic model was used. This was expected since SNAP, being a normal mode acoustic propagation model, provides a complete solution to the wave equation and not an approximate solution characteristic of both PE and FEPE.

When the Rubano site-specific Hamilton geoacoustic model was used for the deep water site, a noticeable difference in model estimates was observed (compare Figures 14a and 28a). As at the Rubano site, little frequency and

receiver depth dependence were noted. As before, PE performed poorly in estimating TL and TL fluctuations at all frequencies. In general, FEPE model estimates were worse than for the Rubano site as were the SNAP model estimates. This poor agreement between the TL models and the measured propagation data at 50 Hz, and to a lesser degree at 140 Hz, suggests the need for a site-specific geoacoustic model. Indeed, a slight improvement was noted when an improved range-dependent geoacoustic model developed by Null (1994) was incorporated. Another possibility for the inaccuracy may lie in the variability of the model estimates caused by the SSP's for the deep site. At both the Rubano site and the shallow site the water conditions were isothermal. This was not the case at the deep site where the SSP's showed a mixed layer from the surface to a depth of approximately 42 m with a slight negative SSP extending to the bottom. No other SSP observations were made at this site to ascertain whether the SSP varied along the propagation path. The extent to which the use of a single SSP or the non site-specific geoacoustic model affects the model results is uncertain.

A shallow water site was examined where the water depth was 9 m less than at the Rubano site and the water conditions were the same (i.e., isothermal). The original assumption of using the initial Hamilton geoacoustic model, derived for the Rubano site, and extending it to the other two sites, was that the entire study area was geoacoustically similar. Making this assumption, it was reasonable to assume that the measured TL at the Rubano site would resemble that at the shallow site. This appeared to be true in terms of average TL but the TL fluctuations at the two sites were found to

vary considerably. The measured data showed less loss at 140 Hz than at 50 Hz because the water depth was much less than one acoustic wavelength at 50 Hz (~30 m). Propagation at 50 Hz was effectively "cut off."

As at the Rubano and deep water sites, PE showed poor agreement in modeling TL and TL fluctuations at both frequencies. In general, FEPE and SNAP performed better at this shallow site than at the deep site previously discussed, but estimates of the TL fluctuations were poor. A possible explanation is that the sedimentary layer at the shallow water site is 5 m instead of the 17 m sedimentary layer used in the Rubano geoacoustic model (Null, 1994). Null showed that when using a geoacoustic model with an initial sedimentary sequence of 5 m rather than 17 m, FEPE performs well in its prediction of TL and SNAP shows much less loss than the data.

The assumption that the GEMINI area was geoacoustically "benign" or range-independent implies that the geoacoustic model developed for the Rubano site could be used for the other two sites with confidence. Since the models fit the measured data reasonably well for the Rubano site and poorly for the deep and shallow sites, it is reasonable to believe that this assumption of a range-independent geoacoustic environment was inappropriate. A seismic model of the sub-bottom layers that "look" flat and range-independent may not be acoustically benign as far as the normal mode interference patterns are concerned. Future work (Null, 1994) will address the derivation of the site-specific Hamilton geoacoustic models for the deep and shallow sites already discussed. Initial results indicate small changes in the geoacoustic model inputs can result in large changes in the TL estimates of SNAP and FEPE. Because the model estimates were far more accurate at

the Rubano site where a site specific geoacoustic model existed, it is speculated that the relatively poor performance at the deep water site may be due to lack of a site specific Hamilton geoacoustic model. In virtually all cases, the PE model, utilizing the LFBL database for its geoacoustic model, performed poorly in its estimation of average TL values and TL fluctuations. The FEPE model was run with a full Hamilton geoacoustic model as input and was much more accurate than PE in predicting average TL and TL fluctuations. The normal mode model, SNAP, which also used a full Hamilton geoacoustic model, was the most accurate in modeling average TL and TL fluctuations. A major unanswered question is why SNAP and FEPE do not agree well with one another as anticipated from a recent workshop on acoustic modeling (Chin-Bing et al., 1992). The answer may be that the synthetic geoacoustic data used in the workshop did not contain the steep gradients observed in the measured geoacoustic data from GEMINI.

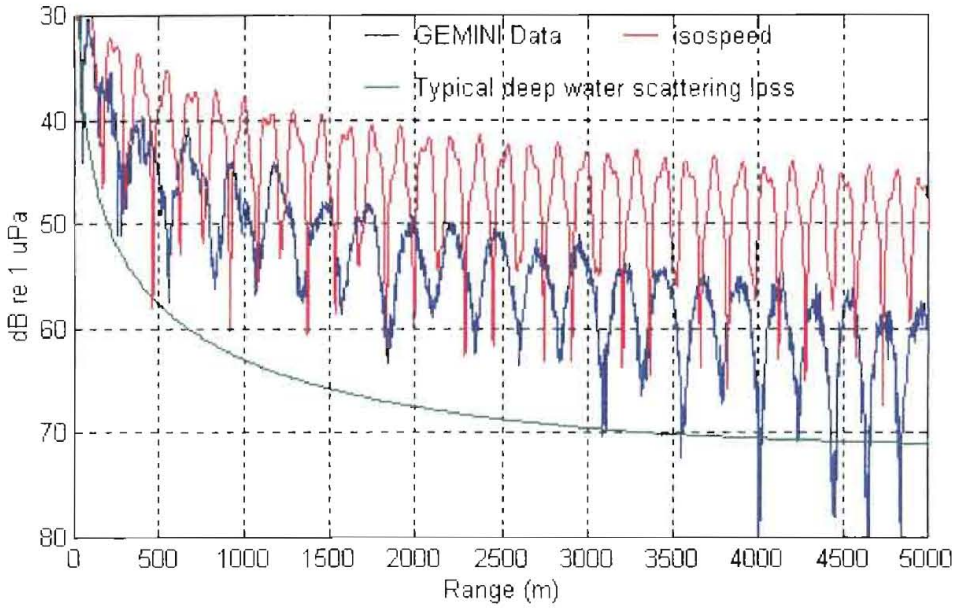

(a)

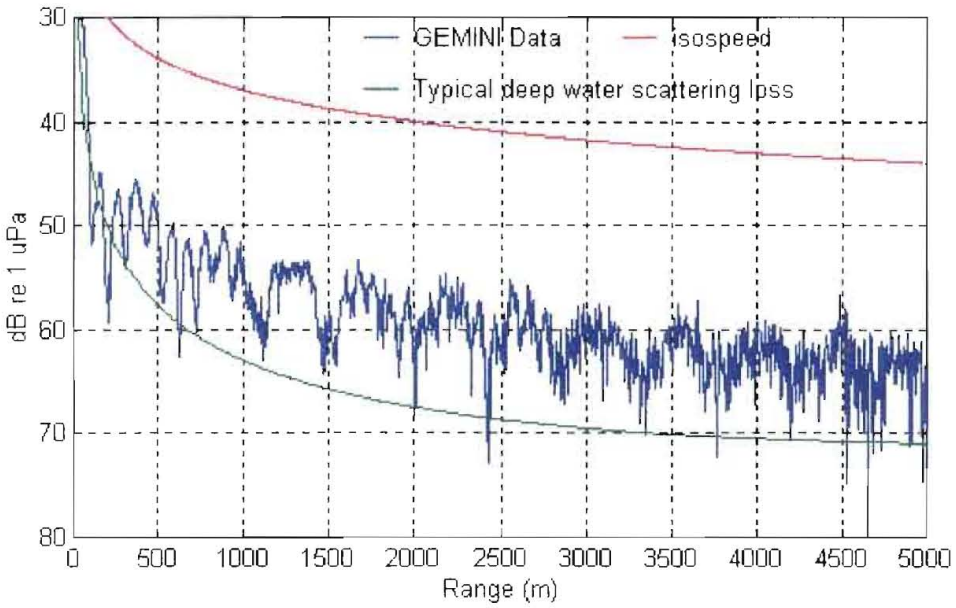

(b)

Figure 11: Plot of GEMINI data versus isospeed model. Source depth: 9 m, receiver depth: 29 m, water depth: 30 m, frequency: 140 Hz (a), 50 Hz (b).

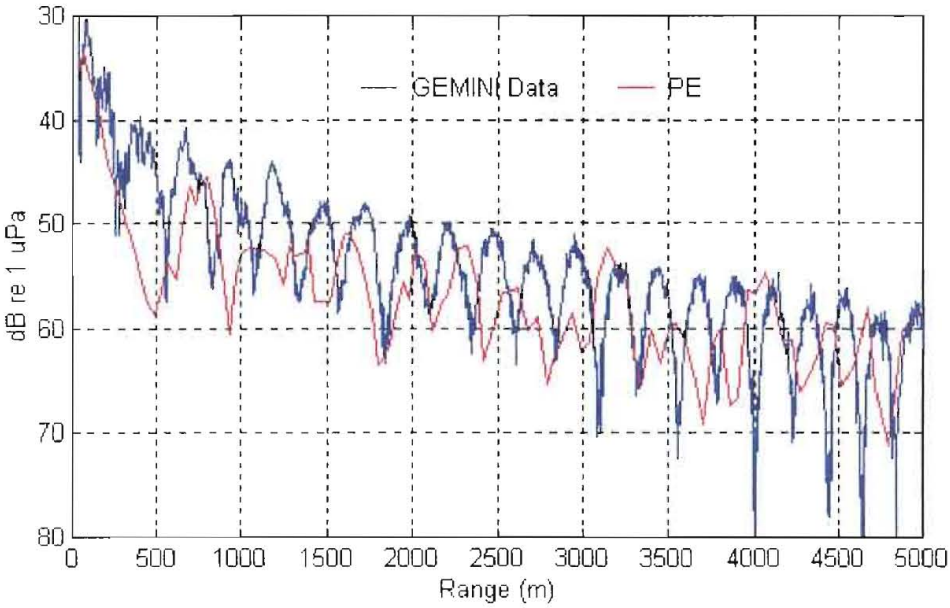

(a)

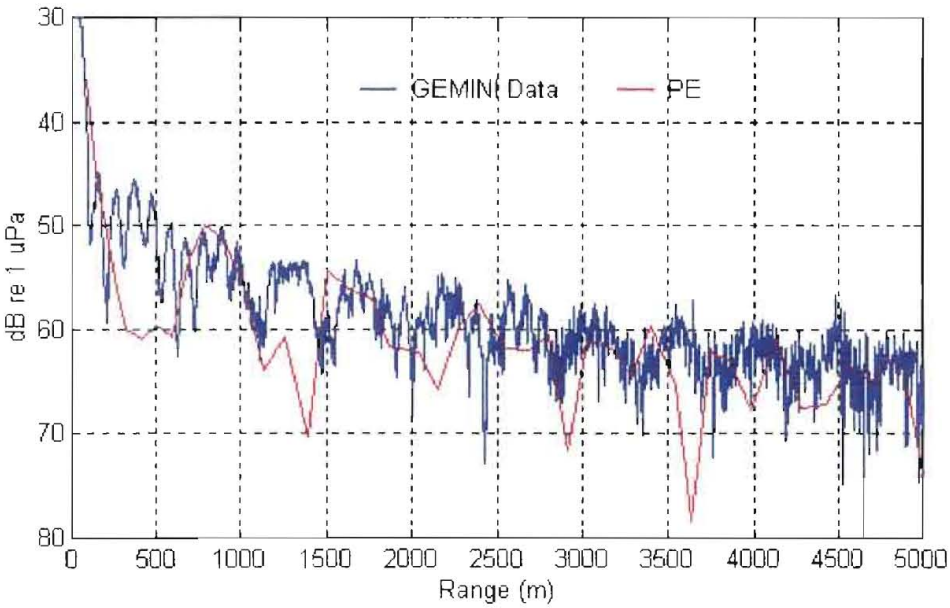

(b)

Figure 12: Plot of GEMINI data versus PE model. Source depth: 9 m, receiver depth: 29 m, water depth: 30 m, frequency: 140 Hz (a), 50 Hz (b).

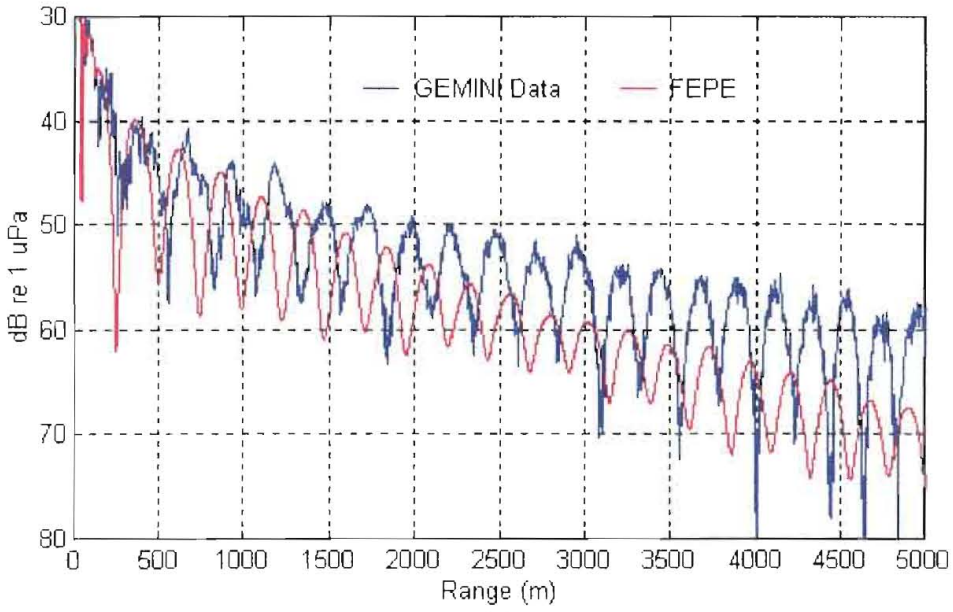

(a)

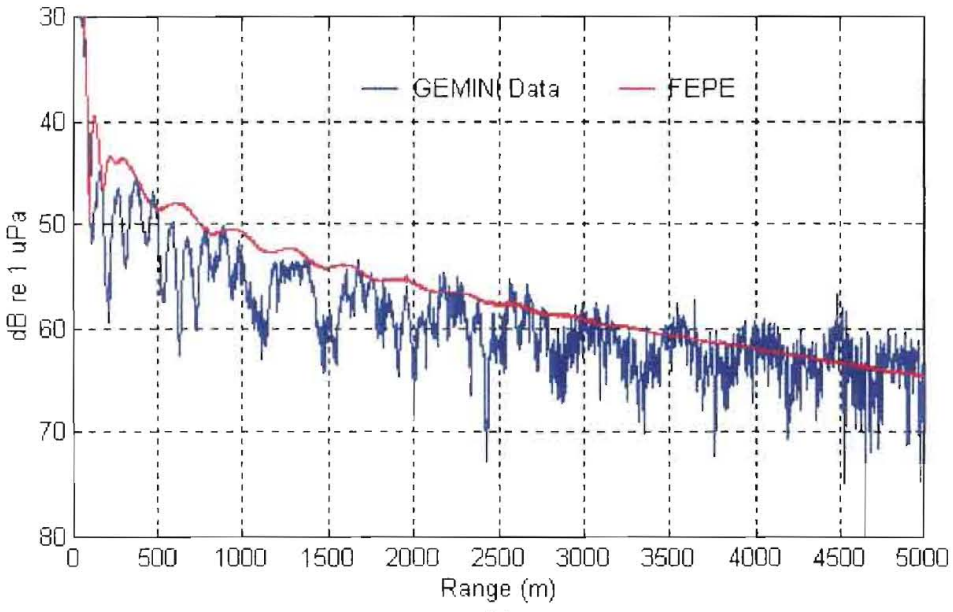

(b)

Figure 13: Plot of GEMINI data versus FEPE model. Source depth: 9 m, receiver depth: 29 m, water depth: 30 m, frequency: 140 Hz (a), 50 Hz (b).

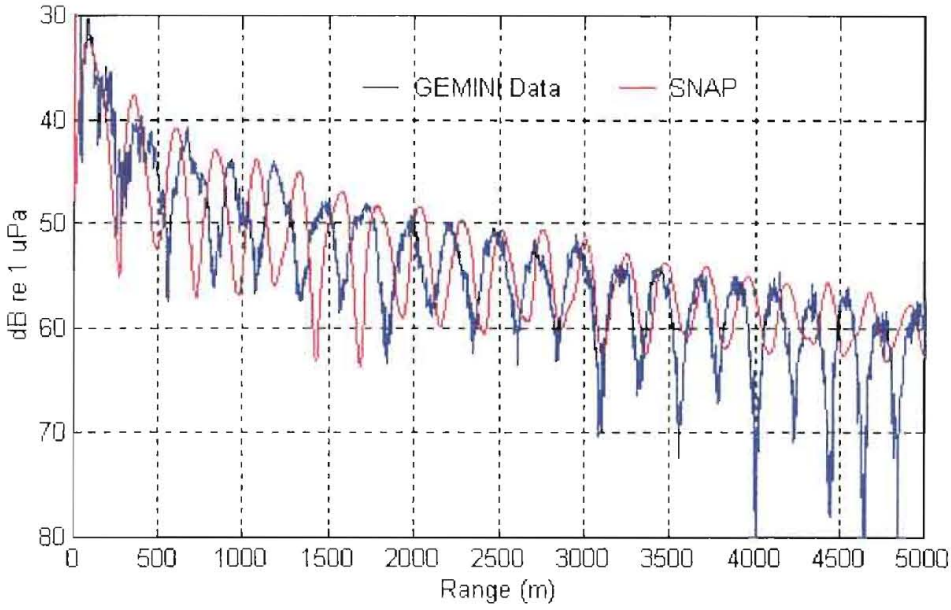

(a)

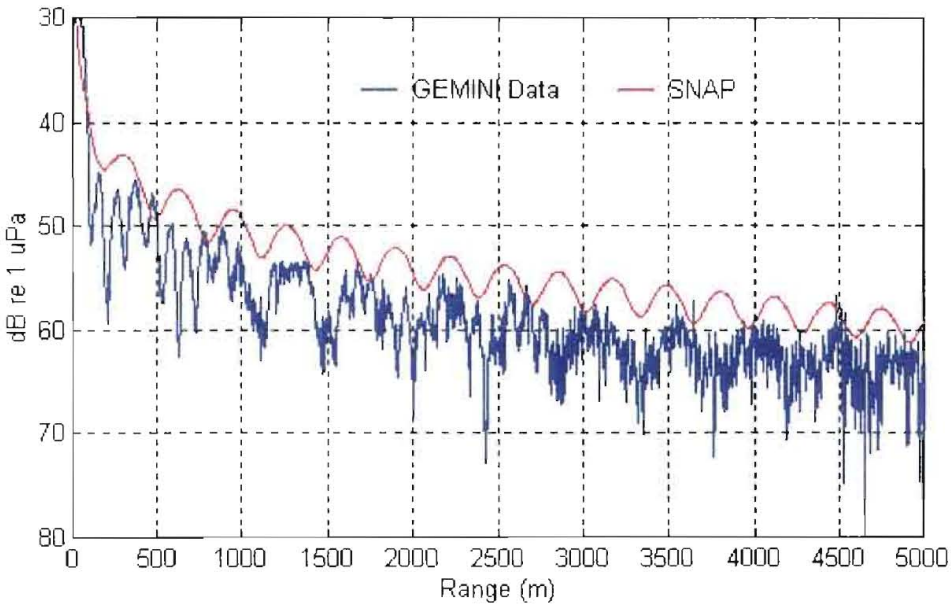

(b)

Figure 14: Plot of GEMINI data versus SNAP model. Source depth: 9 m, receiver depth: 29 m, water depth: 30 m, frequency: 140 Hz (a), 50 Hz (b).

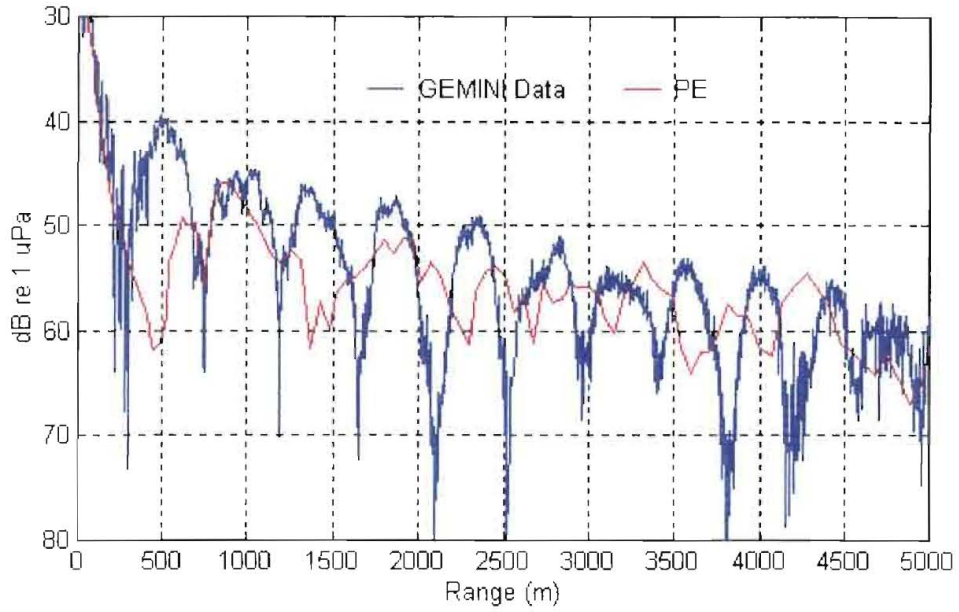

(a)

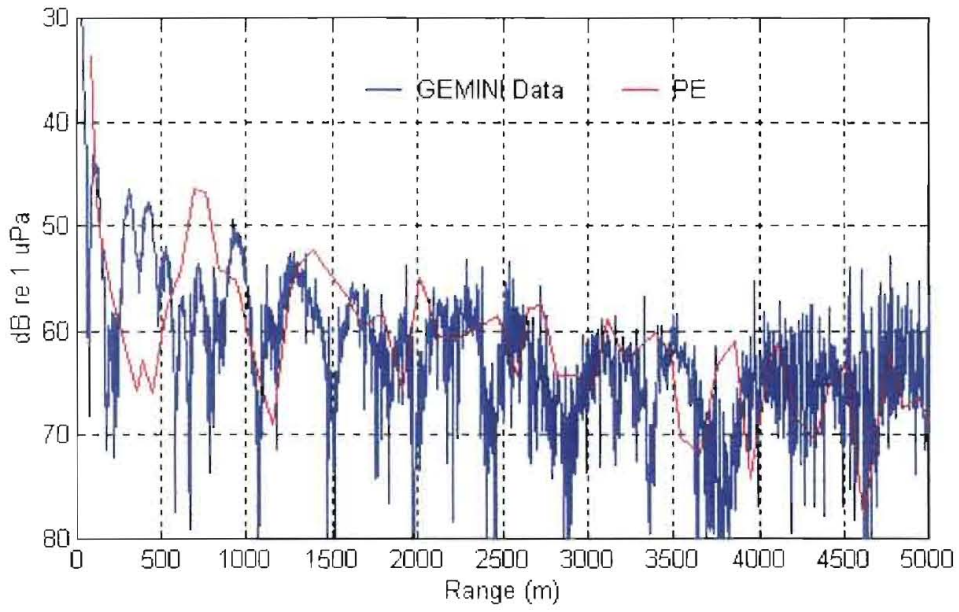

(b)

Figure 15: Plot of GEMINI data versus PE model. Source depth: 9 m, receiver depth: 29 m, water depth: 30 m, frequency: 140 Hz (a), 50 Hz (b).

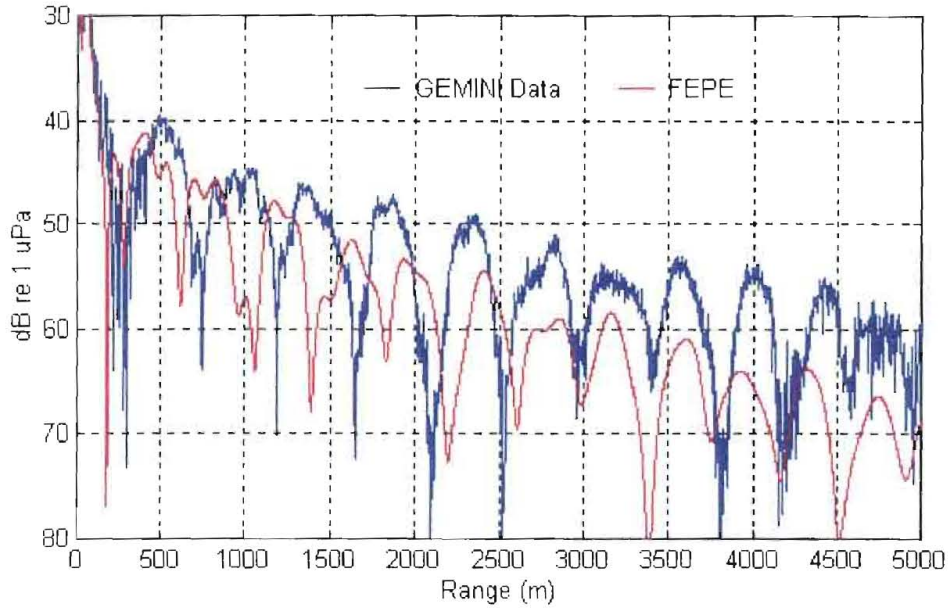

(a)

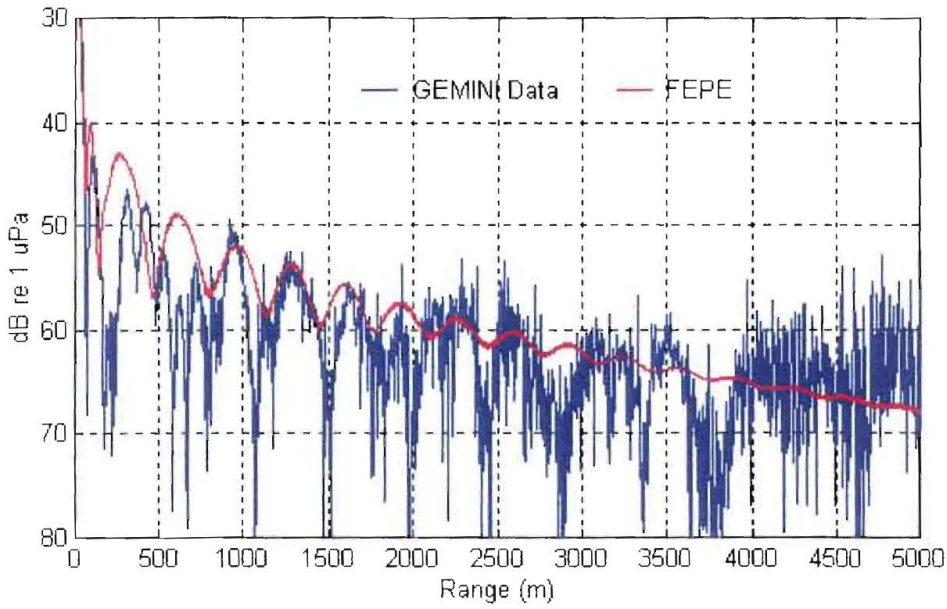

(b)

Figure 16: Plot of GEMINI data versus FEPE model. Source depth: 9 m, receiver depth: 29 m, water depth: 30 m, frequency: 140 Hz (a), 50 Hz (b).

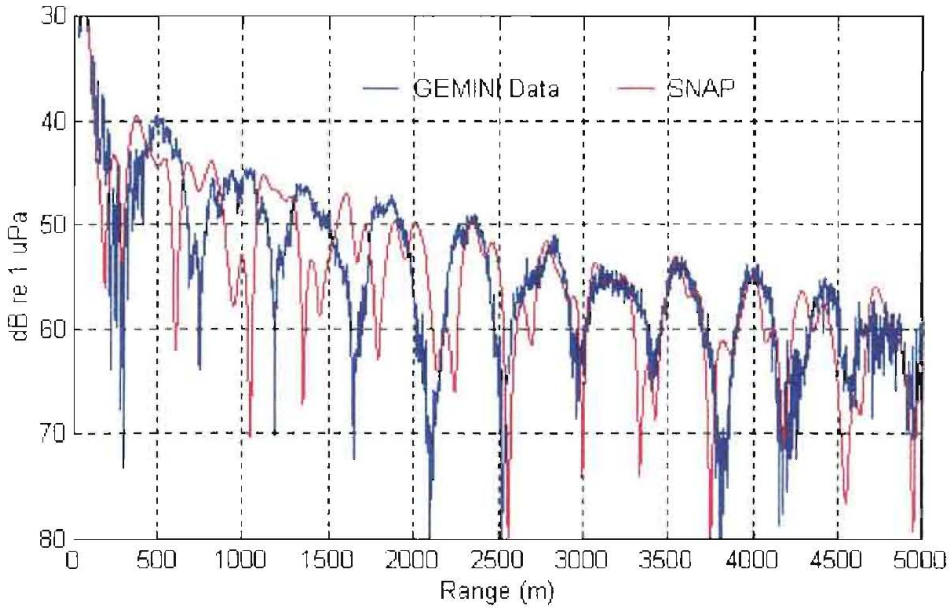

(a)

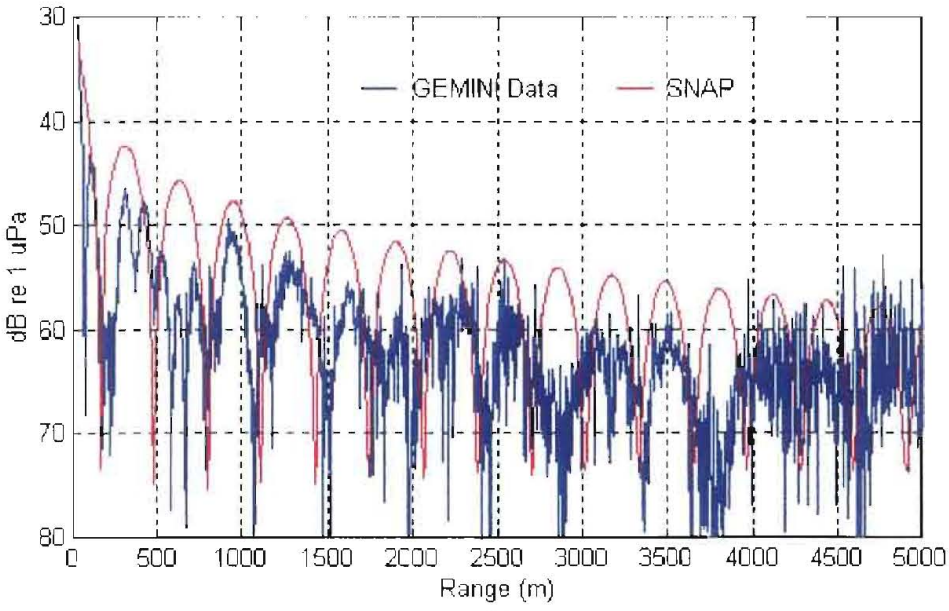

(b)

Figure 17: Plot of GEMINI data versus SNAP model. Source depth: 9 m, receiver depth: 29 m, water depth: 30 m, frequency: 140 Hz (a), 50 Hz (b).

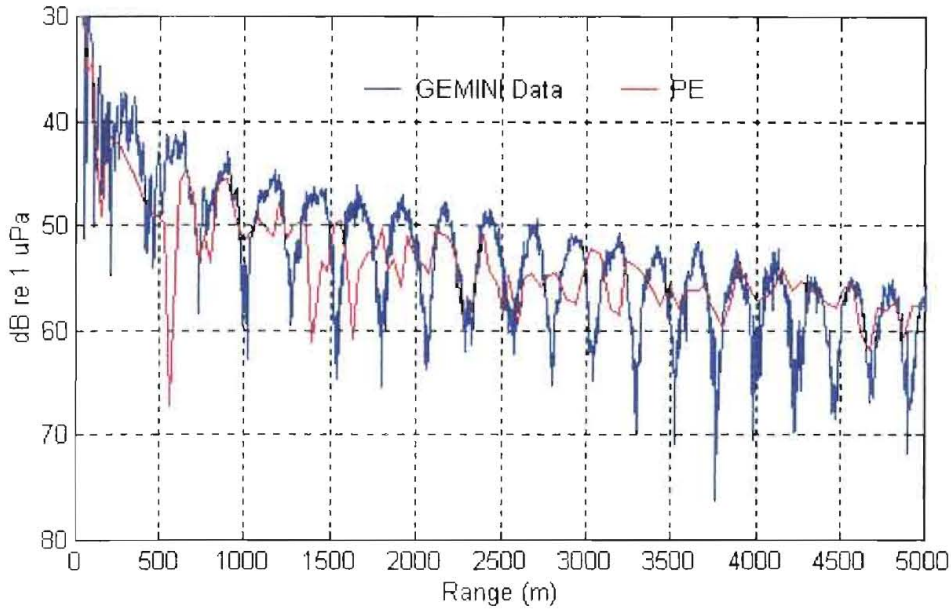

(a)

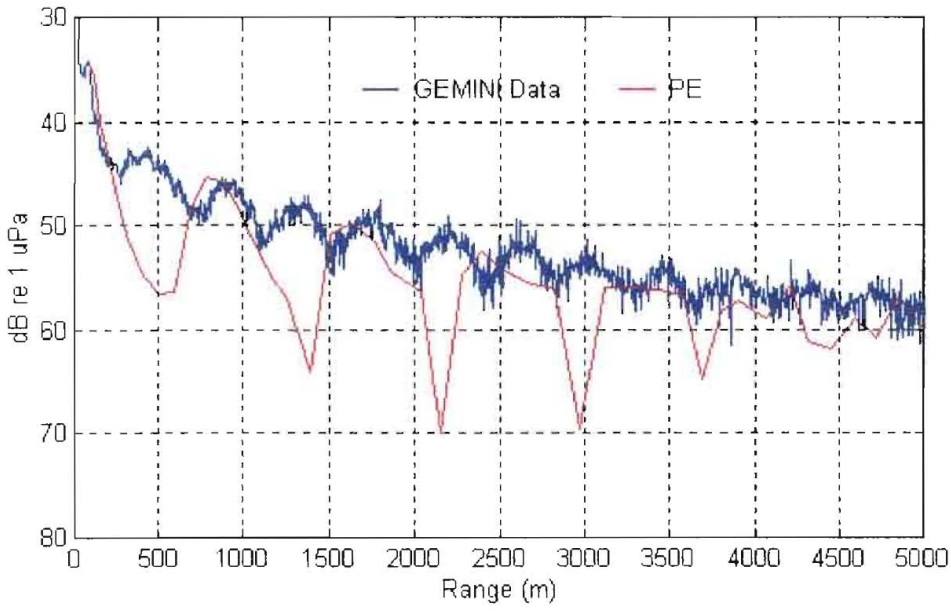

(b)

Figure 18: Plot of GEMINI data versus PE model. Source depth: 9 m, receiver depth: 29 m, water depth: 30 m, frequency: 140 Hz (a), 50 Hz (b).

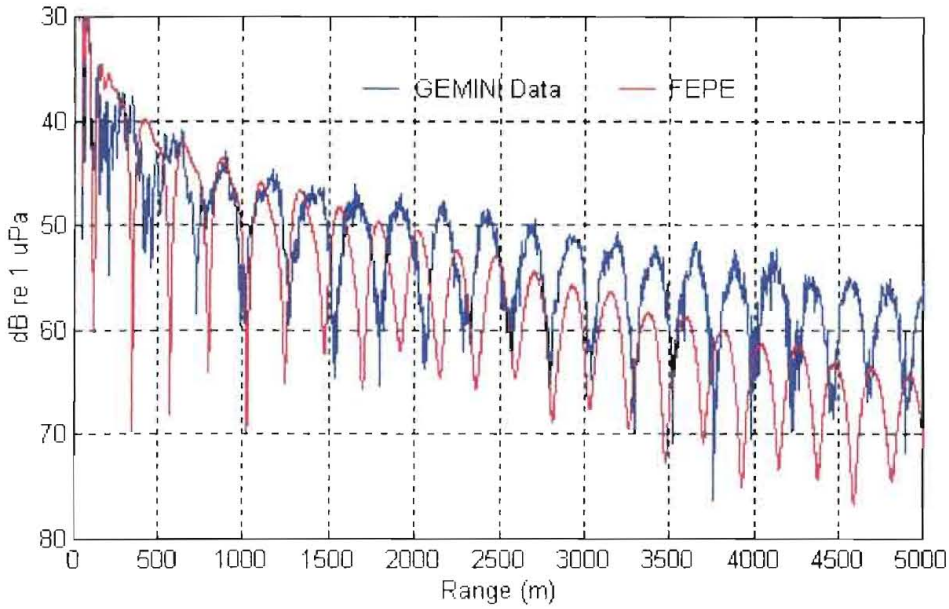

(a)

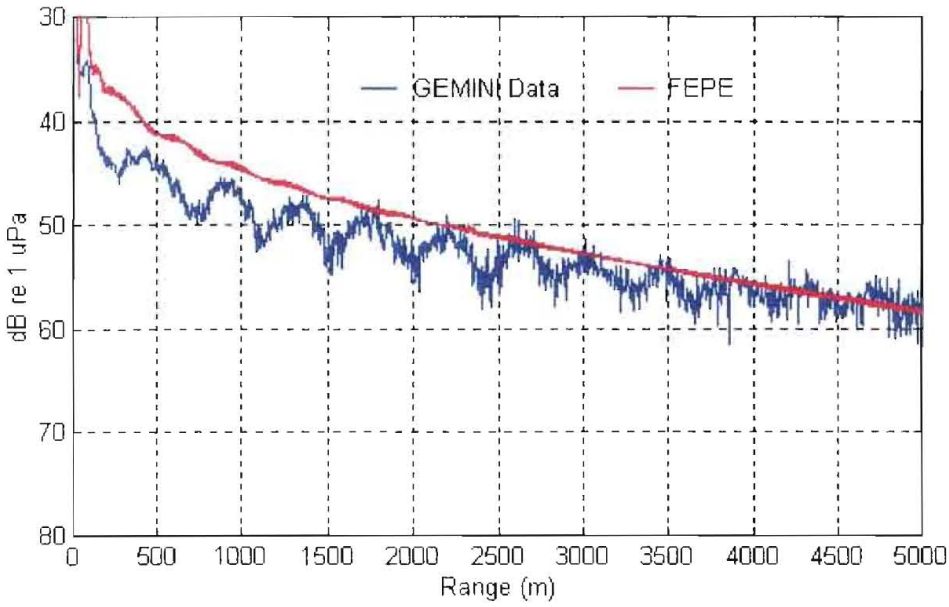

(b)

Figure 19: Plot of GEMINI data versus FEPE model. Source depth: 9 m, receiver depth: 29 m, water depth: 30 m, frequency: 140 Hz (a), 50 Hz (b).

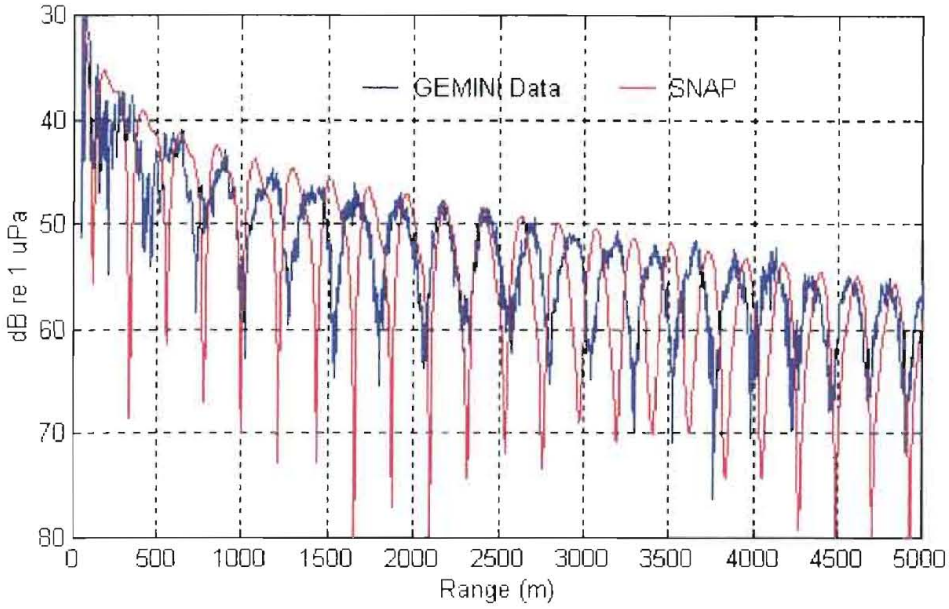

(a)

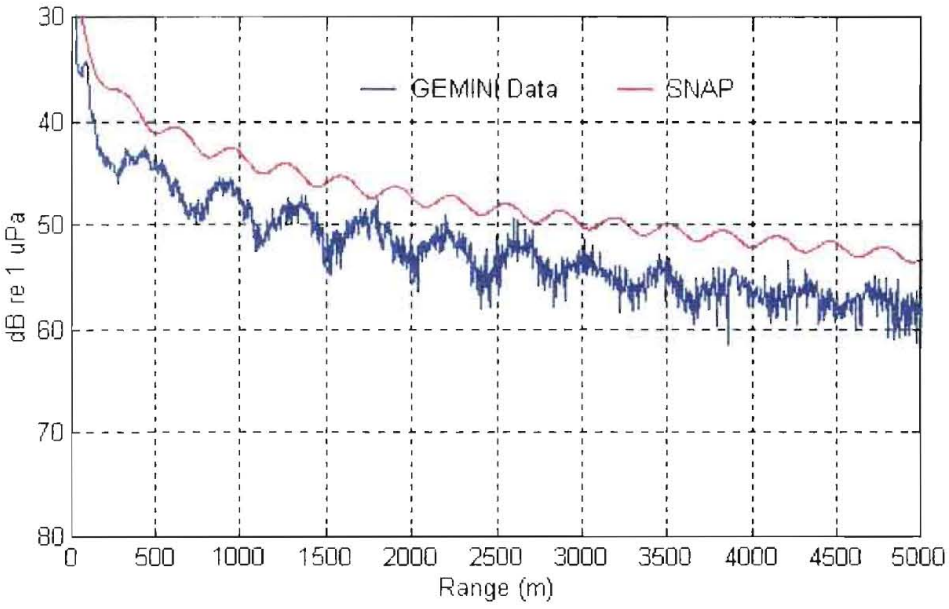

(b)

Figure 20: Plot of GEMINI data versus SNAP model. Source depth: 9 m, receiver depth: 29 m, water depth: 30 m, frequency: 140 Hz (a), 50 Hz (b).

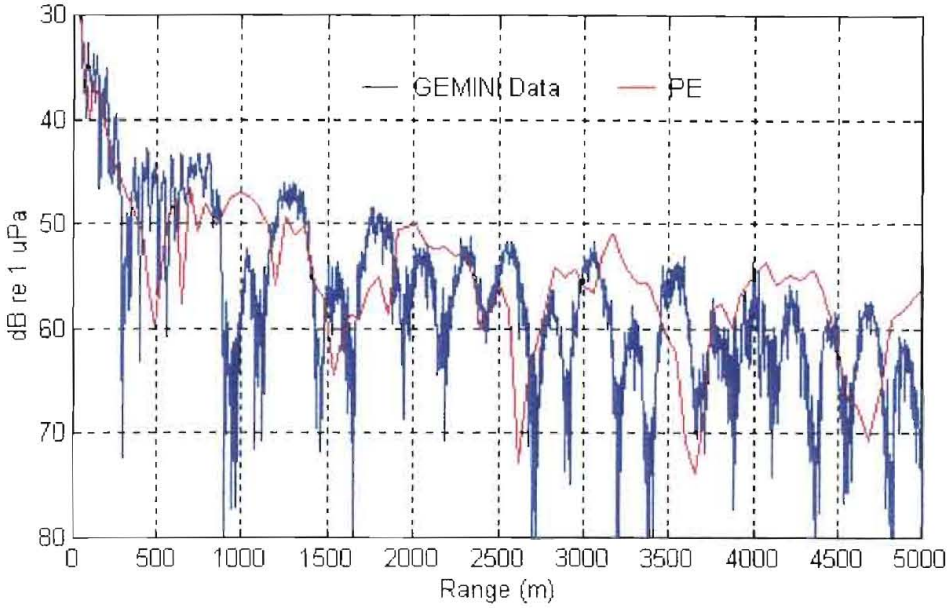

(a)

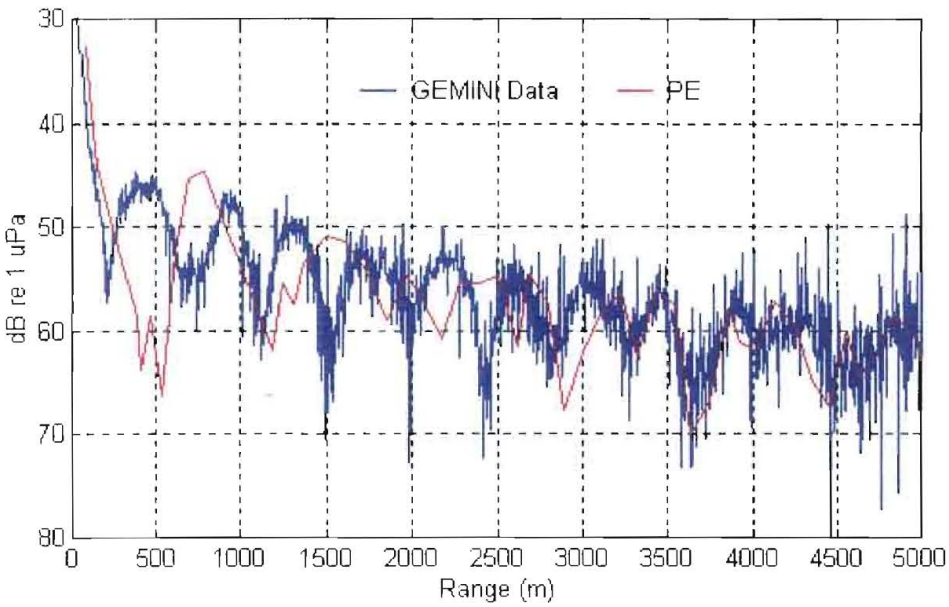

(b)

Figure 21: Plot of GEMINI data versus PE model. Source depth: 9 m, receiver depth: 29 m, water depth: 30 m, frequency: 140 Hz (a), 50 Hz (b).

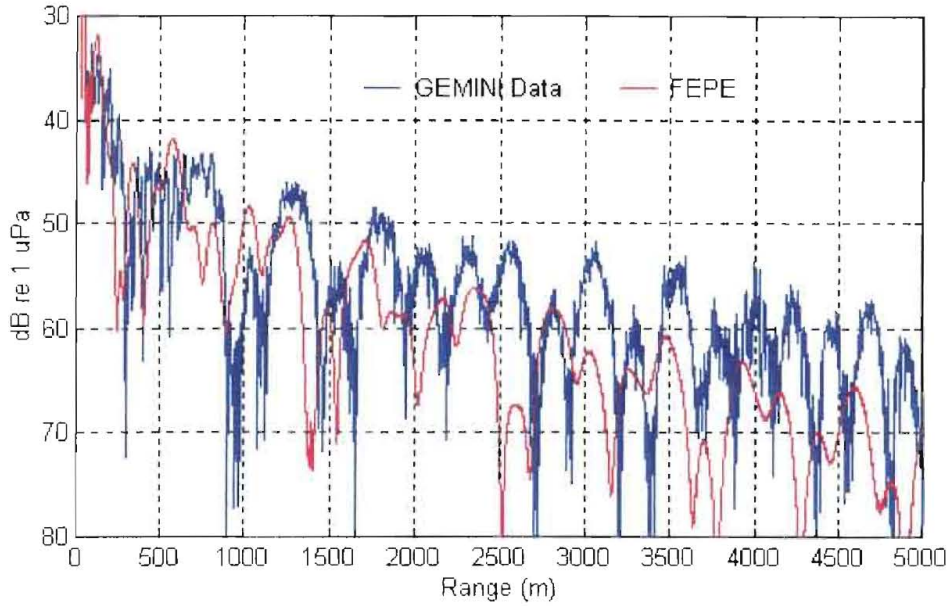

(a)

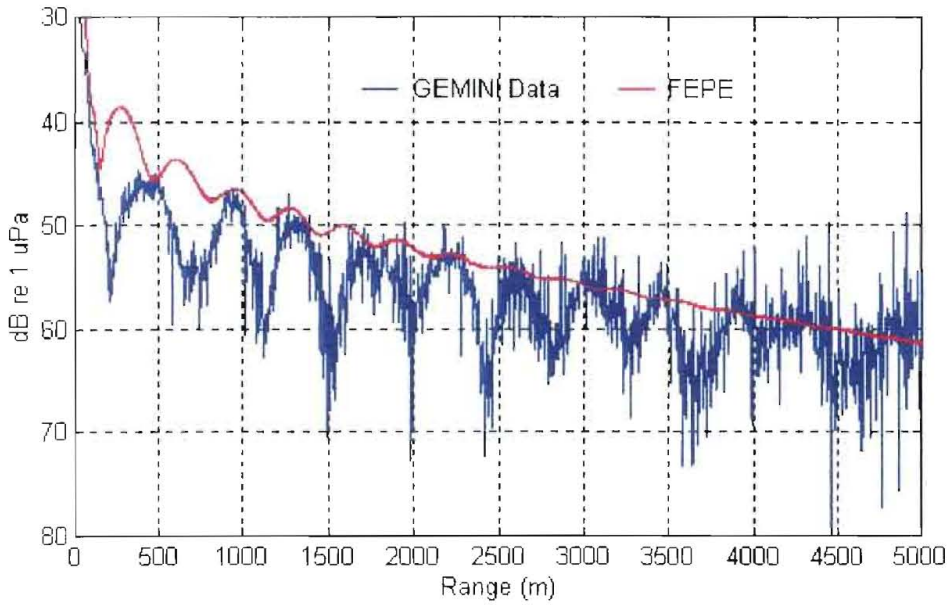

(b)

Figure 22: Plot of GEMINI data versus FEPE model. Source depth: 9 m, receiver depth: 29 m, water depth: 30 m, frequency: 140 Hz (a), 50 Hz (b).

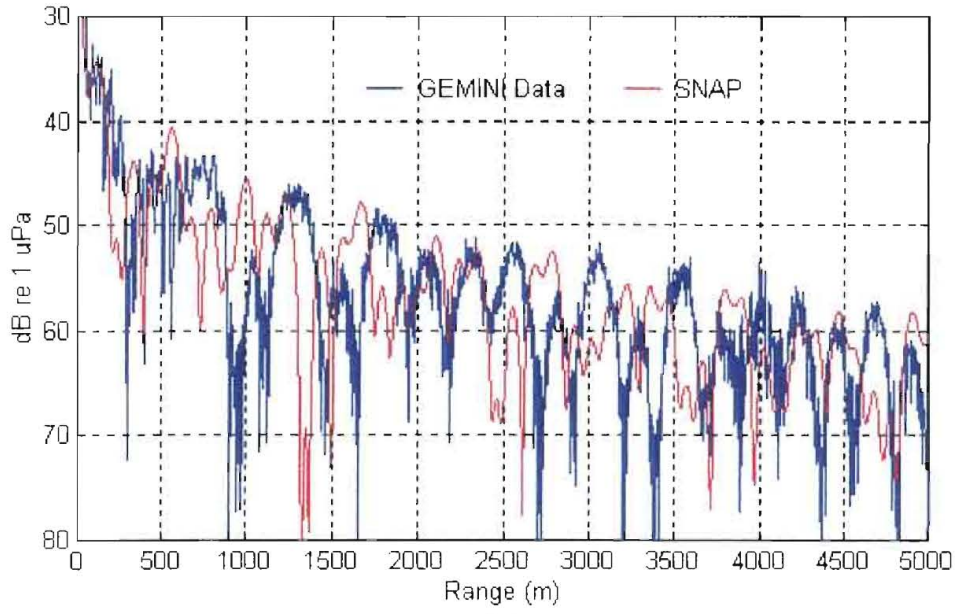

(a)

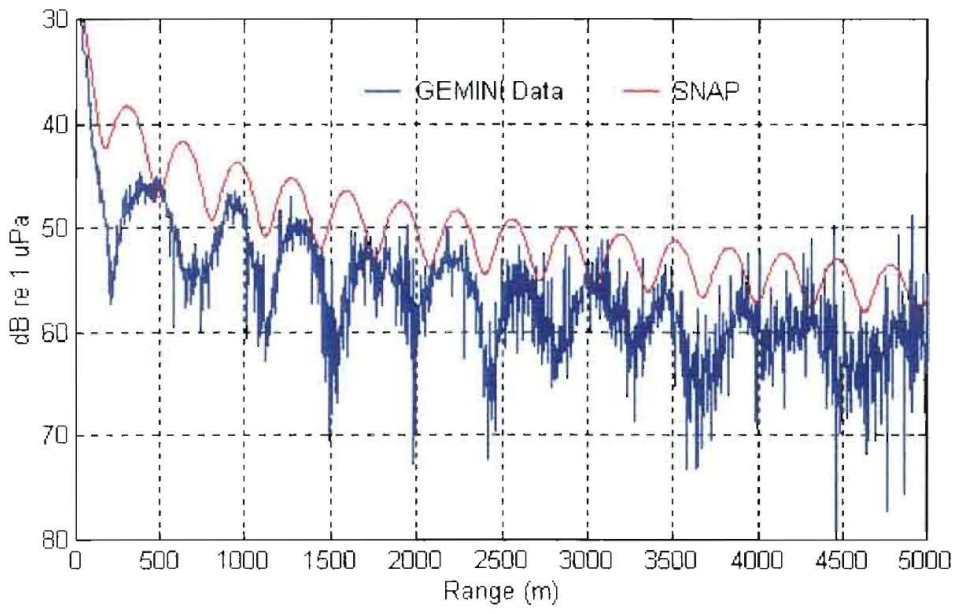

(b)

Figure 23: Plot of GEMINI data versus SNAP model. Source depth: 9 m, receiver depth: 29 m, water depth: 30 m, frequency: 140 Hz (a), 50 Hz (b).

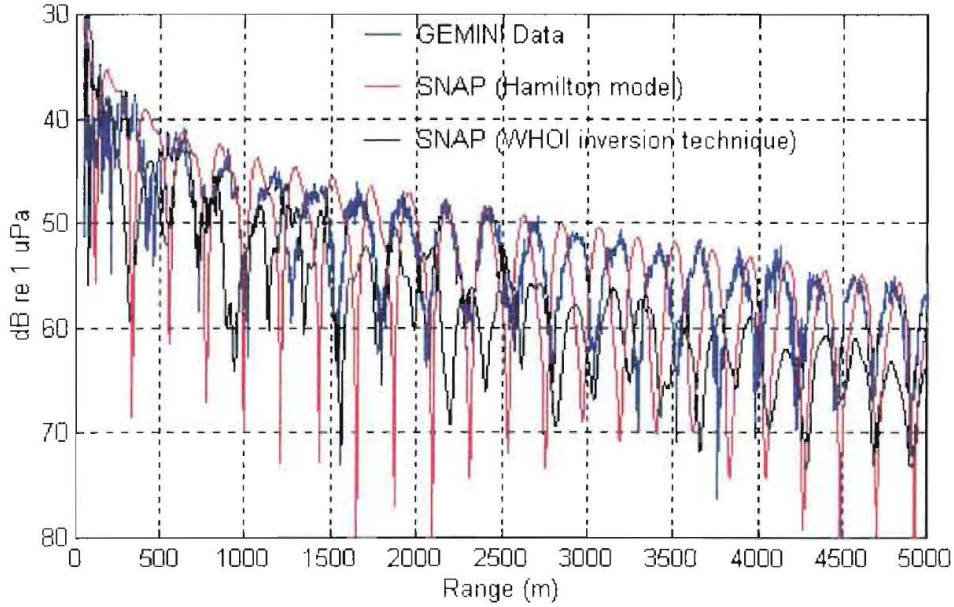

(a)

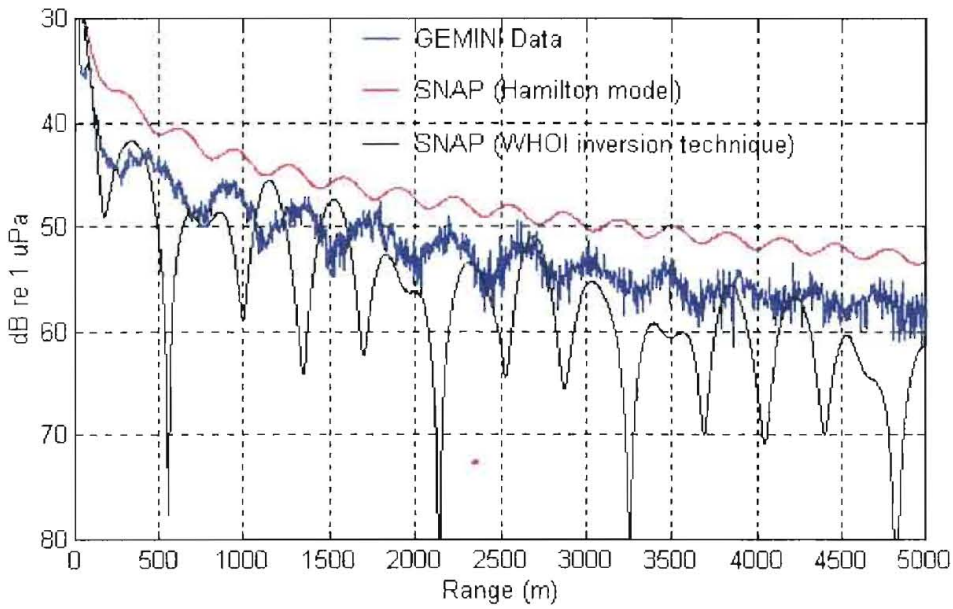

(b)

Figure 24: Plot of GEMINI data versus SNAP using both the WHOI geoacoustic model and the Hamilton "point" geoacoustic model as input. Source depth: 23 m, receiver depth: 29 m, frequency: 140 Hz (a), 50 Hz (b).

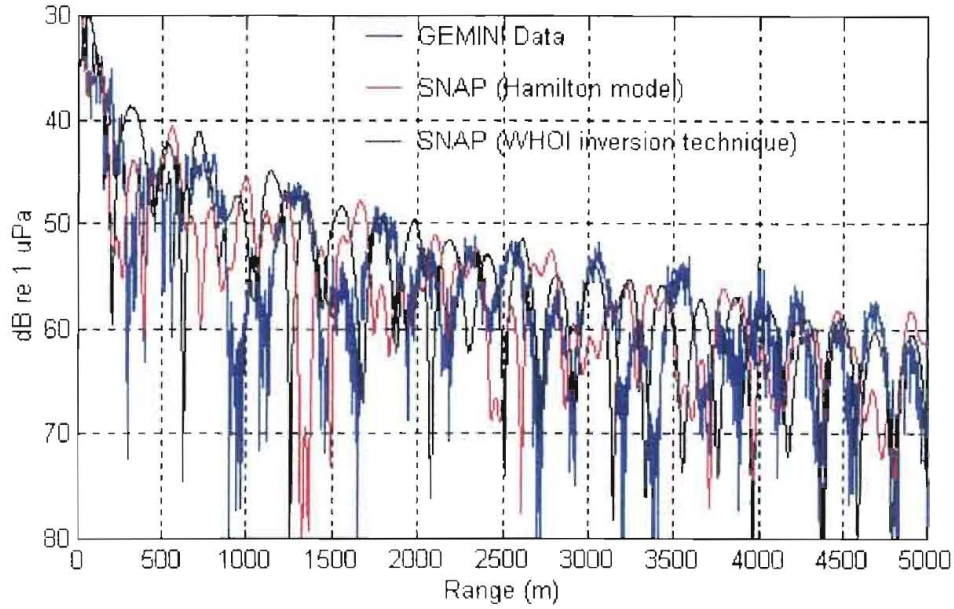

(a)

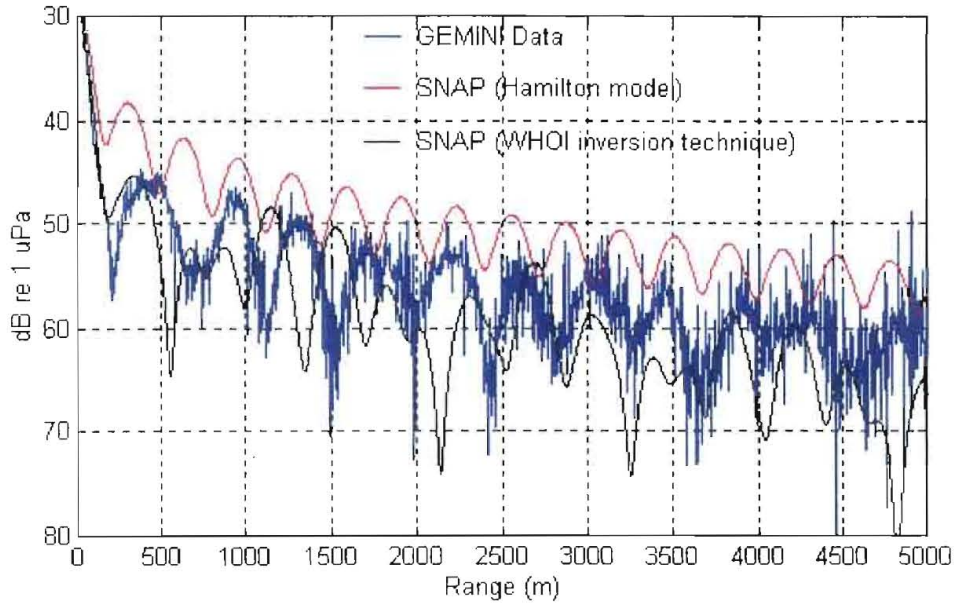

(b)

Figure 25: (a) same as Figure 24a but for 15 m receiver depth. (b) same as Figure 24b but for 15 m receiver depth.

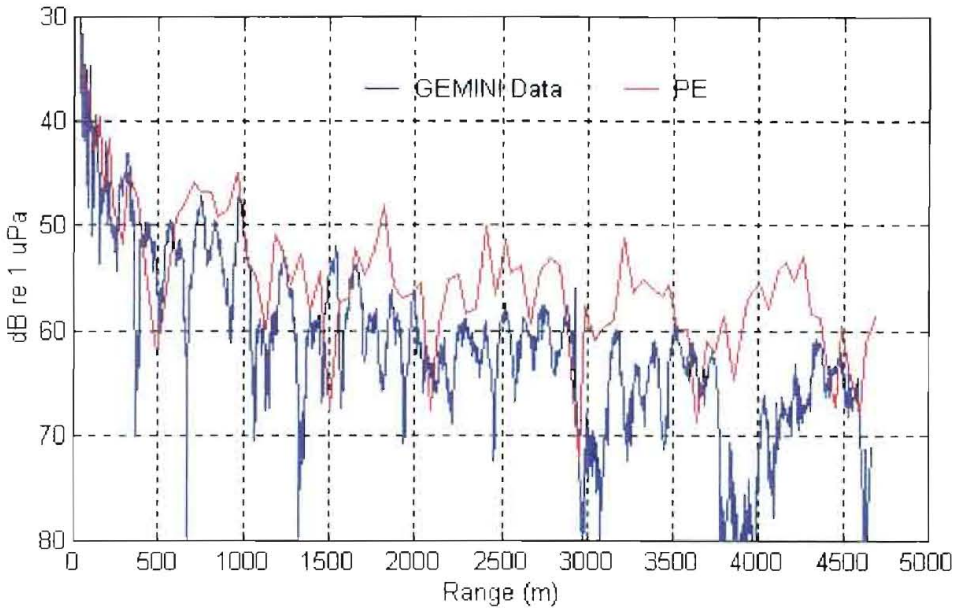

(a)

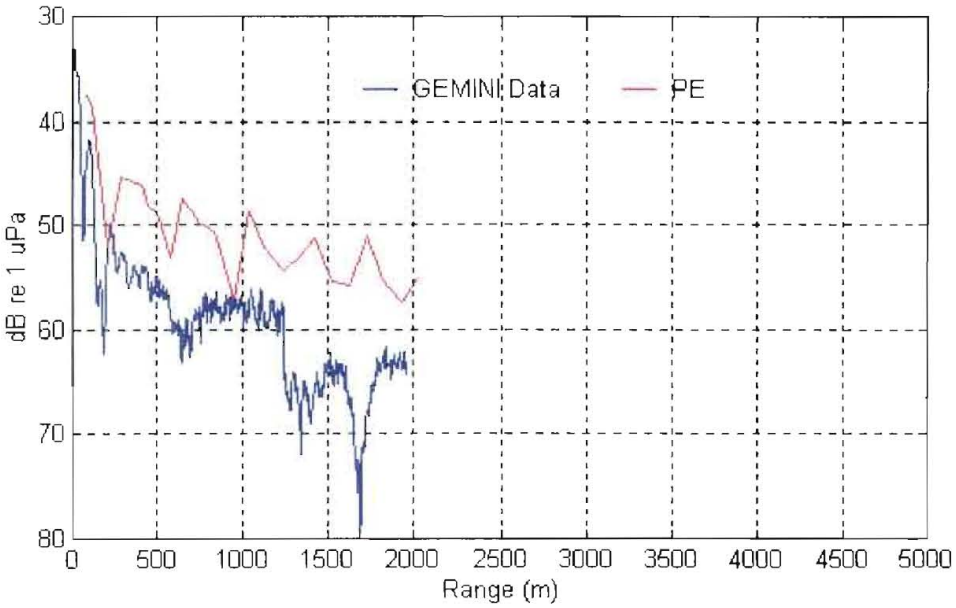

(b)

Figure 26: Plot of GEMINI data versus PE model. Source depth: 46 m, receiver depth: 61 m, water depth: 62 m, frequency: 140 Hz (a), 50 Hz (b).

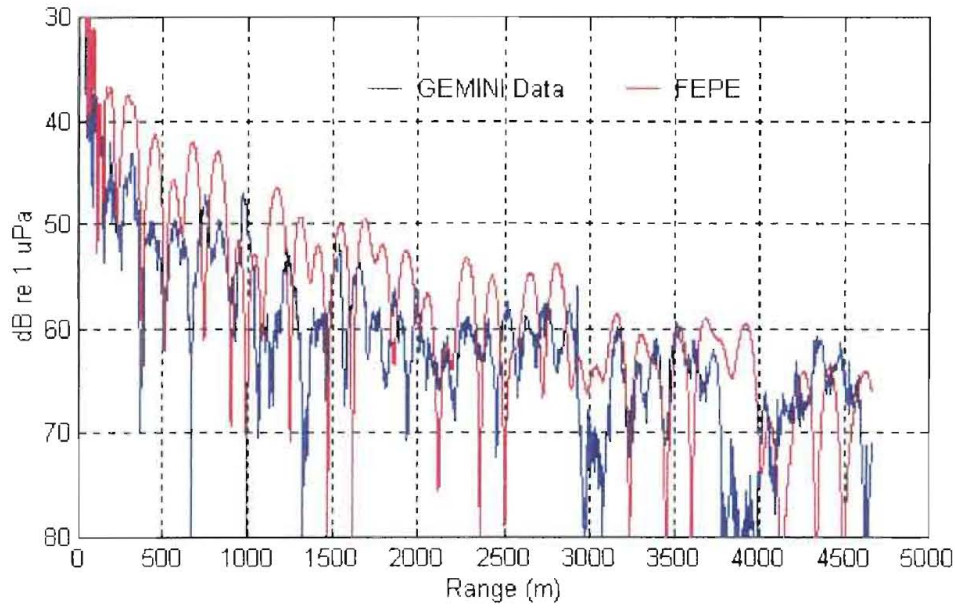

(a)

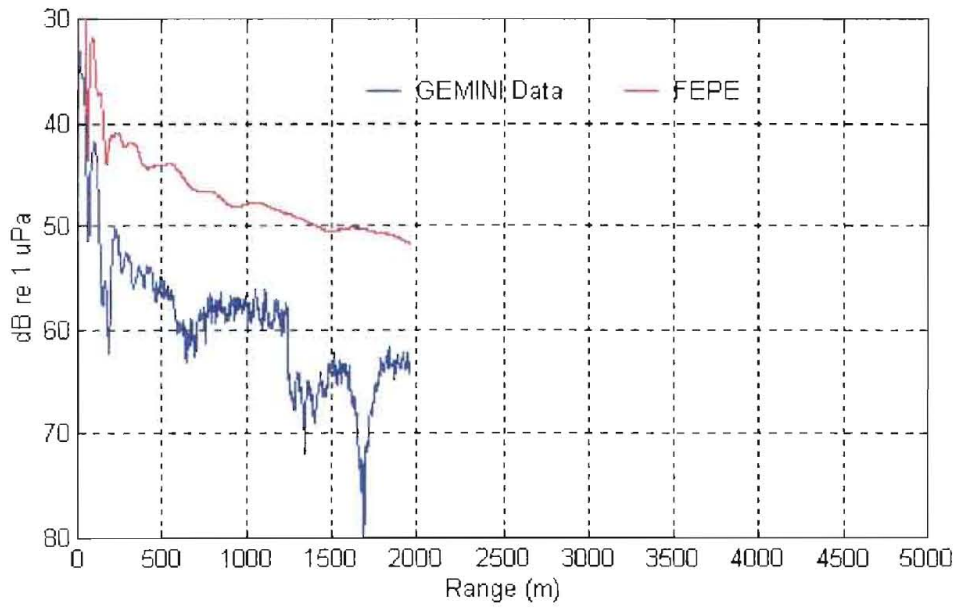

(b)

Figure 27: Plot of GEMINI data versus FEPE model. Source depth: 46 m, receiver depth: 61 m, water depth: 62 m, frequency: 140 Hz (a), 50 Hz (b).

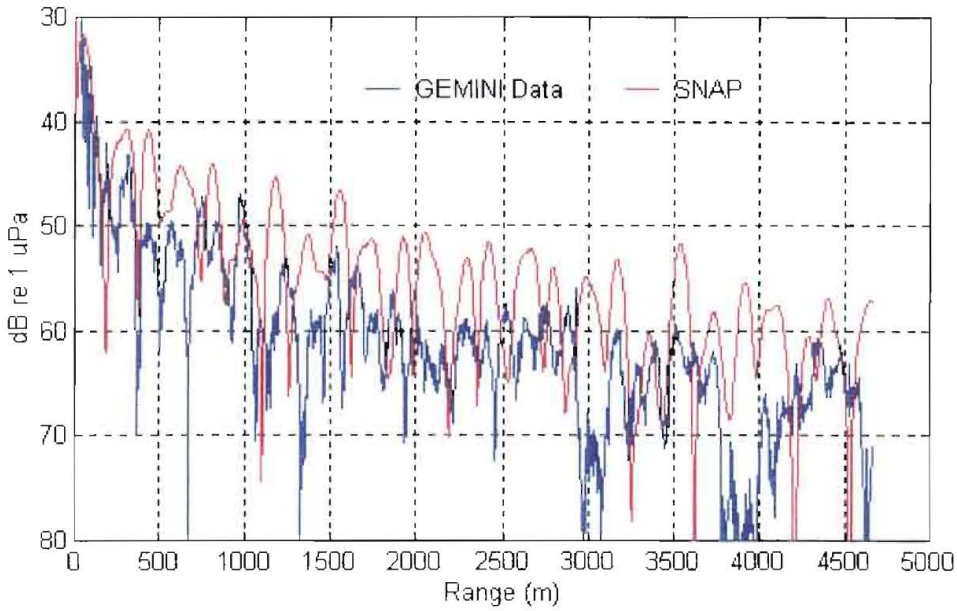

(a)

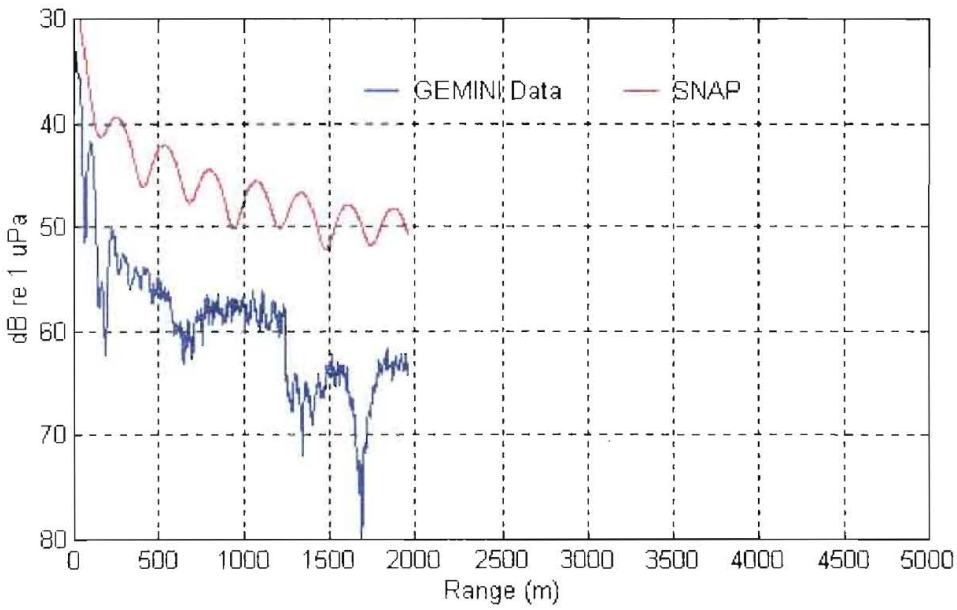

(b)

Figure 28: Plot of GEMINI data versus SNAP model. Source depth: 46 m, receiver depth: 61 m, water depth: 62 m, frequency: 140 Hz (a), 50 Hz (b).

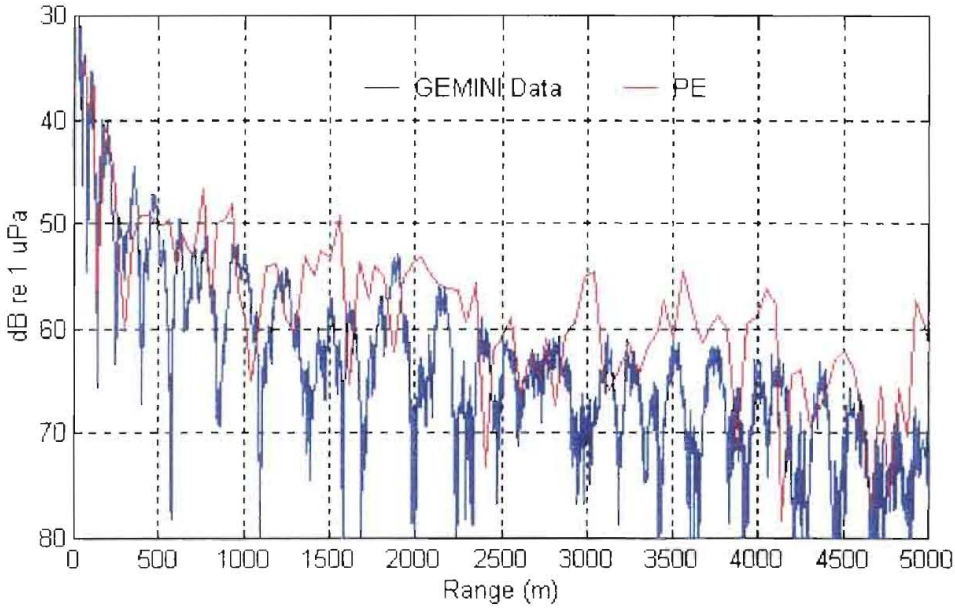

(a)

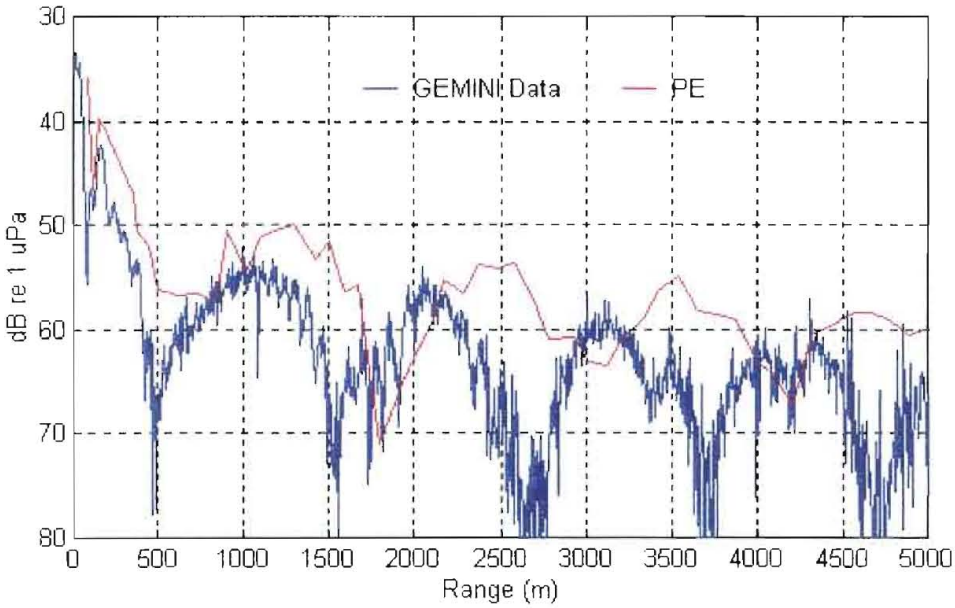

(b)

Figure 29: Plot of GEMINI data versus PE model. Source depth: 46 m, receiver depth: 32 m, water depth: 62 m, frequency: 140 Hz (a), 50 Hz (b).

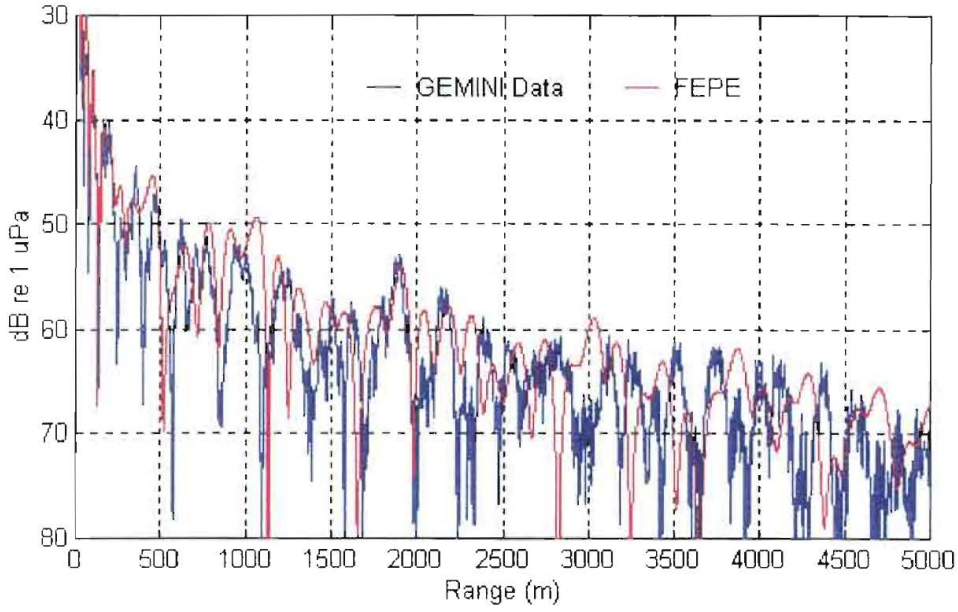

(a)

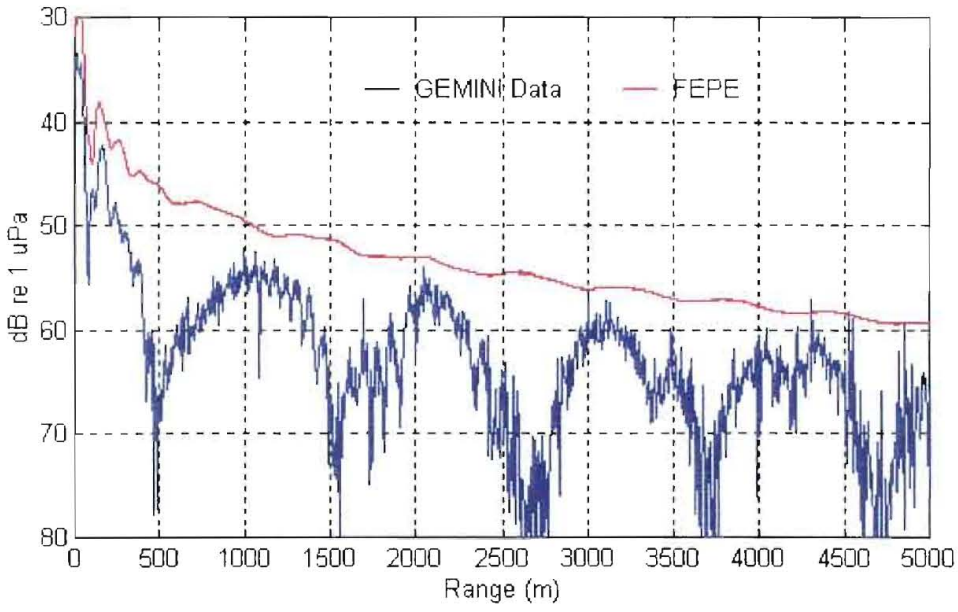

(b)

Figure 30: Plot of GEMINI data versus FEPE model. Source depth: 46 m, receiver depth: 32 m, water depth: 62 m, frequency: 140 Hz (a), 50 Hz (b).

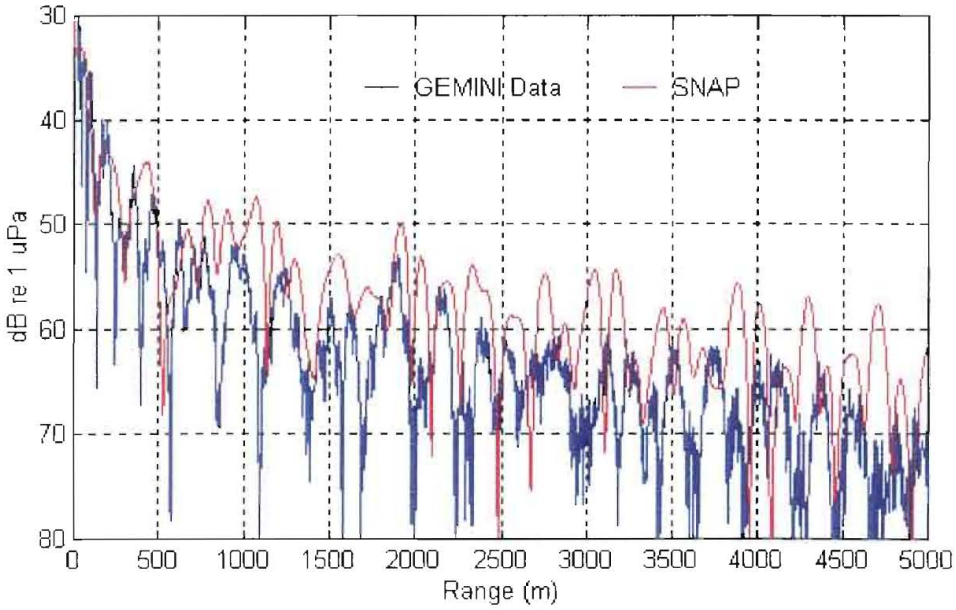

(a)

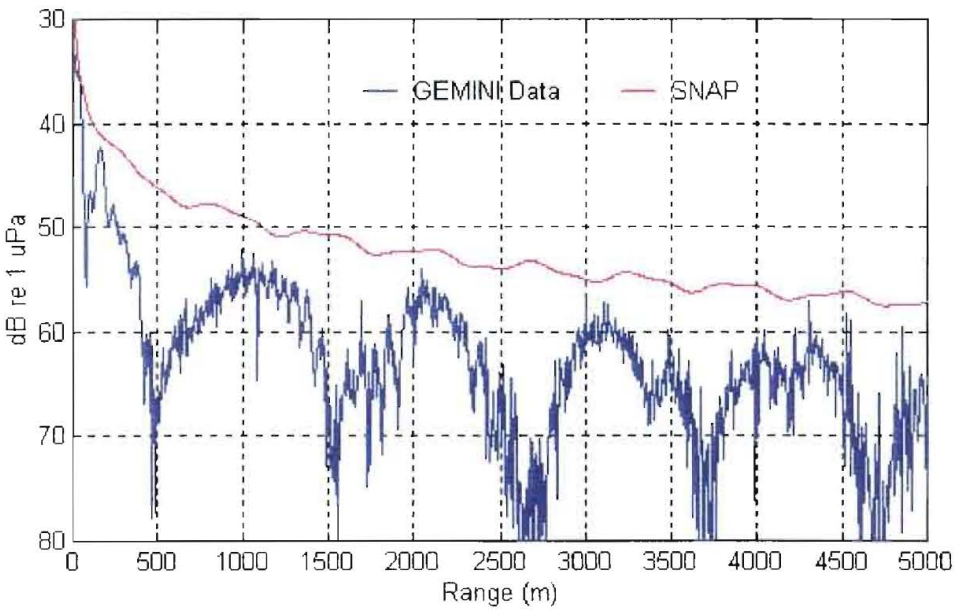

(b)

Figure 31: Plot of GEMINI data versus SNAP model. Source depth: 46 m, receiver depth: 32 m, water depth: 62 m, frequency: 140 Hz (a), 50 Hz (b).

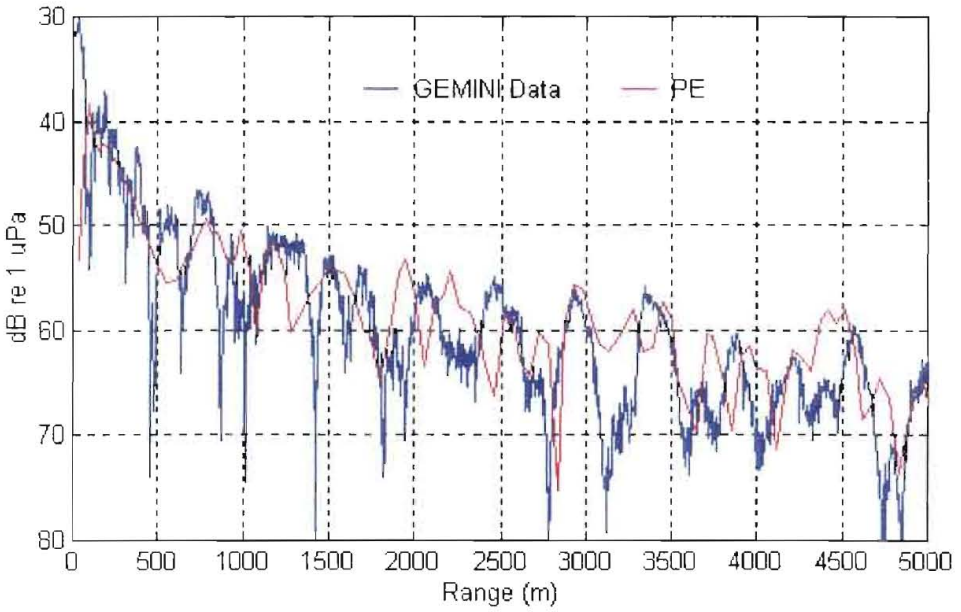

(a)

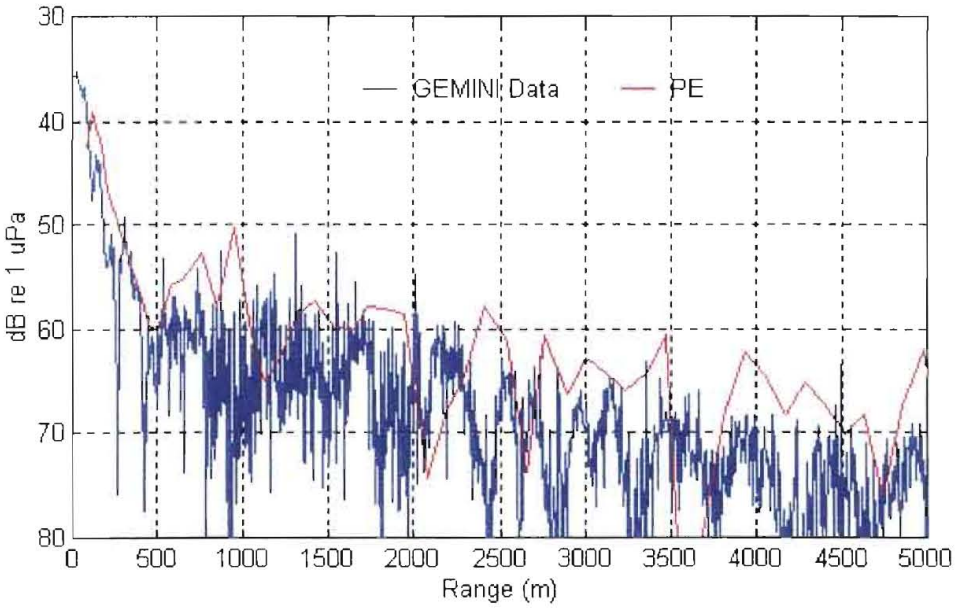

(b)

Figure 32: Plot of GEMINI data versus PE model. Source depth: 9 m, receiver depth: 61 m, water depth: 62 m, frequency: 140 Hz (a), 50 Hz (b).

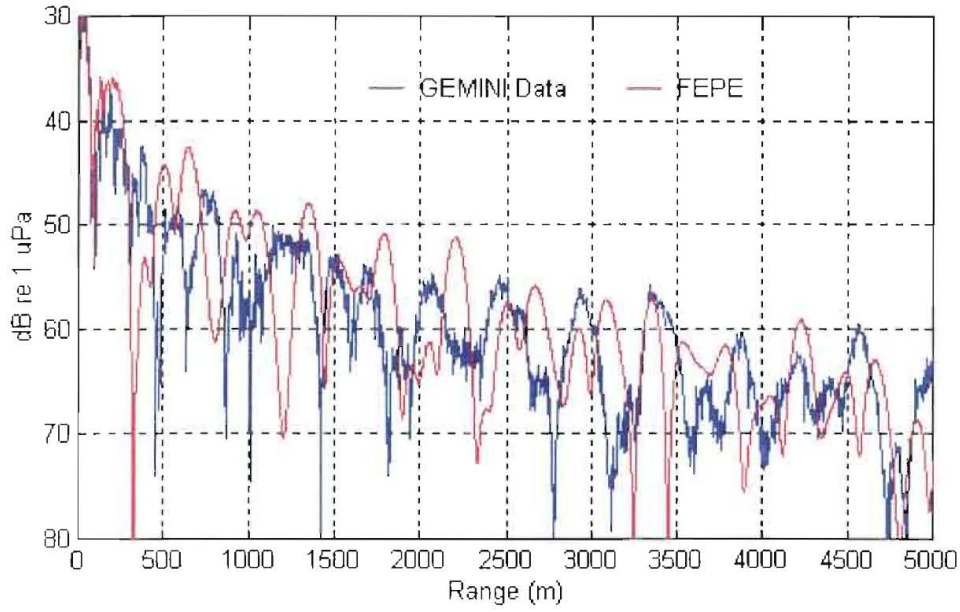

(a)

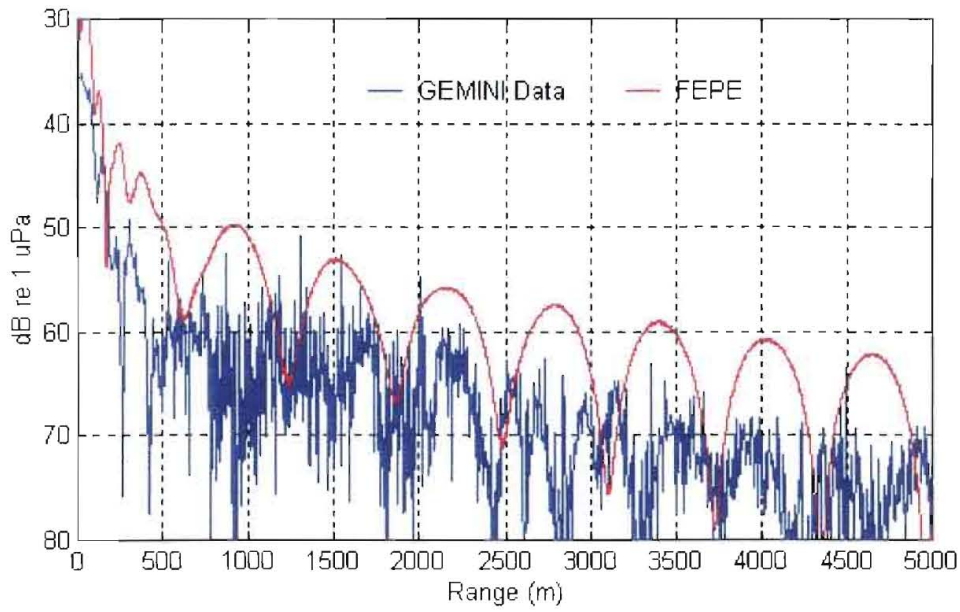

(b)

Figure 33: Plot of GEMINI data versus FEPE model. Source depth: 9 m, receiver depth: 61 m, water depth: 62 m, frequency: 140 Hz (a), 50 Hz (b).

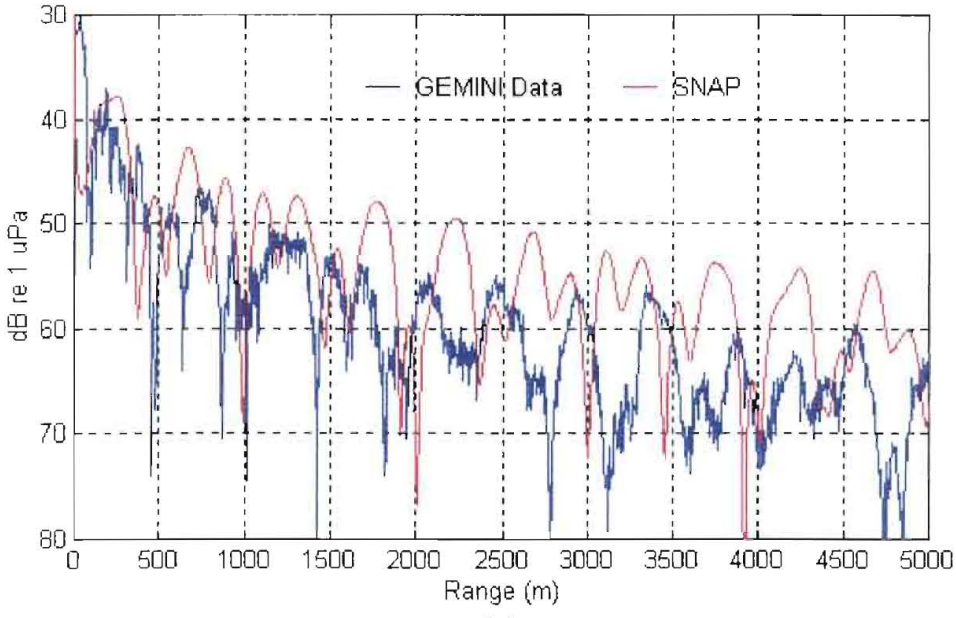

(a)

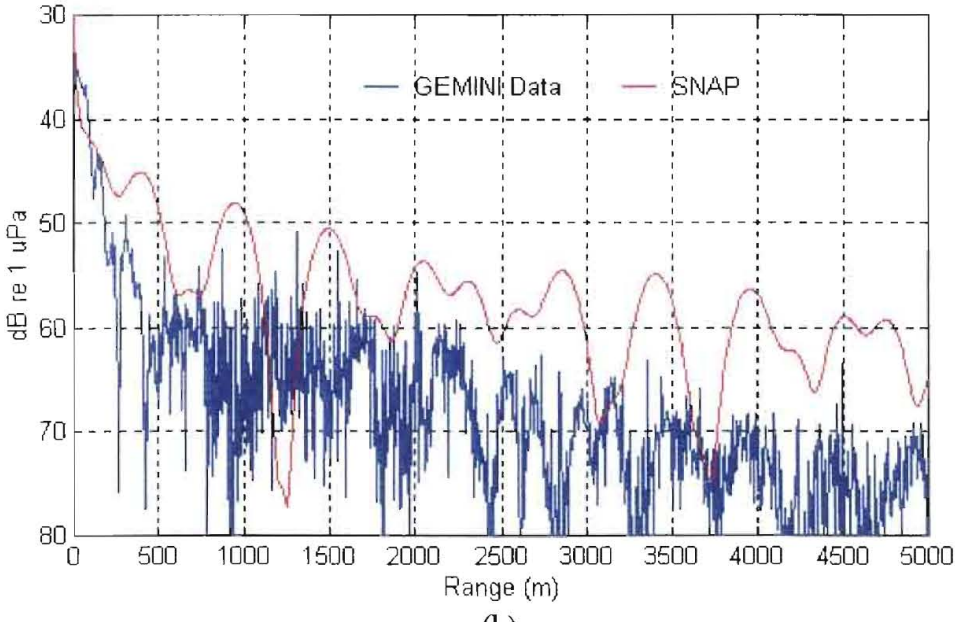

(b)

Figure 34: Plot of GEMINI data versus SNAP model. Source depth: 9 m, receiver depth: 61 m, water depth: 62 m, frequency: 140 Hz (a), 50 Hz (b).

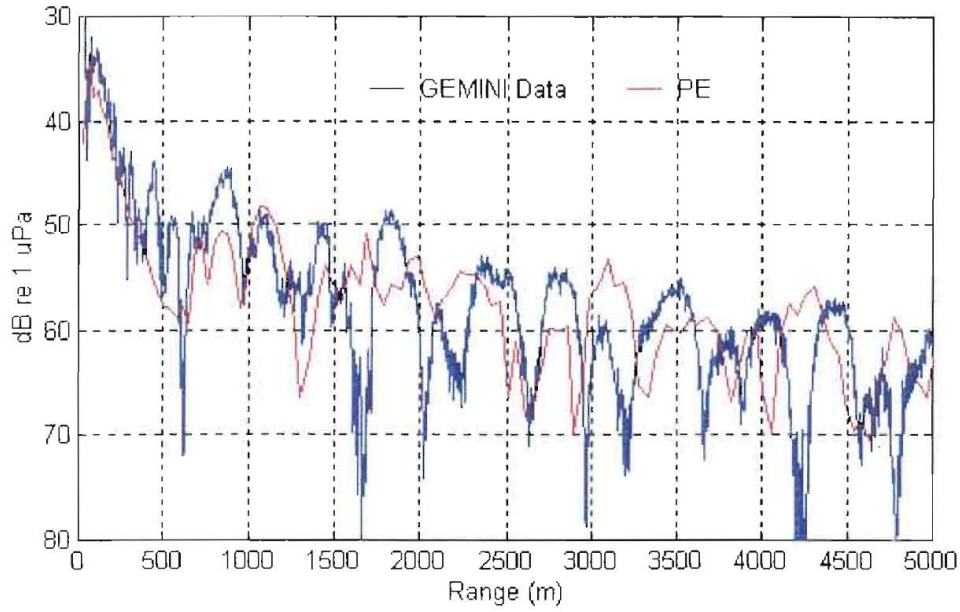

(a)

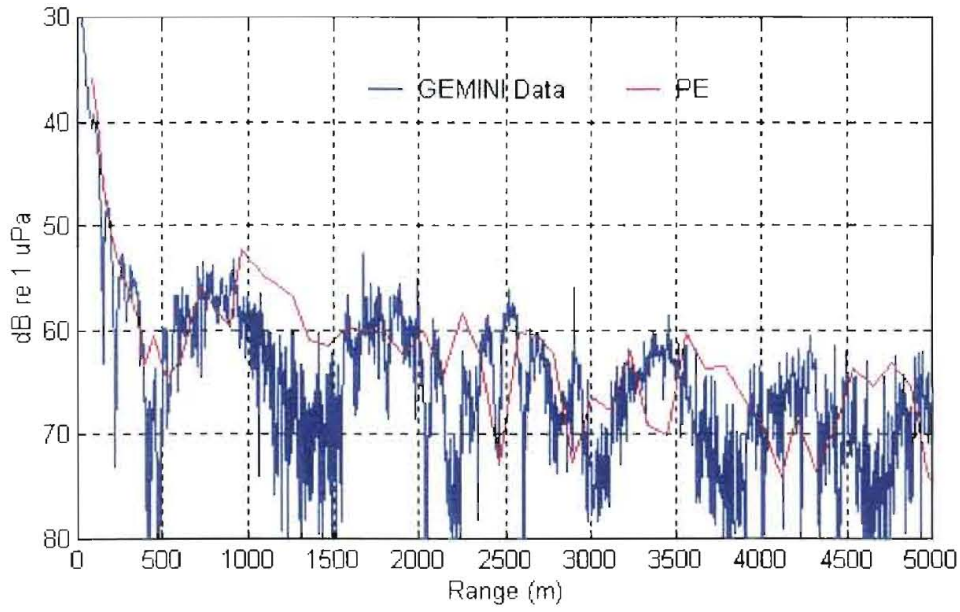

(b)

Figure 35: Plot of GEMINI data versus PE model. Source depth: 9 m, receiver depth: 32 m, water depth: 62 m, frequency: 140 Hz (a), 50 Hz (b).

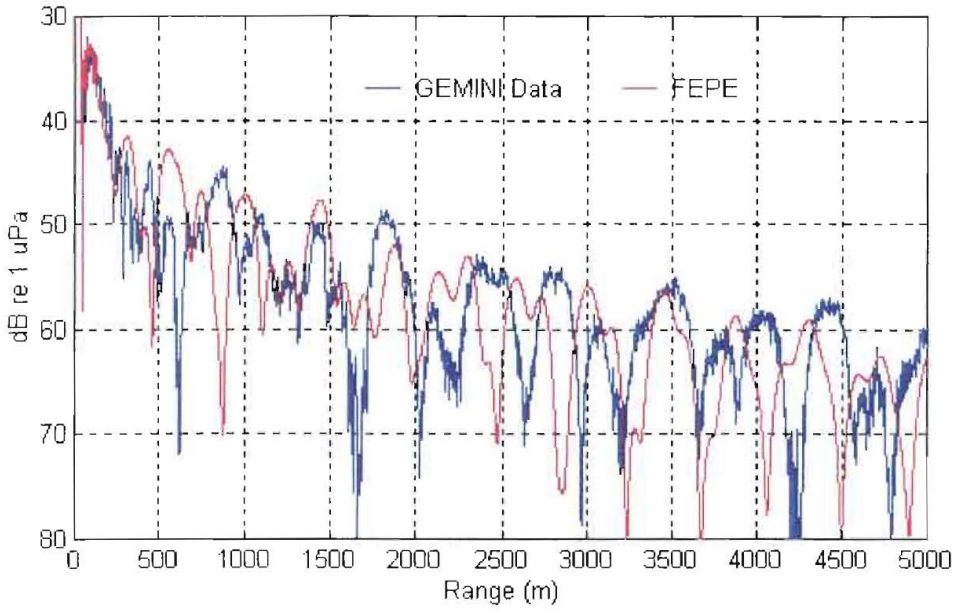

(a)

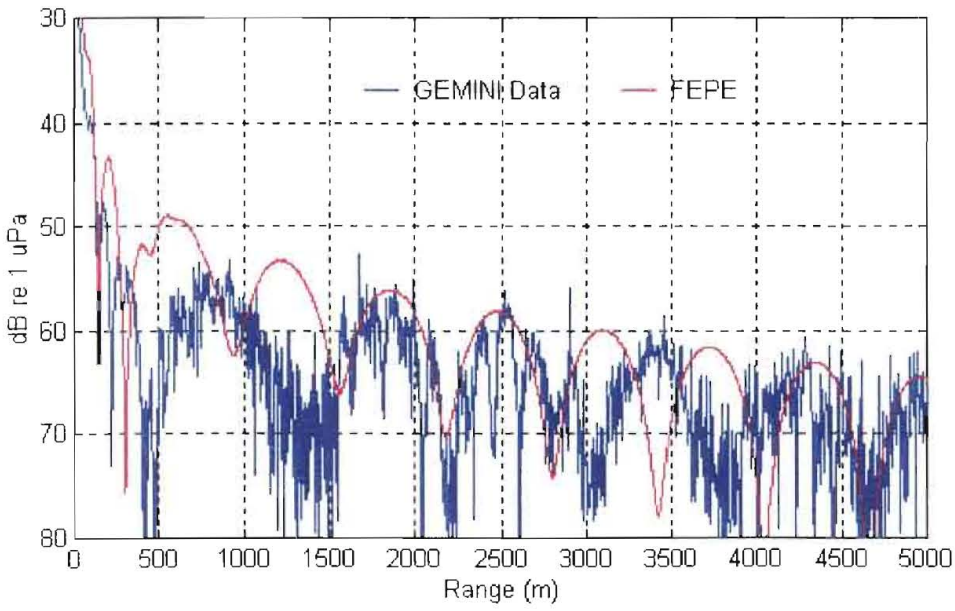

(b)

Figure 36: Plot of GEMINI data versus FEPE model. Source depth: 9 m, receiver depth: 32 m, water depth: 62 m, frequency: 140 Hz (a), 50 Hz (b).

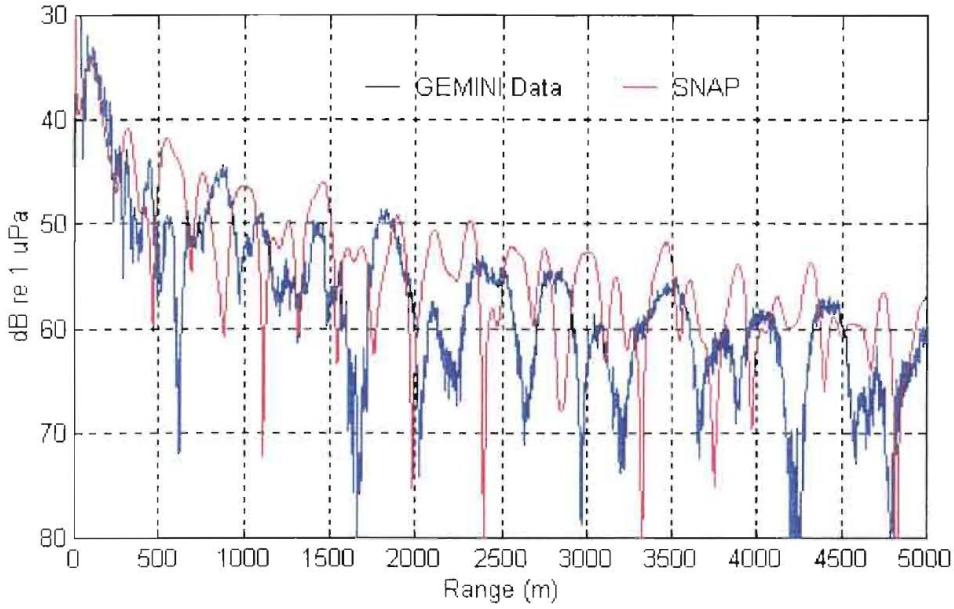

(a)

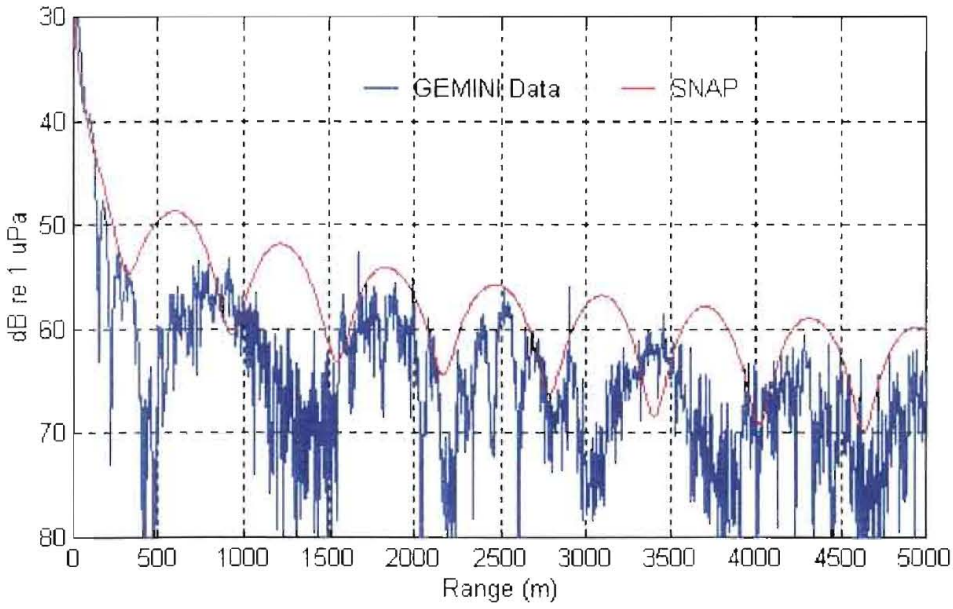

(b)

Figure 37: Plot of GEMINI data versus SNAP model. Source depth: 9 m, receiver depth: 32 m, water depth: 62 m, frequency: 140 Hz (a), 50 Hz (b).

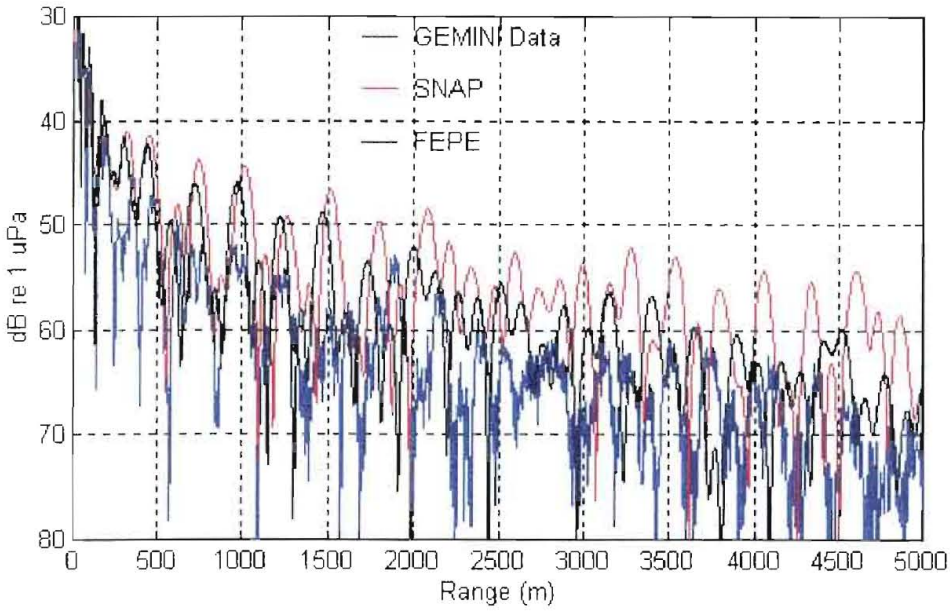

(a)

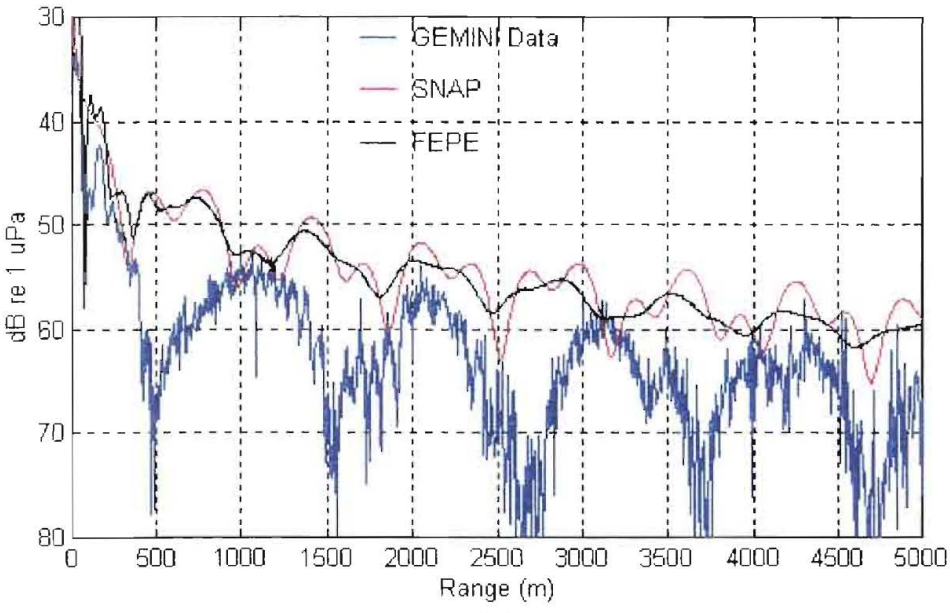

(b)

Figure 38: Plot of GEMINI data versus SNAP and FEPE using an improved geoacoustic model (Null, 1994). Source depth: 46 m, receiver depth: 32 m, frequency: 140 Hz (a), 50 Hz (b).

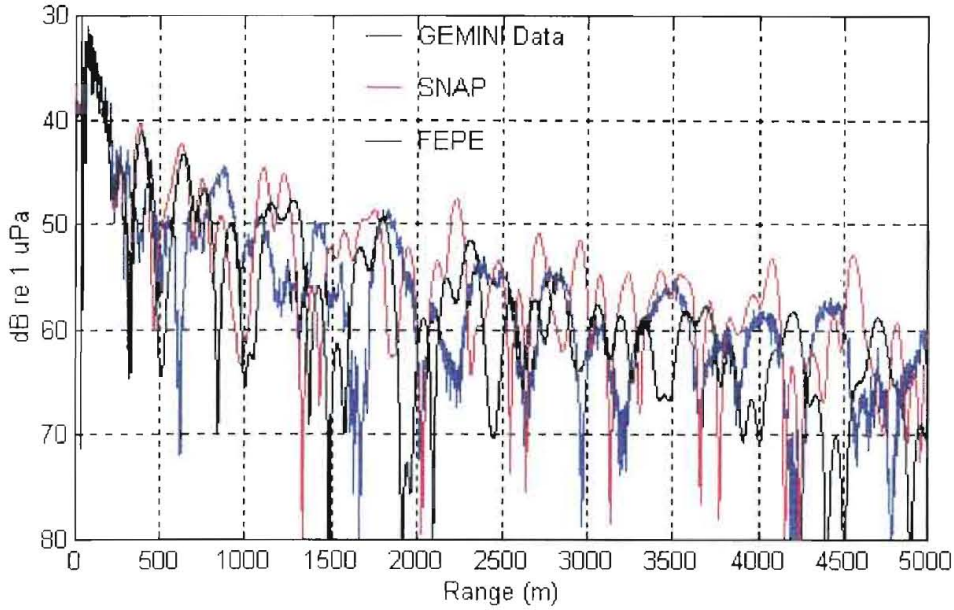

(a)

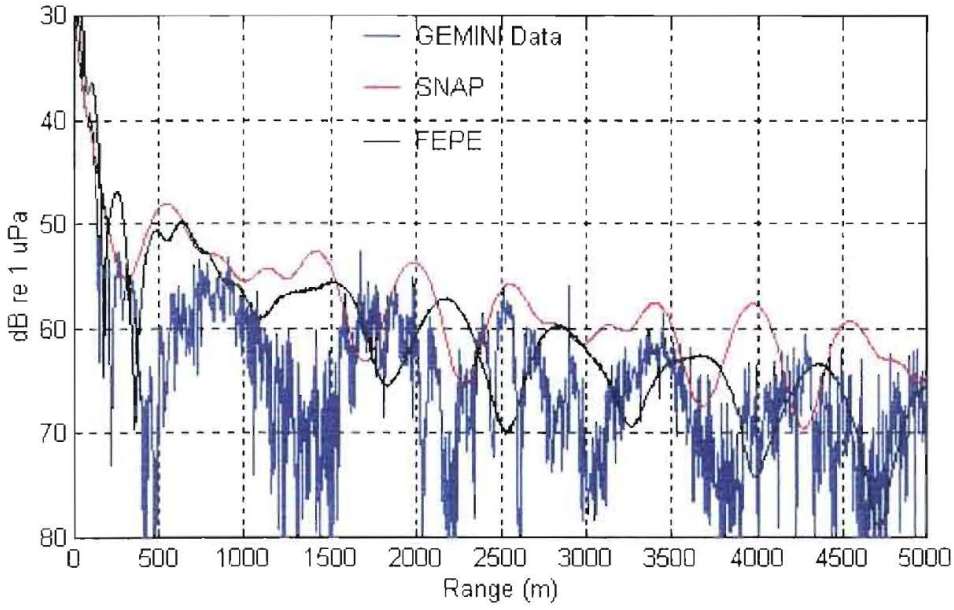

(b)

Figure 39: Plot of GEMINI data versus SNAP and FEPE using an improved geoacoustic model (Null, 1994). Source depth: 9 m, receiver depth: 32 m, frequency: 140 Hz (a), 50 Hz (b).

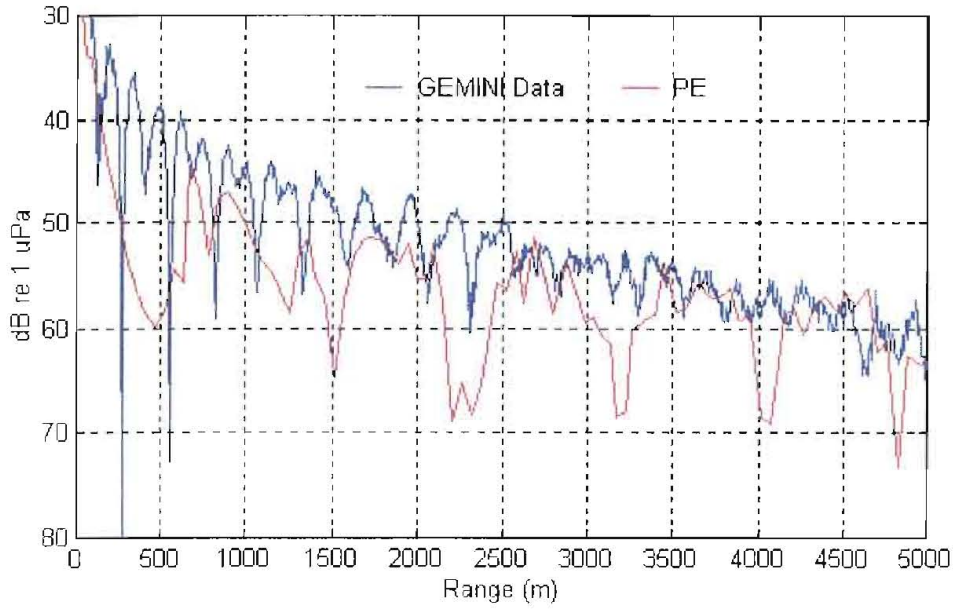

(a)

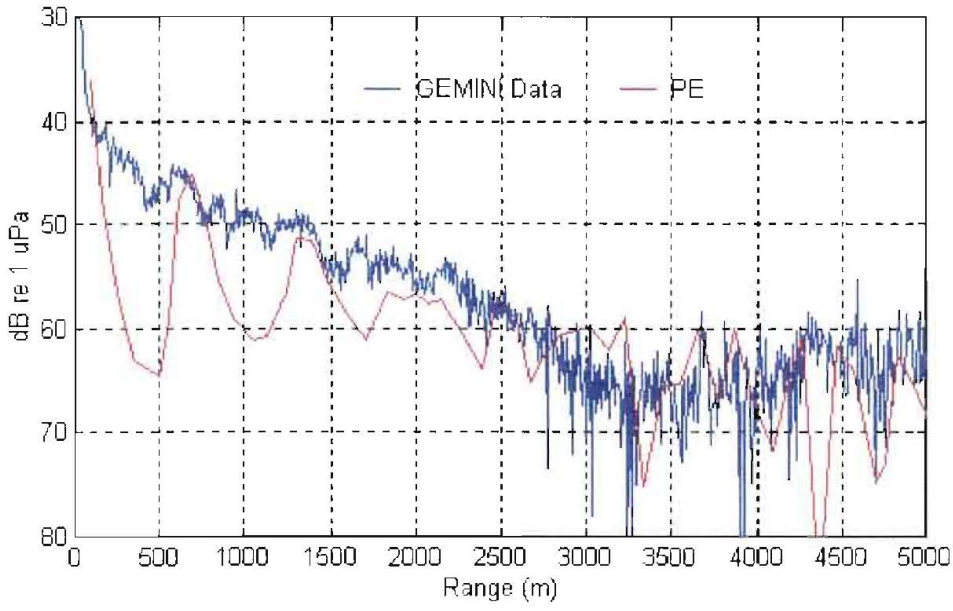

(b)

Figure 40: Plot of GEMINI data versus PE model. Source depth: 9 m, receiver depth: 20 m, water depth: 21 m, frequency: 140 Hz (a), 50 Hz (b).

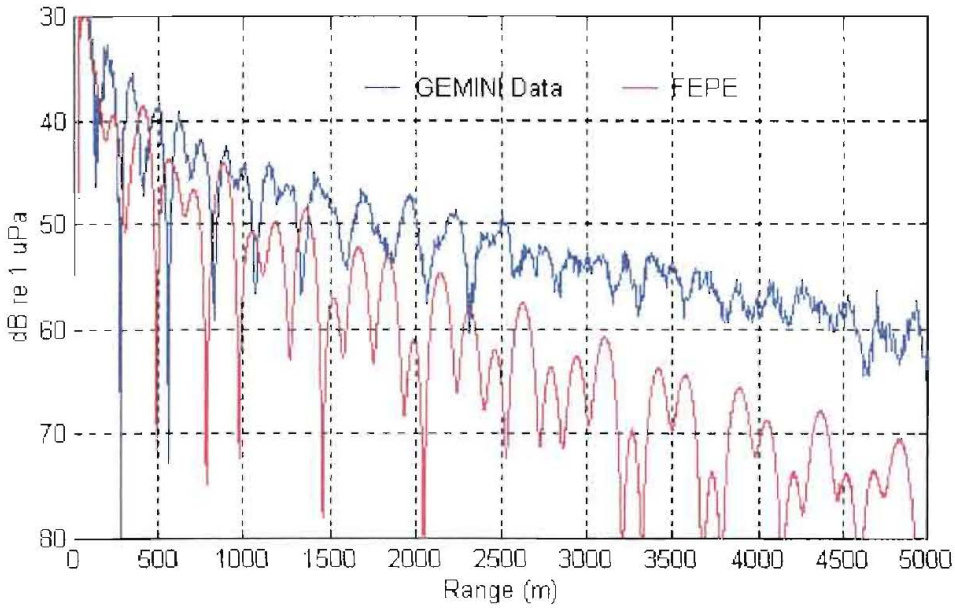

(a)

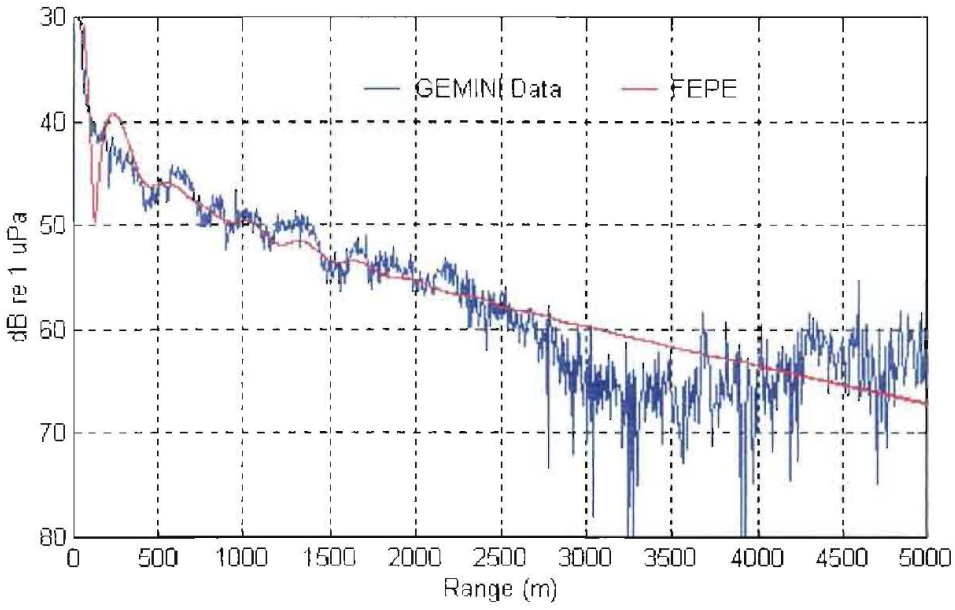

(b)

Figure 41: Plot of GEMINI data versus FEPE model. Source depth: 9 m, receiver depth: 20 m, water depth: 21 m, frequency: 140 Hz (a), 50 Hz (b).

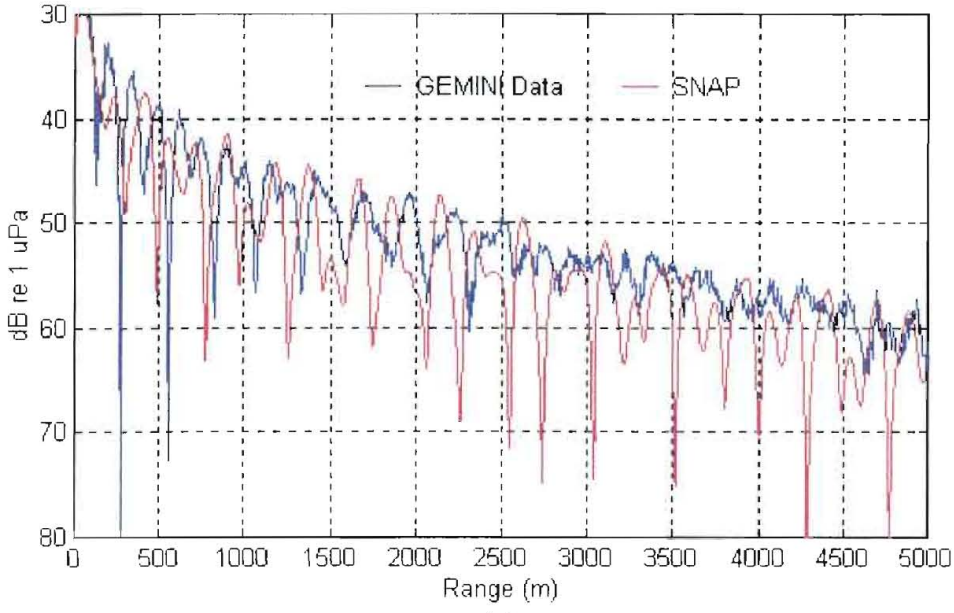

(a)

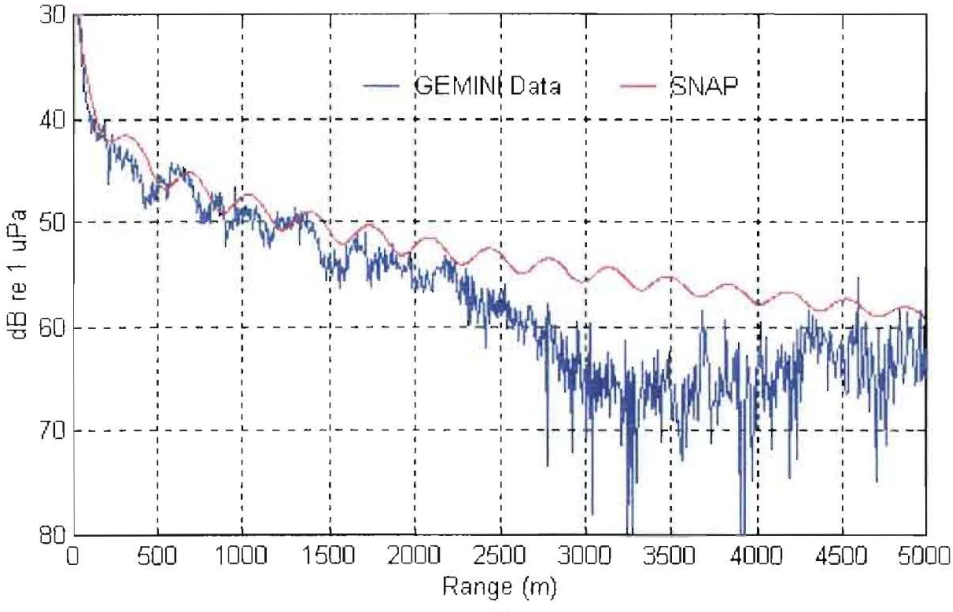

(b)

Figure 42: Plot of GEMINI data versus SNAP model. Source depth: 9 m, receiver depth: 20 m, water depth: 21 m, frequency: 140 Hz (a), 50 Hz (b).

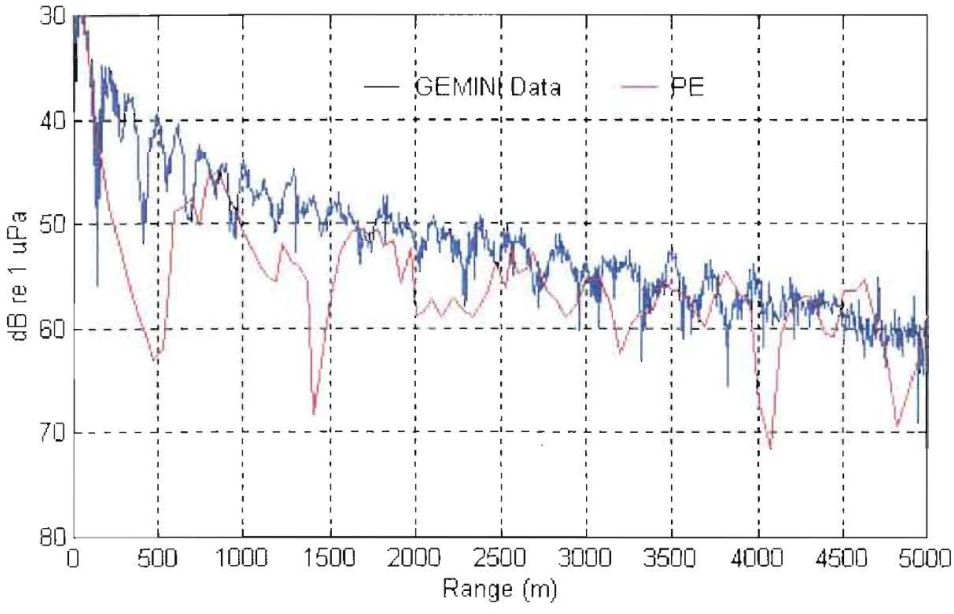

(a)

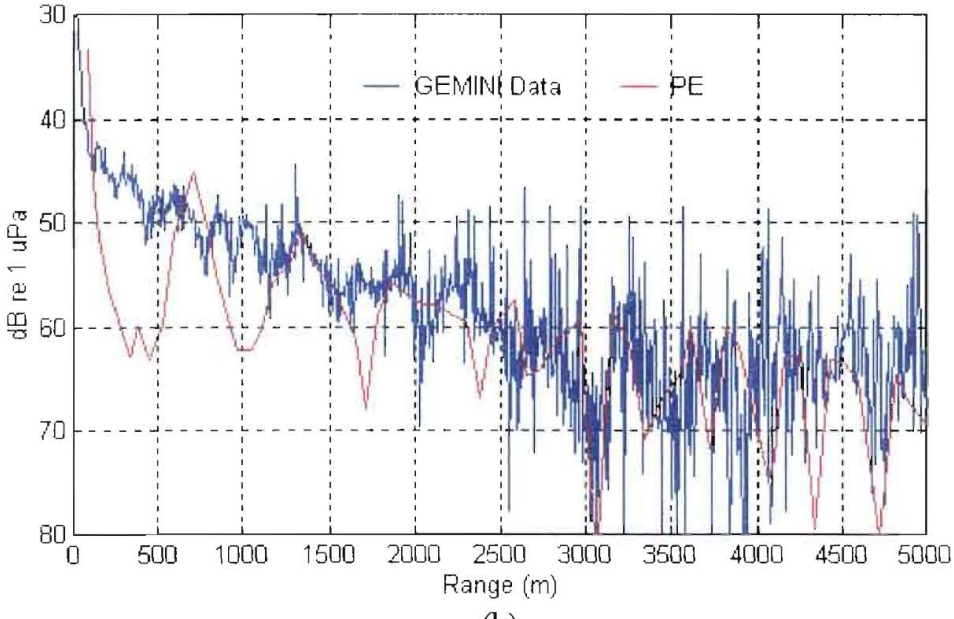

(b)

Figure 43: Plot of GEMINI data versus PE model. Source depth: 9 m, receiver depth: 16 m, water depth: 21 m, frequency: 140 Hz (a), 50 Hz (b).

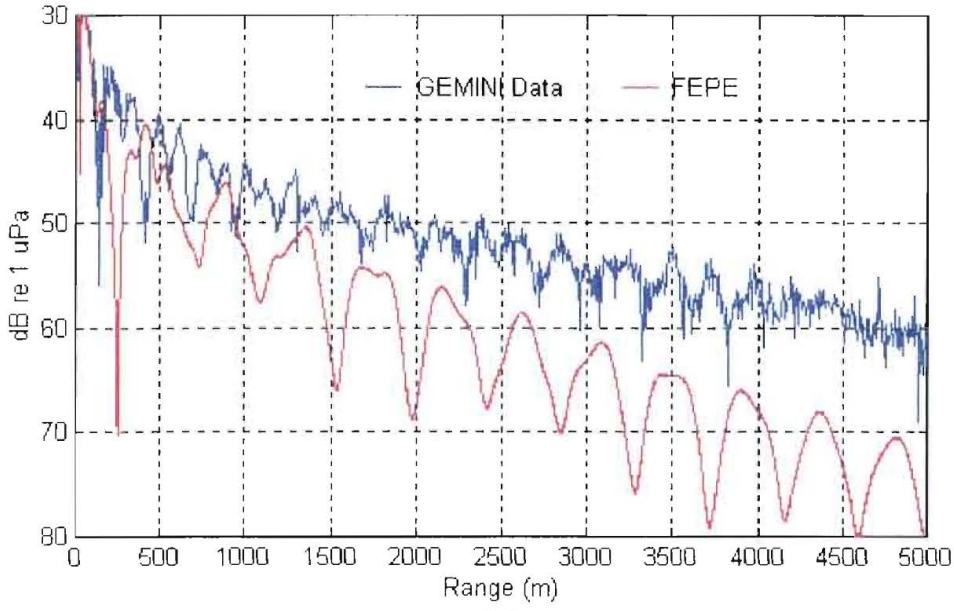

(a)

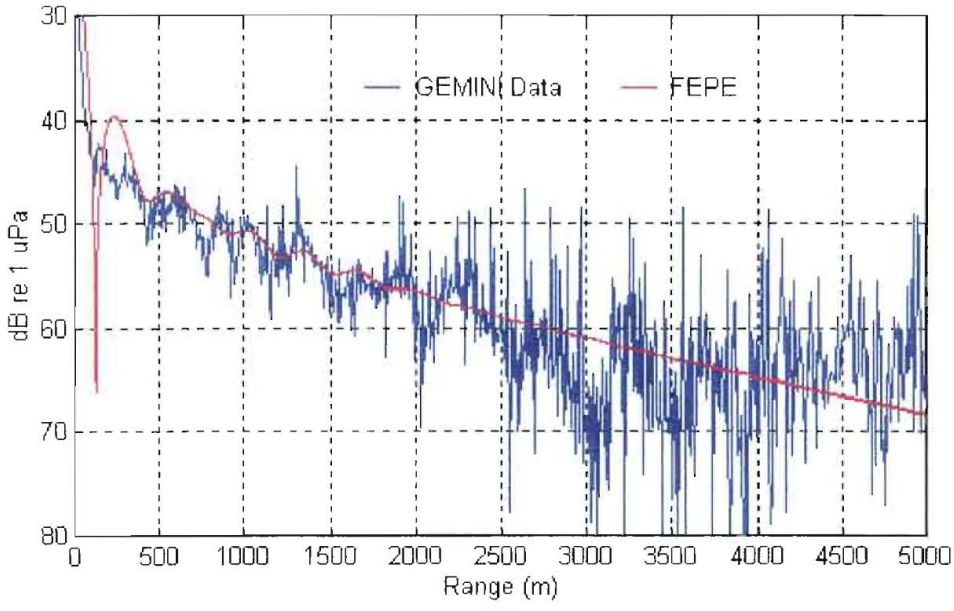

(b)

Figure 44: Plot of GEMINI data versus FEPE model. Source depth: 9 m, receiver depth: 16 m, water depth: 21 m, frequency: 140 Hz (a), 50 Hz (b).

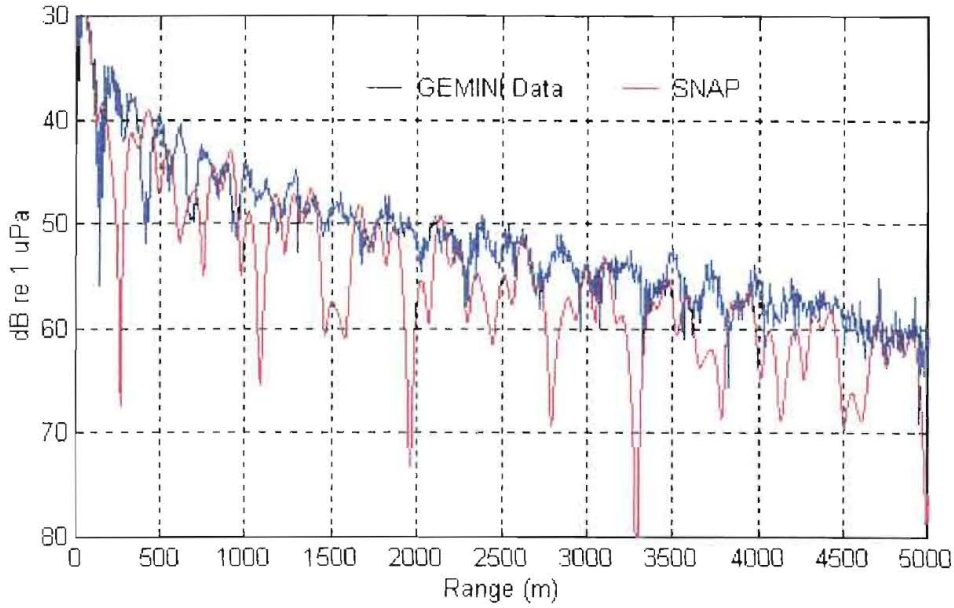

(a)

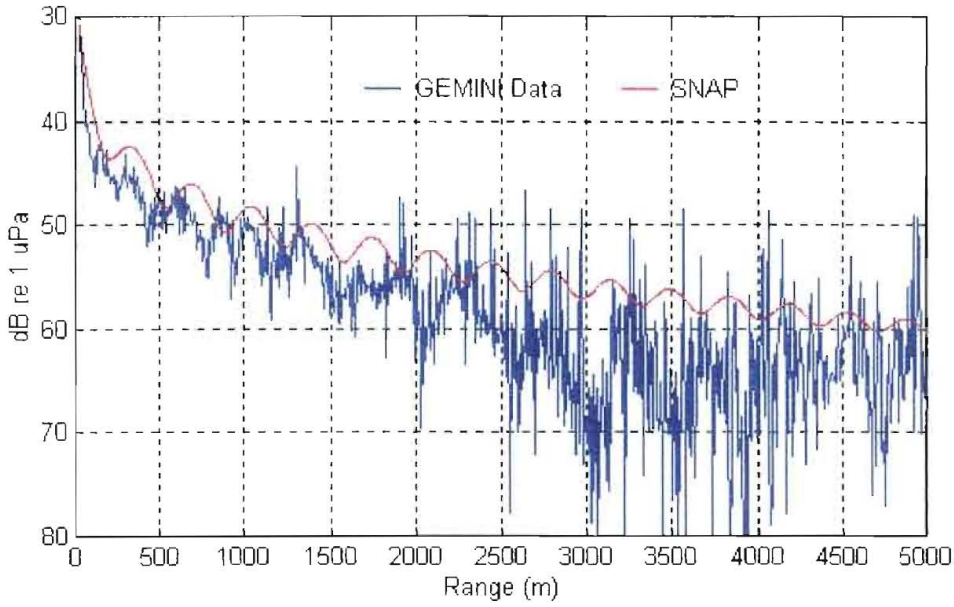

(b)

Figure 45: Plot of GEMINI data versus SNAP model. Source depth: 9 m, receiver depth: 16 m, water depth: 21 m, frequency: 140 Hz (a), 50 Hz (b).

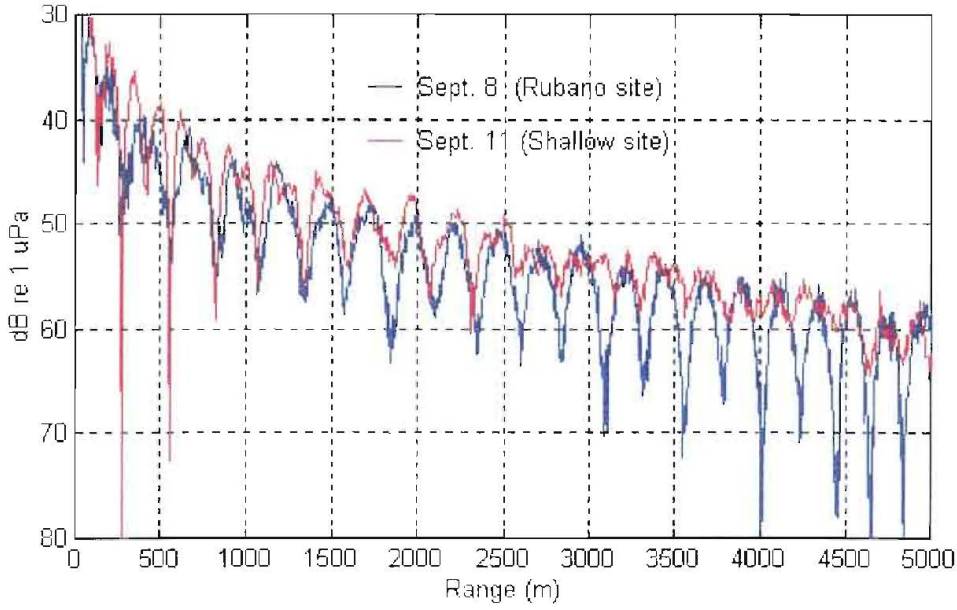

(a)

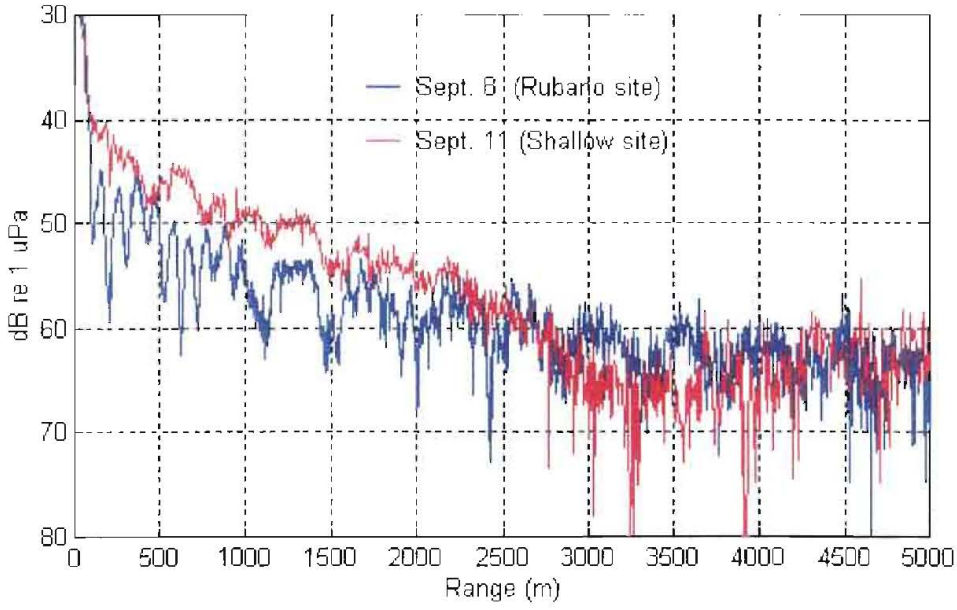

(b)

Figure 46: Plot of 8 and 11 September measured data. Source depth: 9 m, bottom receiver, frequency: 140 Hz (a), 50 Hz (b).

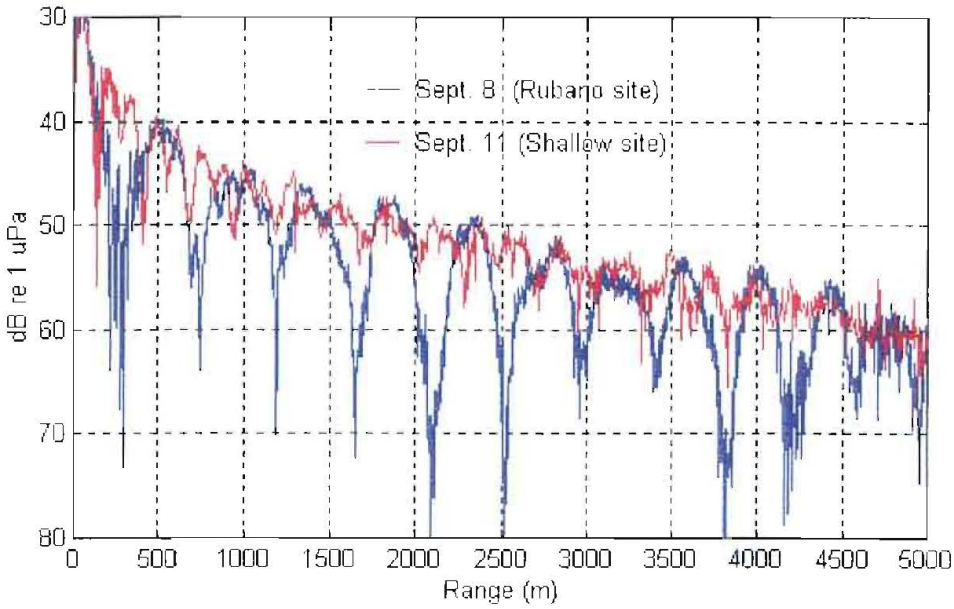

(a)

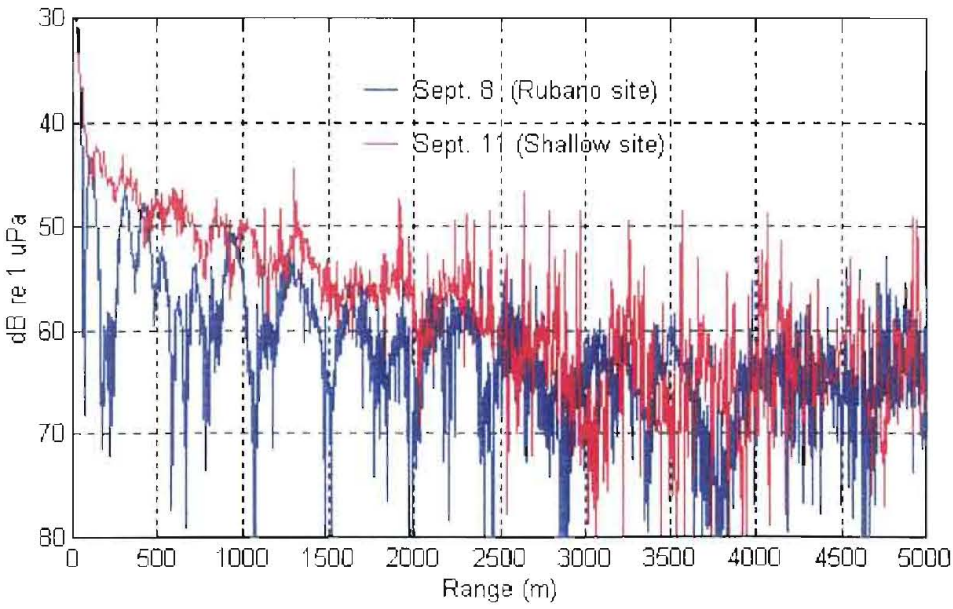

(b)

Figure 47: Plot of 8 and 11 September measured data. Source depth: 9 m, shallow receiver, frequency: 140 Hz (a), 50 Hz (b).

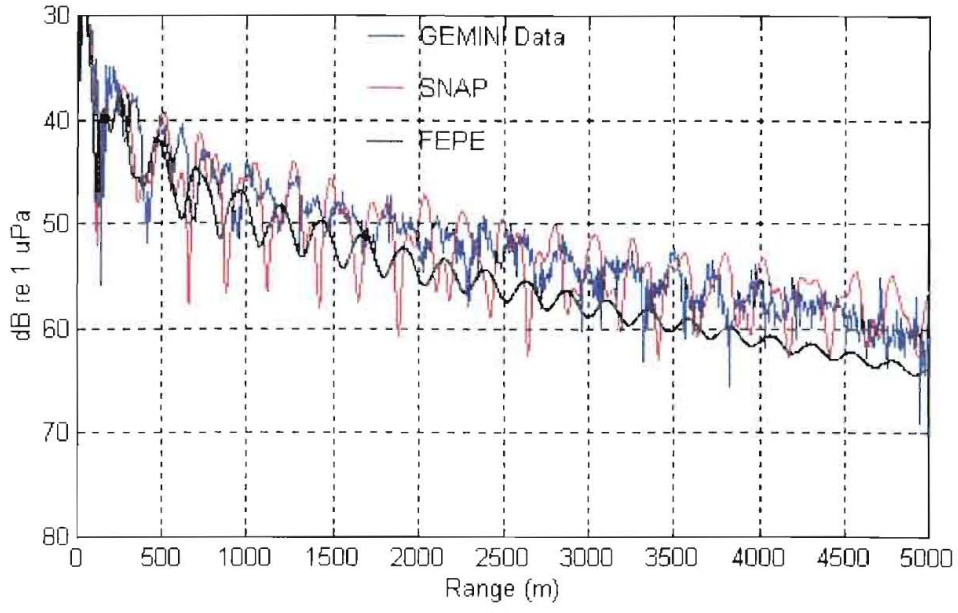

(a)

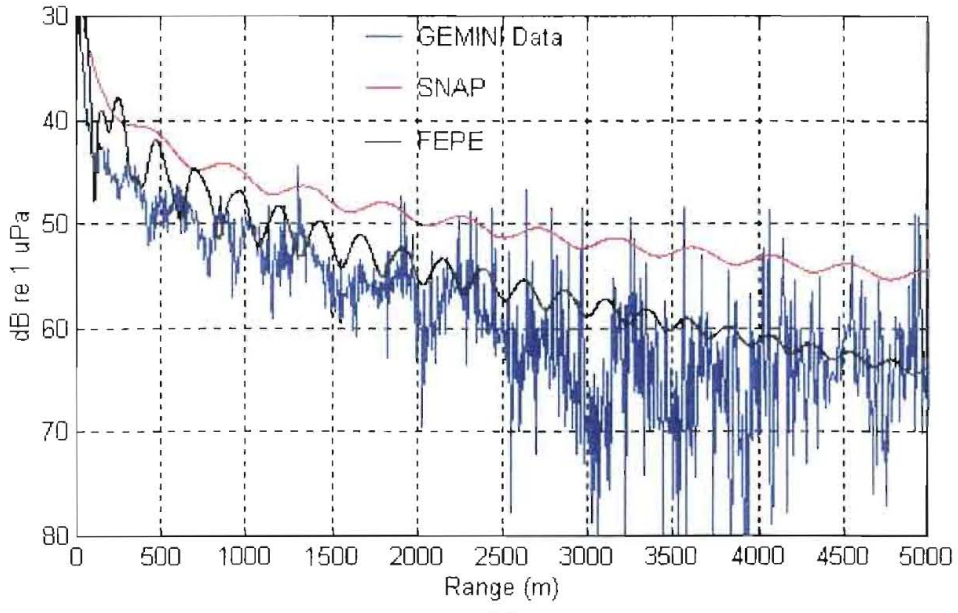

(b)

Figure 48: Plot of GEMINI data versus SNAP and FEPE using an improved geoacoustic model (Null, 1994). Source depth: 9 m, shallow receiver, frequency: 140 Hz (a), 50 Hz (b).

IV. CONCLUSIONS AND RECOMMENDATIONS

The main goal of this thesis was to assess the accuracy of several propagation models using average TL and TL fluctuations compared with measured data for several shallow water environments. The models examined were the Navy standard parabolic equation (PE) model using the LFBL geoacoustic model, the finite element parabolic equation model (FEPE) and the SACLANTCEN normal mode acoustic propagation model (SNAP). Additionally, a comparison of the LFBL geoacoustic model to a Hamilton "point" geoacoustic model was conducted. The comparison was performed at 50 and 140 Hz using data from the Project GEMINI experiment conducted off the shores of Corpus Christi, Texas. This area was previously identified by Matthews et al. (1985) to be a range-independent geoacoustically "benign" environment. The project consisted of five separate experiments conducted at a shallow site (~20 m), a relatively deep water site (~60 m) and a 30 m deep site previously studied by Rubano (1980).

The PE model performed poorly in this geoacoustically "benign" environment and it is recommended that it not be used to model TL in shallow water. The performance of the FEPE model was better in deeper water (deep site) and at the Rubano site than it was at the shallow site. SNAP performed the best overall and shows great potential for modeling average TL and TL fluctuations in shallow water but only if accurate SSP and bottom characteristics are incorporated. It is important to note that

small changes in the geoacoustic model parameters can change the relative performance of the SNAP and FEPE outputs significantly.

The Navy standard PE model, using the OAML approved geoacoustic model LFBL, does not model TL accurately in a "benign", range-independent, well-surveyed area. Hence, one can not expect it to be able to model TL accurately in a complex, range-dependent, unsurveyed shallow water area. The development of a normal mode model using a Hamilton geoacoustic model as input shows the most promise for improved accuracy in the short term. The results of this study provide strong evidence that site-specific Hamilton geoacoustic data must be used. Site-specific geoacoustic models are clearly needed for sites as close as 12 nm from one another, even in a benign, nearly range independent geoacoustic environment.

New algorithms such as the WHOI inverse technique (Rajan, 1987) must be developed to estimate geoacoustic parameters when geoacoustic information, normally obtained from seismic sources, are not available about the shallow water region of interest. Use of the WHOI inverse technique may also prove useful in extending Hamilton vertical or point geoacoustic models horizontally in range between point measurements. Since performing seismic surveys for all the world's shallow water areas is unrealistic, the WHOI inversion technique offers great promise in providing good geoacoustic input parameters for modeling shallow water accurately.

LIST OF REFERENCES

Berryhill, H. L. and A. R. Tippet, "Map showing post-wisconsin sedimentation patterns and faulting in the Corpus Christi 1 x 2 quadrangle, Texas," U. S. Geological Survey, Misc. Inv. Ser. Map I-1287-D, Denver, CO (1981).

Chin-Bing, S. A., D. B. King, J. A. Davis and R. B. Evans, *PE Workshop II: Proceedings of the second parabolic equation workshop*. Naval Research Laboratory, Washington, DC, (1993).

Collins, M. D., "Higher-order Pade' approximations for accurate and stable elastic parabolic equations with application to interface wave propagation," *J. Acoust. Soc. Am.* 89(3), 1050-1057 (1991).

Etter, P. C., *Underwater Acoustic Modeling: Principles, Techniques and Applications*, Elsevier Applied Science, New York (1991).

Hamilton, E. L., "Shear-wave velocity versus depth in marine sediments: a review," *Geophysics* 41(5), 985-996 (1976).

Hamilton, E. L., "Sound attenuation as a function of depth in the sea floor," *J. Acoust. Soc. Am.* 59(3), 528-535 (1976).

Hamilton, E. L., "Sound velocity-density relations in sea-floor sediments and rocks," *J. Acoust. Soc. Am.* 63(2), 366-377 (1978).

Hamilton, E. L., "Geoacoustic modeling of the seafloor," *J. Acoust. Soc. Am.* 68(5), 1313-1340 (1980).

Holland, C., "Shallow water deficiencies in PE," in *Software requirements specification for the low frequency bottom loss model LFBLTAB*, Plannings Systems Inc., Technical Report 014-453, August (1992).

Holland, C. and G. Muncil, "An approximate stochastic model for reflection from quasi-periodic sedimentary sequences," Planning Systems Inc., Technical Report 014-452, February (1992).

Lee, W. H. K. and C. S. Cox, "Time variation of ocean temperatures and its relation to internal waves and ocean heat flow measurements," *J. Geophys. Res.* 71(8), 2101-2111 (1966).

Lynch, J. F., S. D. Rajan and G. V. Frisk, "A comparison of broadband and narrow-band inversions for bottom geoacoustic properties at a site near Corpus Christi, Texas," *J. Acoust. Soc. Am.* 89(2), 648-665 (1991).

Matthews, J. E., P. J. Bucca and W. H. Geddes, "Preliminary environmental assessment of the Project GEMINI site - Corpus Christi, Texas," Naval Ocean Research and Development Activity, Rep. No. 120 (1985).

Mitchell, S. K. and K. C. Focke, "New measurements of compressional wave attenuation in deep ocean sediments," *J. Acoust. Soc. Am.* 67(5), 1582-1589 (1980).

Morton, J. F., "The shallow water diesel: a new priority," *Naval Institute Proceedings*, 119(3), 126-128 (1993).

Null, J. M., Master's Thesis (in preparation), Naval Postgraduate School, Monterey, CA, July (1994).

Porter, M. B., "The KRAKEN Normal Mode Program," SACLANTCEN Memorandum Serial No. SM-245, (1991).

Rajan S. D., J. F. Lynch and G. V. Frisk, "Perturbative inversion methods for obtaining bottom geoacoustic parameters in shallow water," *J. Acoust. Soc. Am.* 82, 998-1017 (1987).

Rajan, S. D., Personal communication with the author, Naval Postgraduate School, Monterey, CA, February (1994).

Ross, C., E. Kelly, L. Reynolds, M. Neil and J. Bowman, "A summary of sediment size, sound velocity and mass physical properties of 16 cores and 15 grab samples from the Gulf of Mexico," USNS LYNCH. U. S. Naval Oceanographic Office, Lab Item 508 (1978).

Rubano, L. A., "Acoustic propagation in shallow water over a low-velocity bottom," *J. Acoust. Soc. Am.* 67(5), 1608-1613 (1980).

Tappert, F. D., "The parabolic approximation method," in *Wave propagation in underwater acoustics*, edited by J. B. Keller and J. S. Papadakis, Springer-Verlag, New York (1977).

Urick, R. J., *Principles of Underwater Sound*, 3rd Edition, McGraw-Hill, New York (1983).

INITIAL DISTRIBUTION LIST

		No. Copies
1.	Defense Technical Information Center Cameron Station Alexandria, VA 22304-6145	2
2.	Library, Code 52 Naval Postgraduate School Monterey, CA 93943-5002	2
3.	Chairman (Code OC/BF) Department of Oceanography Naval Postgraduate School Monterey, CA 93943-5000	3
4.	Dr. James H. Wilson Neptune Sciences, Inc. 3834 Vista Azul San Clemente, CA 92674	3
5.	Ms. Josie Paquin Neptune Sciences, Inc. 150 Cleveland Ave. Slidell, LA 70458	2
6.	Commander Naval Oceanography Command Code 7170 Stennis Space Ctr, MS 39529-5000 Attn: Mr. Jack McDermid	1
7.	Commanding Officer Attn: Dr. Nelson Letourneau Naval Oceanographic Office Stennis Space Ctr Bay St. Louis, MS 39522-5001	1

8. Mr. Jim Donald — 1
Naval Undersea Warfare Center
New London Lab
Code 01Y
New London, CT 06320

9. Mr. Barry Blumenthal — 1
Code C124A
Advanced Environmental Acoustic Support Program
Office of Naval Research
800 N. Quincy St.
Arlington, VA 22217-5660

10. Dr. Bill Cary — 1
ARPA/MSTO
3701 N. Fairfax Drive
Arlington, VA 22203-1714

11. Dr. Subramaniam Rajan — 1
Woods Hole Oceanographic Institution
Applied Ocean Physics and Engineering Department
Woods Hole, MA 02543

12. LT Steven P. Duarte — 1
105 Moran Circle
Monterey, CA 93940

13. LT Mark Null — 1
1040 Spruance Road
Monterey, CA 93940

14. Mr. Ed Chaika/Mr. Dave Small — 2
Advanced Environmental Acoustic Support Program
Code ONR - DET
Building 1020 - Room 184
Stennis Space Center, MS 39529-5000

15. Dr. R. Heitmeyer/Dr. T. C. Yang — 2
Naval Research Laboratory
Code 5123
Washington, DC 20375-5000

16. Commanding Officer 2
Attn: Dr. Homer Bucker/Dr. Frank Ryan
NCCOSC RDTE DIV
53560 Hull St.
San Diego, CA 92152-5001